

**Investigation of
Claystone / Bentonite
Mixtures as
Barrier Material for
Geological Disposal of
Radioactive Waste**

Investigation of Claystone / Bentonite Mixtures as Barrier Material for Geological Disposal of Radioactive Waste

Chun-Liang Zhang
Abram Rogalski
Bernd Zehle
Uwe Hertel

January 2023

Remark:

This report refers to the research project 02E11627 which has been funded by the Federal Ministry for the Environment, Nature Conservation, Nuclear Safety and Consumer Protection (BMUV).

The work was conducted by the Gesellschaft für Anlagen- und Reaktorsicherheit (GRS) gGmbH.

The authors are responsible for the content of the report.

Keywords

Barrier Material, Bentonite, Claystone, Consolidation, Gas Migration, Hydration, Mixture, Performance, Repository, Swelling, Thermal Effects, Water Permeability

Foreword

Crushed Opalinus claystone, MX80 bentonite, and claystone/bentonite mixtures were investigated as engineered barrier material in a radioactive waste repository in the clay formations. Safety-relevant properties and performance of the selected barrier materials were determined under repository-relevant conditions, including

- petrophysical properties (minerals, grain distribution, water content, etc.)
- water absorption and retention capacity
- compressibility for fabrication of compacted blocks
- swelling pressure in relation to dry density
- water permeability in relation to dry density
- gas migration behaviour under water-saturated conditions
- thermo-hydro-mechanical behaviour.

The research work was funded by the Federal Ministry for the Environment, Nature Conservation, Nuclear Safety and Consumer Protection (BMUV) under contract number 02E11627 and was carried out in the GRS Geolaboratory in the period from November 2017 to October 2022. Extensive valuable results were achieved, which are presented in this report. In general, the claystone/bentonite mixtures investigated exhibit favorable properties and performance. The test results can be used to design the engineered barriers in a repository.

Contents

	Foreword	I
1	Introduction	1
2	Geotechnical properties of sample materials: crushed Opalinus claystone, MX80 bentonite and mixtures	7
2.1	Characteristics of sample materials	7
2.1.1	Crushed Opalinus claystone	7
2.1.2	MX80 Bentonite	10
2.1.3	Claystone/bentonite mixtures.....	12
2.1.4	Synthetic pore water	13
2.2	Water retention	14
2.2.1	Test methodology	14
2.2.2	Test results	17
2.3	Compressibility	24
2.3.1	Test methodology	24
2.3.2	Test results	25
2.4	Swelling capacity	30
2.4.1	Test methodology	30
2.4.2	Test results	31
2.5	Water permeability	34
2.5.1	Test methodology	34
2.5.2	Test results	34
2.6	Gas permeability	35
2.6.1	Test methodology	36
2.6.2	Test results	37
3	Barrier performance of selected claystone/bentonite mixtures	45
3.1	Repository relevant conditions considered.....	45
3.2	Test methodology	46
3.2.1	Equipment and samples	46

3.2.2	Test procedure	51
3.3	Results of hydro-mechanical testing	54
3.3.1	Hydration and swelling.....	54
3.3.2	Consolidation and water permeability	56
3.3.3	Gas penetration and impact.....	61
3.3.4	Dismantled samples	65
3.4	Results of thermal testing	68
3.4.1	Thermal effects on hydration and swelling	68
3.4.2	Thermal effects on consolidation and water permeability.....	68
3.4.3	Thermal effect on gas penetration	72
4	Summary and conclusions	77
	Acknowledgements	80
	References	81
	List of figures.....	89
	List of tables	93

1 Introduction

Clay formations are investigated in many countries for deep geological disposal of radioactive waste due to their favourable properties such as large homogeneous rock mass, stable geological structure, extremely low permeability, diffusion-dominated slow transport of fluid, high sorption capacity for retardation of radionuclides, and certain self-sealing capacity. In France and Switzerland, for instance, the potential repositories were proposed to be constructed in the overconsolidated Callovo-Oxfordian (COX) and Opalinus (OPA) argillaceous formations respectively /AND 05/15/ and /NAG 02/. In Germany, two generic models were developed on basis of known data for the Lower Cretaceous Clay and the Opalinus Clay to elaborate the methodology of demonstration of the safety of a repository for high-level radioactive waste (HLW) /LOM 15/ and /JOB 17/.

All disposal concepts established are based on a multi-barrier system, which comprises the natural geological formations and engineering barriers (EBS). The EBS represents engineered materials placed within a repository, including the waste canisters, buffer, backfill, plugs and seals. Once the waste containers are emplaced in deposition holes, the remaining openings such as boreholes, drifts and shafts are to be backfilled and sealed with suitable materials to assure the stability and functionality against release of radionuclides into the biosphere /IAE 92/ and /OEC 03/. The barrier materials must fulfil essential requirements on the safety relevant properties such as

- sufficiently high density to ensure the other required attributes;
- certain mechanical stiffness to guarantee the stability of the engineered barrier system;
- sufficiently high swelling capacity to seal engineered gaps and voids in the barrier system and to resist the propagation of the damaged rock zone (EDZ);
- sufficiently low hydraulic conductivity to limit or avoid advective water transport and to retard migration of radionuclides;
- low gas entry/breakthrough pressures to allow gas release without compromising the integrity of the geological and engineered barrier system;
- chemical-mineralogical compatibility with the host rock to keep the long-term stability of the engineered barrier system;
- adequate thermal conductivity of the buffer around HLW to transfer heat and thus avoid high temperatures as well as thermal impact on the barrier functions.

In most of the concepts, bentonite-based materials have been considered and widely investigated as engineered barrier material for retardation of radionuclides due to favourable properties of bentonite such as high sorption capacity for radionuclides, certain swelling capacity and low hydraulic conductivity when emplaced to certain densities. In addition to the bentonite-based materials, crushed claystone from excavation of a repository and its mixture with bentonite have been recently investigated as the barrier material for the potential repository in COX clay rock /ZHA 10/13/14/17a/18a/, /ZEN 19/, /MID 20/, /ROB 21/. The preliminary results showed a good suitability of the crushed claystone for backfilling and the claystone/bentonite mixture for sealing the repository.

Within the German generic repository models, a preliminary backfilling/sealing concept was developed /LOM 15/, /JOB 17/. Figure 1.1 illustrates the principle of the concept. All remaining openings including deposition boreholes and drifts, access and main drifts, and shafts will be backfilled and sealed with suitable materials. For the generic repository in the OPA formation with a limited thickness of 100 to 130 m, POLLUS casks of HLW will be disposed in horizontal drifts (figure 1.2). The casks will be laid down on highly compacted blocks consisting of prepared excavated rock material. If necessary, expansive clay minerals (bentonite) will be added to ensure a sufficient swelling capacity. The remaining spaces in the deposition drifts will be backfilled using the granules of the same material. Similarly, the access and main drifts will be backfilled with the crushed claystone and sealed with the compacted clay-based blocks and/or bentonite pellets (figure 1.3). The seal cores must have certain swelling capacity to compress and cut off the surrounding damaged zone (EDZ). The seal cores are confined by three concrete plugs at each end and in the middle to ensure the mechanical stability. It is also considered to add asphalt/bitumen elements between the seal cores and plugs as immediate active seal elements. The backfill is expected to take the long-term barrier function.

It is to be pointed out that the utilization of excavated claystone provides many advantages such as chemical-mineralogical compatibility with the host rock, environmental and economic efficiency with no or less occupancy of the ground surface for the excavated claystone and low costs of material preparation and transport, and others.

To support the design and safety assessment of a potential repository in the clay formations in Germany, a research programme was initiated and conducted by GRS to investigate crushed OPA claystone and mixtures with MX80 bentonite as the engineered barrier material. The project was funded by the German Federal Ministry for Economic

Affairs and Climate Action (BMWK) under contract number 02E11627 and conducted from November 2017 to October 2022.

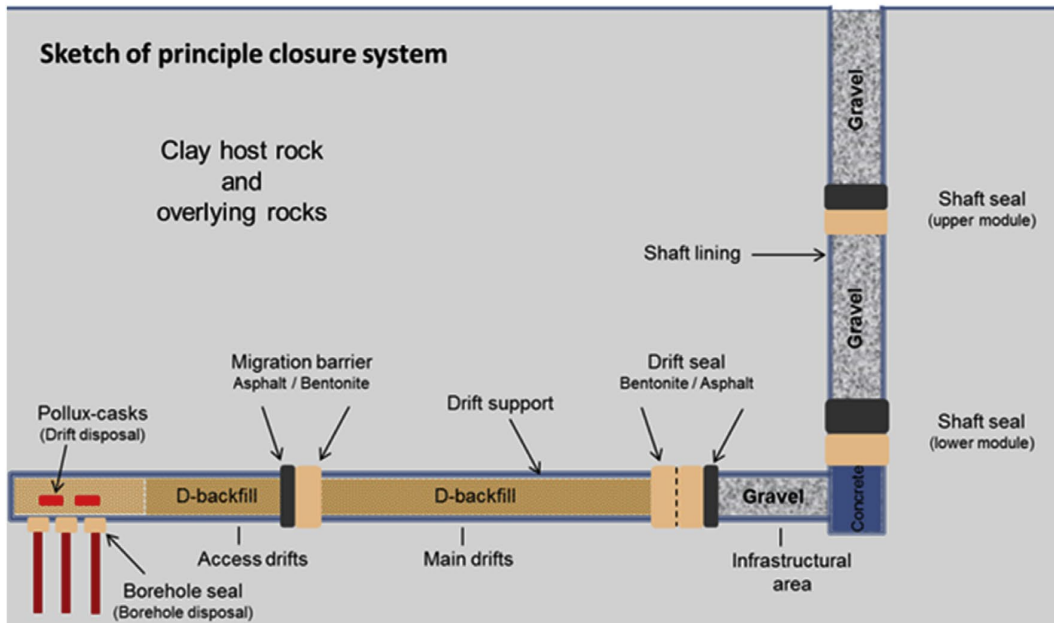


Fig. 1.1 Sketch of the proposed backfilling/sealing concept /JOB 17/

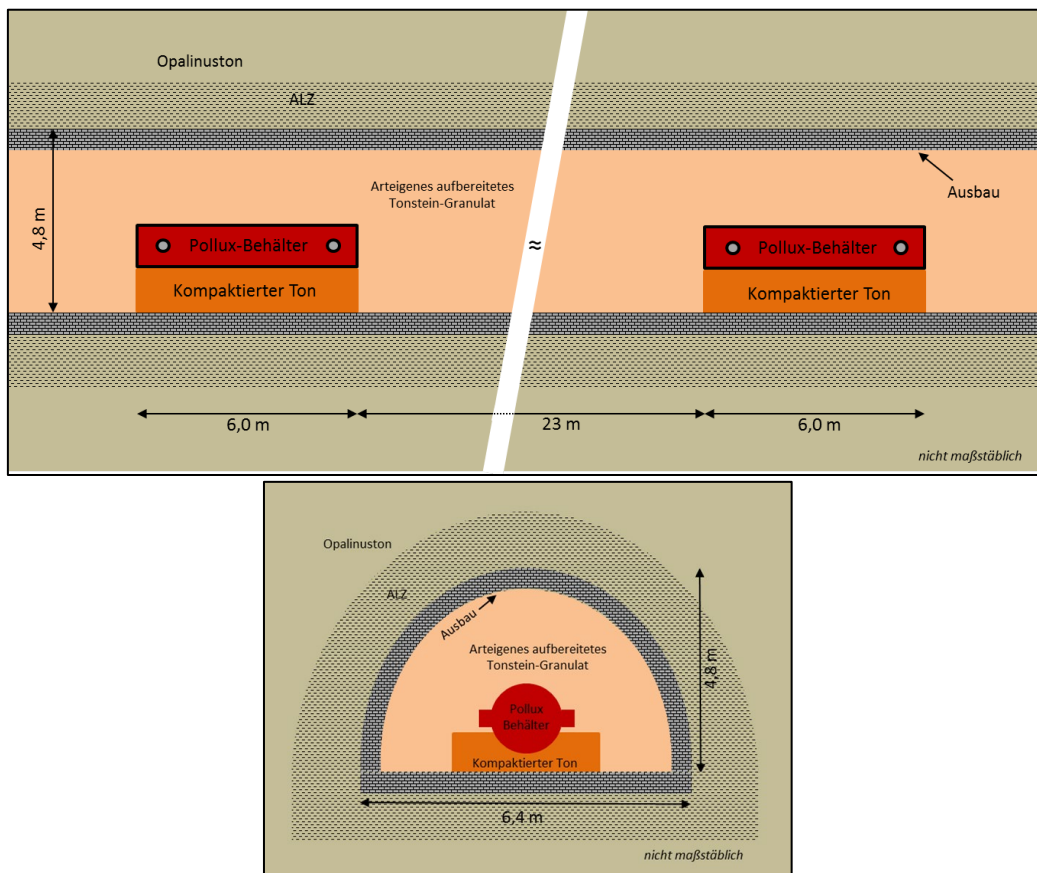


Fig. 1.2 HLW disposal concept in horizontal drifts in Opalinus Clay /JOB 17/

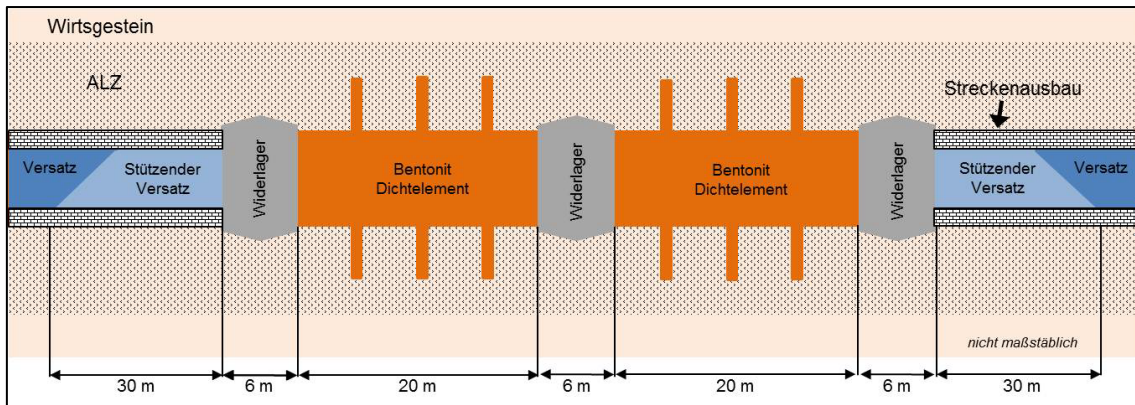


Fig. 1.3 Concept for backfilling and sealing horizontal drifts /LOM 15/

Within the present project, different materials were selected and investigated for the engineering barriers in a repository

- Buffer material: a) precompacted claystone/bentonite mixture for supporting POLLUS casks and b) bentonite granules for backfilling the remaining space in the deposition drifts (figure 1.2);
- Seal material: a) bentonite granules and b) precompacted claystone/bentonite mixture for sealing the boreholes, drifts and shafts at selected locations (figures 1.1 and 1.3);
- Backfill material: a) excavated claystone or b) claystone/bentonite mixture for backfilling the residual openings (boreholes, drifts, and shafts) in the repository (figures 1.1 and 1.3).

These barrier materials can be loosely emplaced and compacted on site, or precompacted to blocks and constructed on site. After the emplacement, the materials will be subjected to a hydration process by taking up water from the saturated host rock. Upon water uptake, the materials will expand and seal the engineered voids/gaps remaining in the filled openings and then swelling pressure may build up, depending on the content of swellable clay minerals and emplaced density. The swelling pressure is responsible for the integrity and stability of the engineered barrier and host rock system. On the other side, the barrier materials will also be consolidated from the rheological deformation of the surrounding rock. Their most important barrier functions will be ensured by low hydraulic conductivities to limit transport of radionuclides with water flow. Furthermore, when moisture contacts the metallic canisters and construction components, anaerobic corrosion will occur and produce gases. Gas accumulation could lead to high gas pressures accessing certain thresholds and impairing the integrity of the geological-

engineered barrier system. Thus, sufficient knowledge of gas migration in these barriers is also necessary for safety assessment of the repository. Moreover, the buffer around HLW canisters will sustain thermal loading from the heat emission. The properties of the buffer will be altered but must not affect its required barrier functions negatively.

Under consideration of the repository relevant conditions, various laboratory experiments were carried out to determine geotechnical properties and barrier performance of the claystone-based materials, including:

- petrophysical properties of sample materials
- water uptake and retention capacity
- compressibility for fabrication of compacted blocks
- swelling capacity (pressure and strain) in relation to dry density
- water permeability in relation to dry density
- gas breakthrough pressure and permeability under water-saturated conditions
- response to hydro-mechanical loading
- thermal effects on barrier performance.

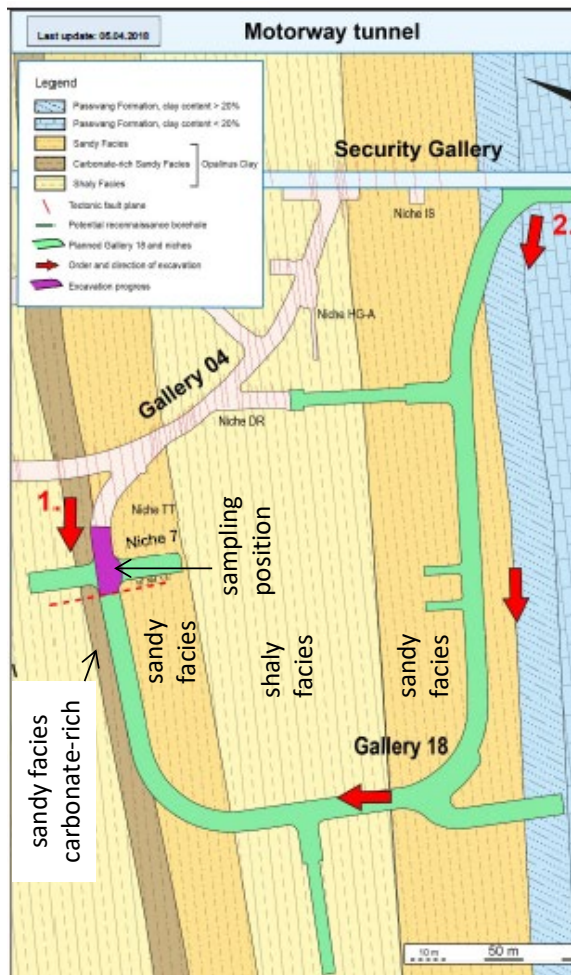
New testing systems and methods were developed for conducting the proposed experiments. Main results obtained are presented and discussed in this report.

2 Geotechnical properties of sample materials: crushed Opalinus claystone, MX80 bentonite and mixtures

2.1 Characteristics of sample materials

2.1.1 Crushed Opalinus claystone

Crushed claystone was extracted from excavation of Gallery 18 in the sandy facies of the Opalinus Clay in the Underground Research Laboratory (URL) at Mont-Terri. Figure 2.1 shows the sampling position and the picture of a road header used for the gallery excavation and the collected and piled material. The sample material was taken from the pile in a mass of about 500 kg. To avoid desaturation and alteration, the extracted material was sealed in plastic drums and stored at room temperature until testing.



a. Gallery 18 and sampling position (April 2018)



b. Excavation using a road header



c. Collection of crushed claystone



d. Sampling from the pile of the excavated claystone

Fig. 2.1 Sampling of the crushed claystone from excavation of Gallery 18 in the sandy facies of Opalinus Clay at Mont-Terri rock Laboratory

The excavated claystone was characterized by its grain size distribution, water content, grain density, and mineralogical composition. Figure 2.2 shows the grain size distributions of the crushed OPA claystone with grain sizes of $d < 32$ mm (excavated material), $d < 10$ mm and 5 mm by removing the respective larger grains, compared to those of the crushed COX claystone tested previously /ZHA 10/13/14/17a/18a/. The raw OPA aggregate ($d < 32$ mm) has a relatively large fraction of small grains compared to the raw COX aggregate. The other two grain distributions of $d < 10$ mm and < 5 mm were selected for mixtures with bentonite and for suitable sample sizes. The grain distributions of OPA and COX aggregates with $d < 10$ mm are quite similar, while OPA aggregate with $d < 5$ mm has more fine grains than COX aggregate with $d < 5$ mm. The comparison of the grain sizes of both materials may be helpful for comparing their geotechnical properties.

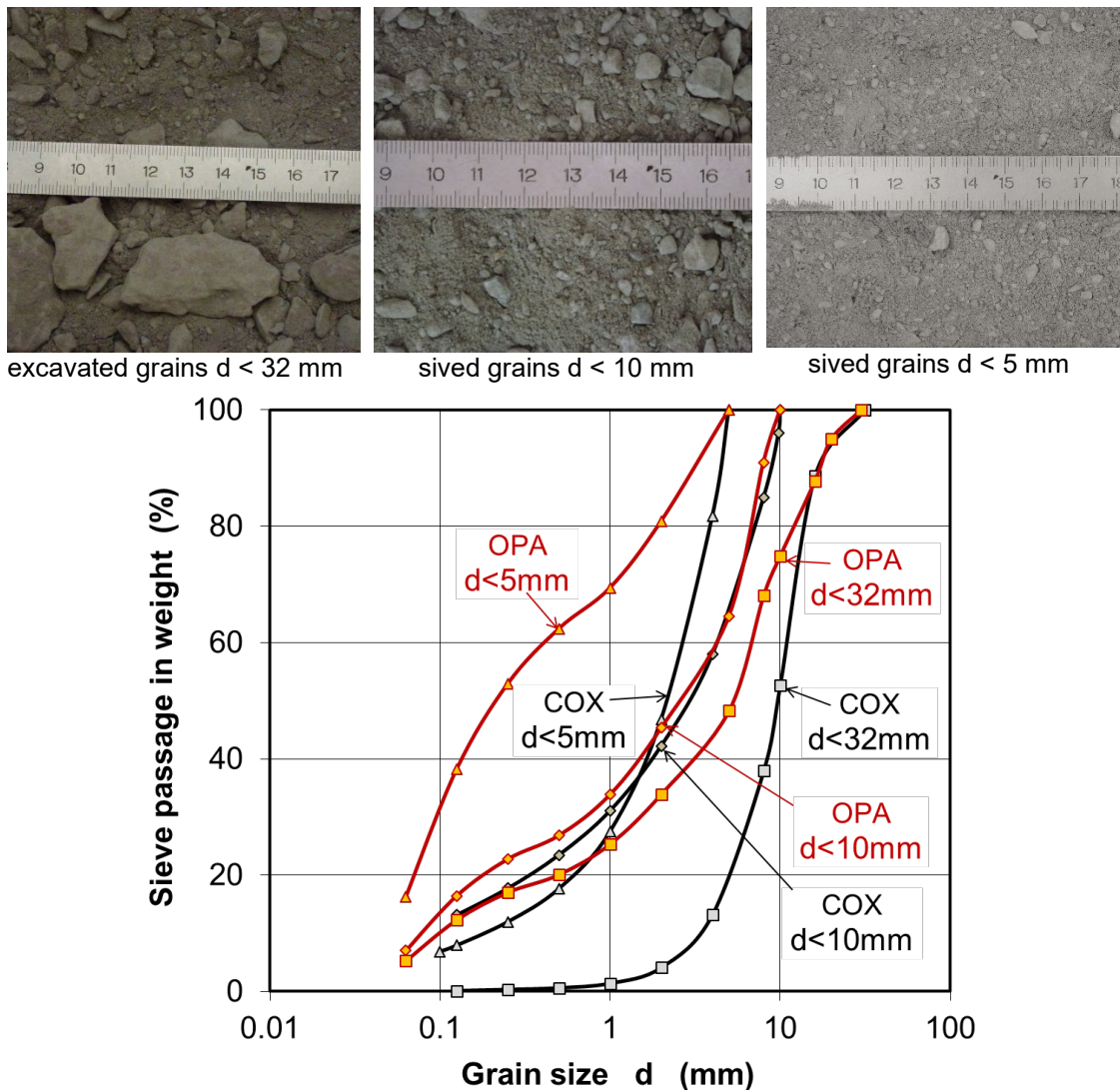


Fig. 2.2 Pictures of crushed OPA claystone with different grain sizes and the corresponding distribution curves compared with crushed COX claystone

Due to exposing to air during the sampling, the excavated material was somewhat de-saturated. The remaining water content was determined after drying in oven at 105 °C for 2 days to $w = 3.63\%$ for the grains $d < 32\text{ mm}$, $w = 3.61\%$ for $d < 10\text{ mm}$, and $w = 3.20\%$ for $d < 5\text{ mm}$, respectively. The remaining water content decreased with decreasing grain sizes because the fine-grained material with relatively large specific surfaces had been more exposed to air and thus more desaturated.

The grain density was measured using a helium gas pycnometer on different grain fractions after drying at 105 °C for 2 days. The results are summarized in table 2.1. The measured values are close to each other with an average value of 2.704 g/cm^3 .

Tab. 2.1 Grain densities measured on different grain fractions of crushed OPA claystone

Grain size (mm)	Grain density (g/cm ³)
4-2	2.711
2-1	2.704
1-0.5	2.702
0.5-0.25	2.700
0.25-0.125	2.704
0.125-0.063	2.693
< 0.063	2.716
mean value	2.704
std. deviation	0.007

The mineralogical composition of the OPA sandy claystone was obtained from two cores BPE-1-2 and BPE-1-3 drilled in the sampling region. The tests were carried out at the German Federal Institute for Geosciences and Natural Resources (BGR) by means of X-ray diffraction and Rietveld analysis. The results are summarised in table 2.2. The main components are clay minerals of 31 %, quartz of 44 % - 45 %, carbonates of 17 % - 23 %, feldspar of 8 % - 10 %, pyrite of < 1 %, and small amounts of other accessory minerals. The results are consistent with those given in literature /KAU 11/, /ZHA 20/. Compared to the COX claystone with clay minerals of 40 - 55 %, quartz of 17 - 27 % and carbonates of 20 - 35 % /ARM 14/, /CON 18/, the OPA sandy claystone has a relatively lower clay content but more quartz and carbonates. The mechanical properties of the claystones are determined by the mineralogical components. Generally, the stiffness and strength increase with increasing carbonate cementation and with decreasing clay minerals. In the presence of expansive clay minerals such as smectite of 13 % - 23 % in the COX /TOU 07/ and 5 % - 20 % in the OPA /PEA 03/, these claystones also exhibit certain swelling capacities upon water uptake /ZHA 17b/. The mechanical behaviour of individual

claystone particles may affect geotechnical properties of the aggregate. The detailed characteristics of the claystones can be found in literature, e. g., for the OPA sandy claystone in /ZHA 20/ and for the COX claystone in /ZHA 18b/.

Tab. 2.2 Main mineralogical components of the OPA sandy claystone determined on drilled cores BPE-1-2/3

Sample	Clay (%)	Quartz (%)	Carbonates (%)	Feldspar (%)	Pyrite (%)
BPE-1-2	31	45	23	8	< 1
BPE-1-3	31	44	17	10	< 1

2.1.2 MX80 Bentonite

In the Swiss and French concepts /NAG 02/, /AND 15/, expansive bentonite will be used as engineered barrier material in form of fabricated blocks, compacted pellets, granules, and bentonite/sand mixture. As a reference material, sodium bentonite MX80 from Wyoming in the USA has been extensively investigated. For instance, the granulated bentonite was used for backfilling a full-scale horizontal drift (FE experiment) at URL Mont-Terri /KÖH 15/, /MÜL 17/, and for sealing a full-scale drift (FSS experiment) /FOI 15/, /BOS 16/. The same bentonite was provided by ANDRA with different grain sizes for our experiments: (a) fine-grained granules $d < 2$ mm, (b) crushed pellets $d < 5$ mm and (c) pellets with a same grain size $d = 7$ mm. The grain size distributions are illustrated in figure 2.3.

Water contents of the delivered samples were measured after drying at 105 °C for 2 days. The results are $w = 7$ % for the pellets $d = 7$ mm, 5.5 % for the crushed pellets $d < 5$ mm and 15% for the powder $d < 2$ mm. The relatively higher water content of the powder resulted from its larger specific surface available for water adsorption.

The compacted pellets had a dry density of 2.0 g/cm³ /BOS 16/. The grain density was measured with a helium gas pycnometer on different grain fractions after drying at 105 °C for 2 days. The results are summarized in table 2.3. The average grain density is 2.67 g/cm³. Additionally, quartz sand was also used for a mixture with bentonite. Its grains are smaller than 2 mm (figure 2.3) and the grain density is 2.68 g/cm³.

The mineralogical composition of the bentonite was determined at the German Federal Institute for Geosciences and Natural Resources (BGR) by means of X-ray diffraction and Rietveld analysis. The mineralogical analysis was performed on the samples preheated at 105 °C for 14 days or without heat treatment. The measured results are summarized in table 2.4. It is obvious that the preheating did not affect the mineralogical compositions of the bentonite. The dominating component montmorillonite is responsible for high capacities of water adsorption and swelling of the bentonite.

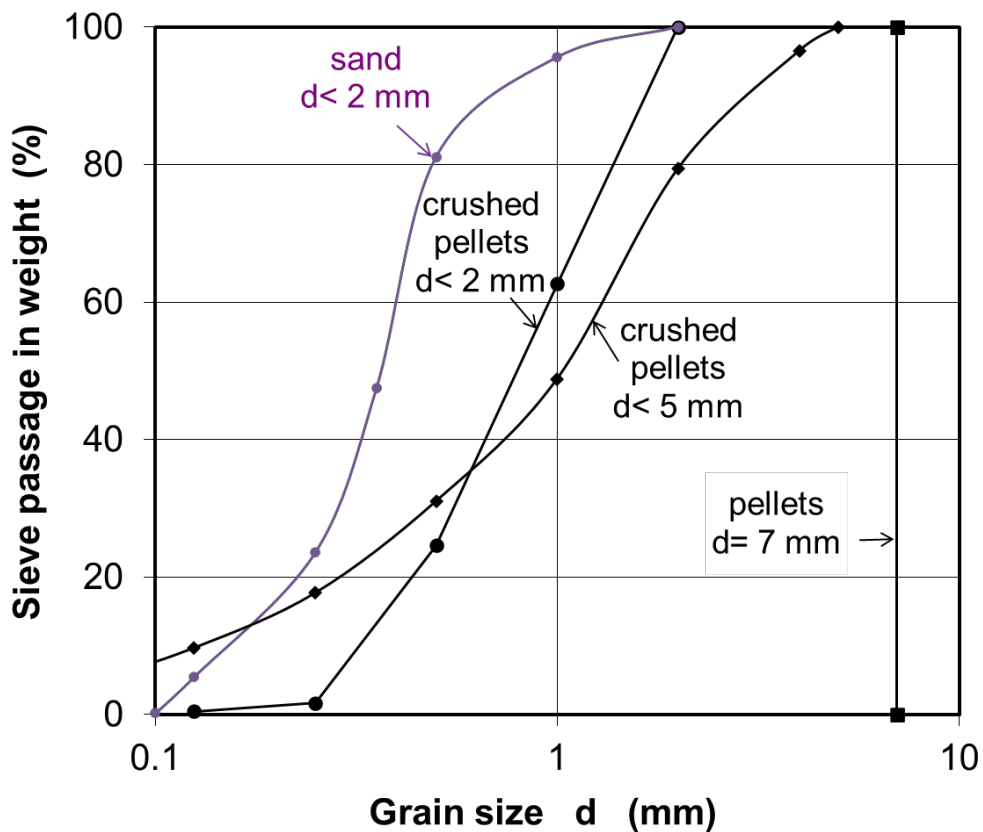
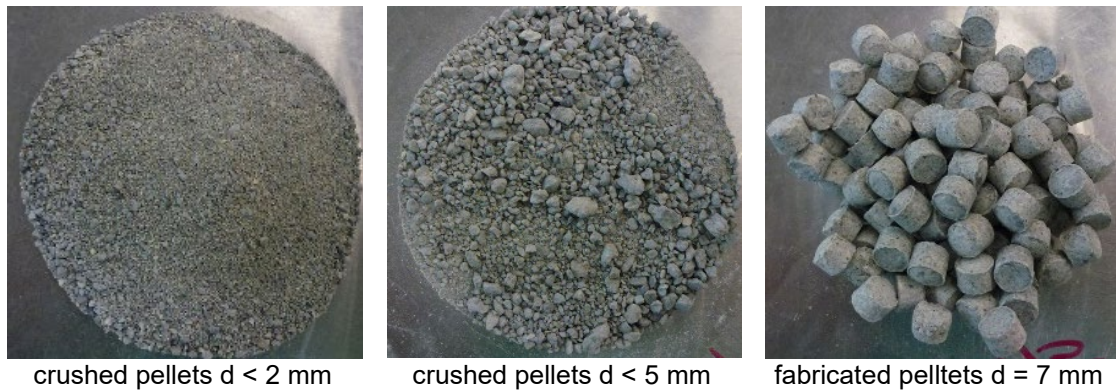


Fig. 2.3 Grain size distributions of the granules, crushed and fabricated pellets of MX80 bentonite

Tab. 2.3 Grain densities of the different fractions of tested MX80 bentonite

Grain size (mm)	Grain density (g/cm ³)
4-2	2.675
2-1	2.666
1-0.5	2.668
0.5-0.25	2.667
0.25-0.125	2.675
0.125-0.063	2.671
< 0.063	2.666
mean value	2.670
std. deviation	0.013

Tab. 2.4 Mineralogical components of tested MX80 bentonite

Mineral content (%)	No heated	Preheated at 105 °C
Montmorillonite	86	86
Quartz	6	6
Cristobalite	1	1
Plagioclase	2	3
Feldspar	3	1
Gips	< 1	2
Pyrite	< 1	< 1
Apatite	< 1	< 1

2.1.3 Claystone/bentonite mixtures

Within the project, the following materials were selected for testing:

- Crushed OPA claystone with the grain size distribution $d < 32$ mm as backfill material and $d < 5$ mm or $d < 10$ mm for mixtures with bentonite as barrier material;
- MX80 bentonite granules and pellet/powder mixture as buffer/seal material;
- Claystone/bentonite mixtures compacted to high densities as buffer/seal material.

Considering the emplacement techniques and the requirements on the engineered barriers, the materials were prepared in loose and/or precompacted blocks for testing. The selected mixtures are similar like those crushed COX claystone/bentonite mixtures tested previously /ZHA 10/13/14/17a/18a/. Therefore, it is possible to compare the properties of both OPA and COX claystone/bentonite mixtures.

2.1.4 Synthetic pore water

For hydraulic testing, synthetic clay water was manufactured based on the chemistry of the porewater in the OPA /PEA 99/ (table 2.4), compared with synthetic COX porewater /AND 05/ (tables 2.5).

Tab. 2.5 Main chemical components of synthetic OPA clay water

Component	Na ⁺	Cl ⁻	Mg ²⁺	Ca ²⁺	SO ₄ ²⁻	K ⁺
Content (mmol/L)	240	300	16.9	25.8	14.1	1.6

Tab. 2.6 Main chemical components of synthetic COX clay water

Component	Na ⁺	Cl ⁻	Mg ²⁺	Ca ²⁺	SO ₄ ²⁻	K ⁺
Content (mmol/L)	27.7	31.1	11.0	13.3	25.0	6.8

Their density and viscosity were measured at different temperatures from 25 to 80 °C. Figure 2.4 shows the results. The density and viscosity of the synthetic OPA and COX porewaters are quite similar and higher than those of the distilled water. The water density and viscosity decrease with increasing temperature. These data are used for calculations of water saturation and water permeability of samples.

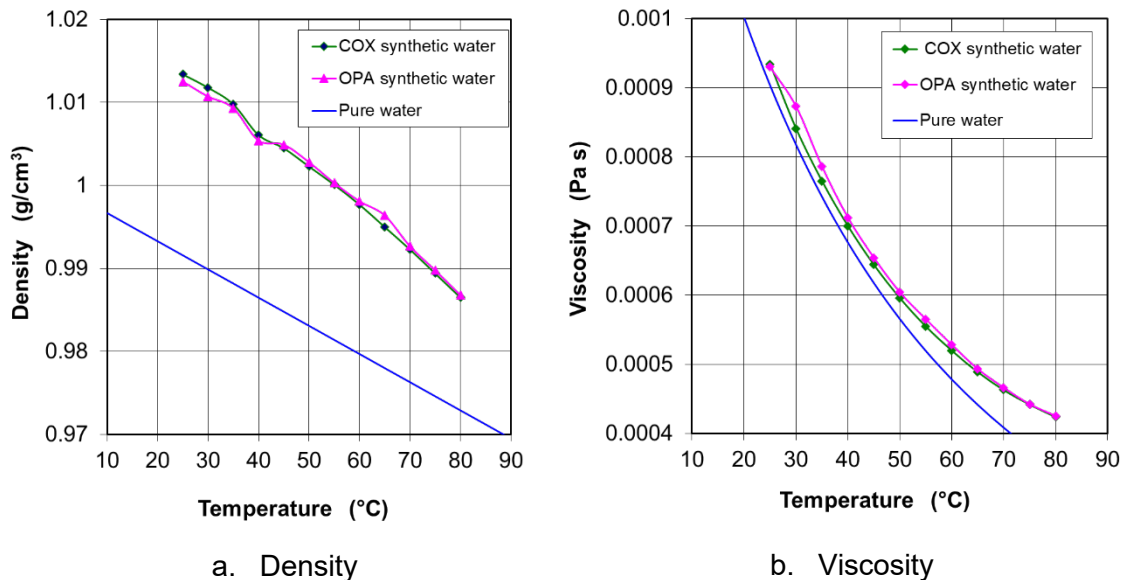


Fig. 2.4 Density and viscosity of synthetic OPA and COX porewaters as a function of temperature in comparison with pure water

2.2 Water retention

An initially unsaturated clay-based material will take up water from humid environment. Under effect of vapour-pressure gradient or suction gradient, water molecules migrate by diffusion into pores from the low suction boundary to the high suction region inside the material. The water molecules are adsorbed in interlayers and on external surfaces of clay particles. The amount of water uptake reaches constant as equilibrium is reached at a given suction. The relationship between suction and water content or degree of saturation is essential for understanding and modelling of the hydro-mechanical behaviour of the material, which is usually called water retention curve. In most of the disposal concepts, “air” dry clay-based materials will be emplaced in the repository openings. A water saturation process will take place in the barrier system by water uptaking from the humid surrounding host rock. The degree of water saturation is a significant factor determining the material properties and behaviour such as water and gas transport, deformation and strength, thermal conductivity, and others. Therefore, the selected claystone/bentonite mixtures as engineered barrier material were firstly characterised by determination of their water uptake and retention capacities.

2.2.1 Test methodology

Vapour transfer technique was adapted for determination of water uptake and retention capacities of the selected materials under free and confined boundary conditions. The samples under free conditions were weighted to an initial weight of 50 g each and placed in bowls, whereas the others were compacted and confined in stainless steel cells of 50 mm diameter and 20 mm height, as shown in figure 2.5. The confined samples were covered with two sintered porous discs and fixed by screwing the bottom and top platen at the end sides of the cells. The porous discs allow exchange of water vapour between in- and outside. The samples were placed in desiccators at different relative humidity values adjusted using different salt solutions as given in table 2.7. The relative humidity RH is correlated to the matrix suction s by the psychrometric law /FRE 93/:

$$s = -\frac{\rho_w RT}{M_w} \ln(RH) \quad (2.1)$$

where T is the absolute temperature, R is the universal gas constant, ρ_w and M_w are the density and the molecular mass of water, respectively. A range of RH -values of 20 % to 100 % was applied, corresponding to $s = 210$ to 0 MPa at the testing temperature of 24 °C. The evolution of RH in each desiccator was continuously recorded by transistor

psychrometer sensors, while the amount of water uptake was measured at time intervals of 1 - 3 months. The total durations lasted for 4 to 12 months until equilibrium. The final water content of each sample was measured after drying in oven at 105 °C for 2 days.



a. Samples placed in bowls and confined in cells



b. Samples placed in desiccators at different relative humidities

Fig. 2.5 Pictures of the samples placed in desiccators for the measurement of water uptake and retention capacities at different humid conditions

Tab. 2.7 Salt solutions used for the measurement of water retention capacities of the selected barrier materials at different relative humidities

Salt solution	Relative humidity <i>RH</i> (%)	Suction <i>s</i> (MPa)
LiCl	22.0	207.1
CaCl ₂	34.5	145.6
Mg(NO ₃) ₂ ·2H ₂ O	55.0	81.8
KJ	67.0	54.8
NaCl	73.0	43.0
KCl	81.3	28.3
ZnSO ₄ ·7H ₂ O	86.7	19.5
Na ₂ HPO ₄ ·12H ₂ O	95.0	7.0
CuSO ₄ ·5H ₂ O	96.5	4.9
H ₂ O	100.0	0.0

The water uptake and retention capacities of the crushed OPA claystone, MX80 bentonite and a claystone/bentonite (7/3) mixture were determined on their samples under free and confined conditions. Their initial characteristics are summarized in tables 2.8 and 2.9. All the samples had grains $d < 5$ mm. The compacted claystone aggregate and claystone/bentonite mixture had the same dry density of 2.0 g/cm^3 .

Currently, thermal effects on bentonite at high temperatures up $150 - 200 \text{ }^\circ\text{C}$ are being investigated in the framework of the EC project EURAD-HITEC /VIL 20/ for evaluating the feasibility of the deep disposal of high heat generating wastes (HHGW) in clay formations. For the same purpose, temperature influence on the water retention capacity of MX80 bentonite was examined with free samples, which were preheated to different temperatures of $25, 50, 105, 150$ and $200 \text{ }^\circ\text{C}$ for $14, 28, 42, 56, 70$ days respectively (sample groups A-E in table 2.9). Samples in the other two groups E and F were preheated to 25 and $200 \text{ }^\circ\text{C}$ for 14 and 70 days respectively, and then compacted to a dry density of 1.50 g/cm^3 and confined in the cells. The targeted density is close to those achieved in the full-scale drift emplacement experiments FE /KÖH 15/, /MÜL 17/ and FSS /FOI 15/, /BOS 16/. The different initial water contents of the samples were resulted from their exposure to air over different time periods before testing. Each group consisted of 6 samples, each of them was placed in a desiccator at a defined relative humidity or suction.

Tab. 2.8 Initial characteristics of the crushed OPA claystone and claystone/bentonite mixture (7/3) for the measurement of water uptake and retention

Samples	Crushed OPA claystone	Compacted OPA claystone	Crushed claystone/bentonite (7/3)	Compacted claystone/bentonite (7/3)
Dry density ρ_d (g/cm ³)	-	2.0	-	2.0
Water content w_o (%)	3.0	3.0	3.7	3.7
Porosity ϕ_o (%)	-	25.9	-	25.7
Confinement	free	confined	free	confined

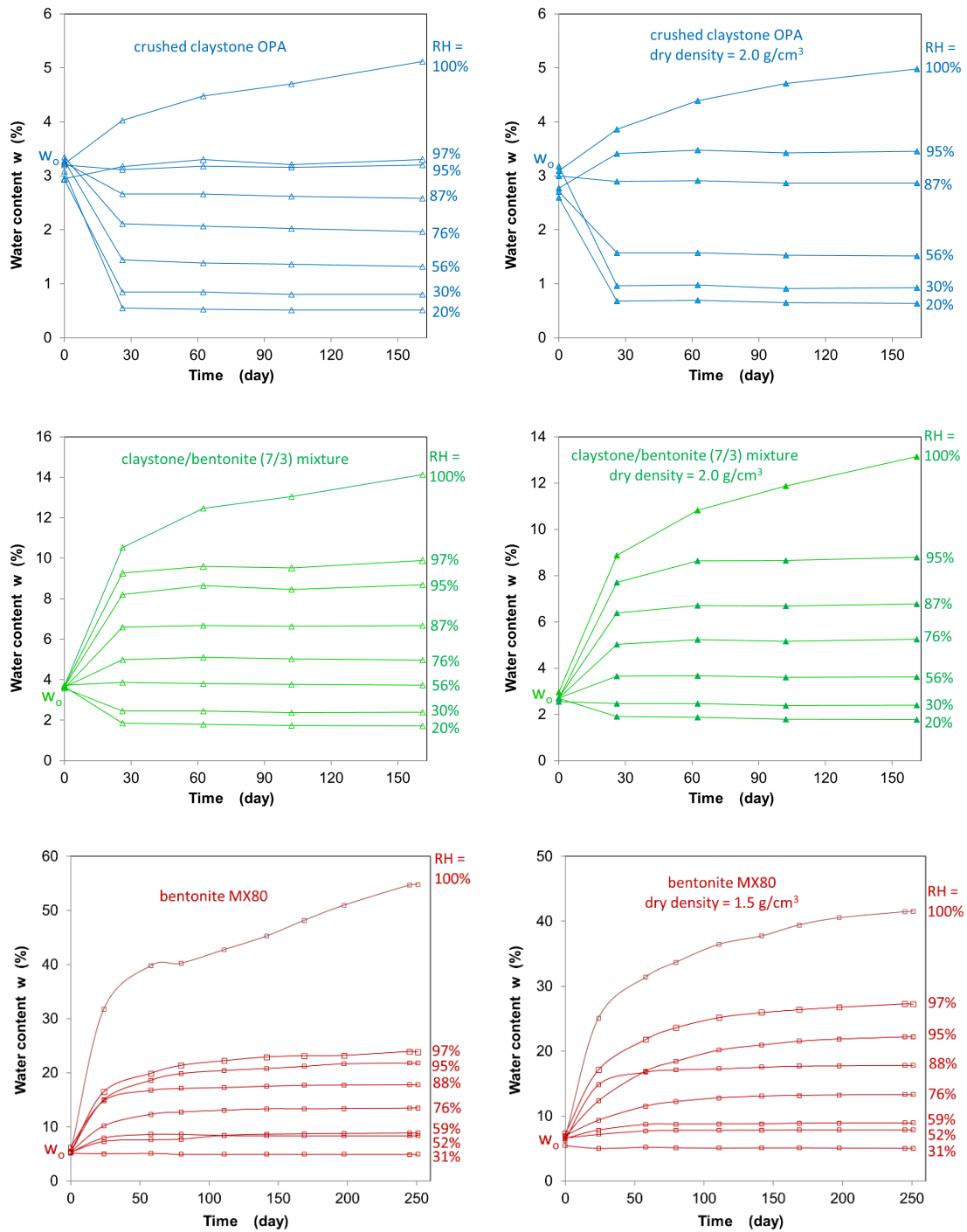
Tab. 2.9 Initial characteristics of MX80 bentonite samples for the measurement of water uptake and retention

MX80 samples	A	B	C	D	E	F	G
Dry density ρ_d (g/cm ³)	-	-	-	-	-	1.5	1.5
Water content w_o (%)	5.4	1.9	0.4	0.3	0.4	13.0	11.0
Porosity ϕ_o (%)	-	-	-	-	-	43.8	43.8
Heating temperature (°C)	25	50	105	150	200	25	200
Heating duration (day)	14	28	42	56	70	14	70
Confinement	free	free	free	free	free	confined	confined

2.2.2 Test results

2.2.2.1 Evolution of water uptake

Figure 2.6 presents typical evolution of water uptake measured on the crushed claystone, claystone/bentonite mixture and bentonite at different humidity values of $RH = 20\%$ to 100% and under free and confined conditions, respectively. It shows that each material took up water when the environment humidity was higher than the initial value RH_o , which was about 90% for the claystone, 50% for the mixture, and 30% for the bentonite, almost independent of applied confinements (free or confined). On the contrary, at dry conditions, $RH < RH_o$, the pre-existing pore water was releasing from particle surfaces into the pore space. Both processes of hydration at $RH > RH_o$ and dehydration at $RH < RH_o$ tended to equilibrium with time. The duration to equilibrium increased with increasing sample density, bentonite content, and relative humidity in the circumstance. The hydration of the bentonite at high relative humidity $RH > 95\%$ took several months to reach equilibrium, much longer than that of the claystone and the claystone/bentonite mixture.



a. under free conditions

b. under confined conditions

Fig. 2.6 Evolution of water uptake measured on the crushed OPA claystone, claystone/bentonite (7/3) mixture and MX80 bentonite under free and confined conditions

2.2.2.2 Water retention capacity

The water contents reached at equilibrium are shown in figure 2.7 as a function of suction for the crushed claystone and claystone/bentonite (7/3) mixture and in figure 2.8 for the bentonite, respectively. Some findings can be derived from the water retention curves:

- The water content of each material increased with decreasing suction exponentially.
- The claystone and the claystone/bentonite (7/3) mixture took up more water under free conditions than under confined conditions, whereas the amounts of water uptake by the bentonite under free and confined conditions are quite similar at suctions $s > 5$ MPa but the unconfined bentonite took much more water at $s < 5$ MPa.
- The preheating up to 105 °C for the claystone and the claystone/bentonite (7/3) mixture did not affect their water uptake capacity, whereas the confined bentonite preheated at 200 °C showed a relatively lower water uptake capacity with $w_{\max} = 35$ % at $s = 0$ compared to the unheated sample with $w_{\max} = 42$ % at $s = 0$.
- The bentonite showed the maximum capacity of water uptake due to the high content of montmorillonite with high capacity of water adsorption. In contrast, the water uptake capacity of the claystone is limited due to the small contents of expansive clay minerals. At zero suction, the amount of water uptake reaches the maximum of $w_{\max} = 56$ % - 59 % at the bentonite under free condition, which is about 3 and 9 times higher than $w_{\max} = 13$ - 14 % at the claystone/bentonite (7/3) mixture and $w_{\max} = 5$ % at the claystone, respectively.

2.2.2.3 Water saturation – suction relationship

Conventionally, the water retention curve of a porous soil material is expressed by degree of water saturation in relation with suction. The degree of water saturation is defined by

$$S_w = \frac{V_w}{V_v} = \frac{\rho_d \cdot w}{\rho_w \cdot \phi} \quad (2.2)$$

where V_w is the volume of the pore water, V_v is the volume of the pores, ρ_d is the dry density of the sample, ρ_w is the density of the pore water, w is the mass water content, and ϕ is the porosity.

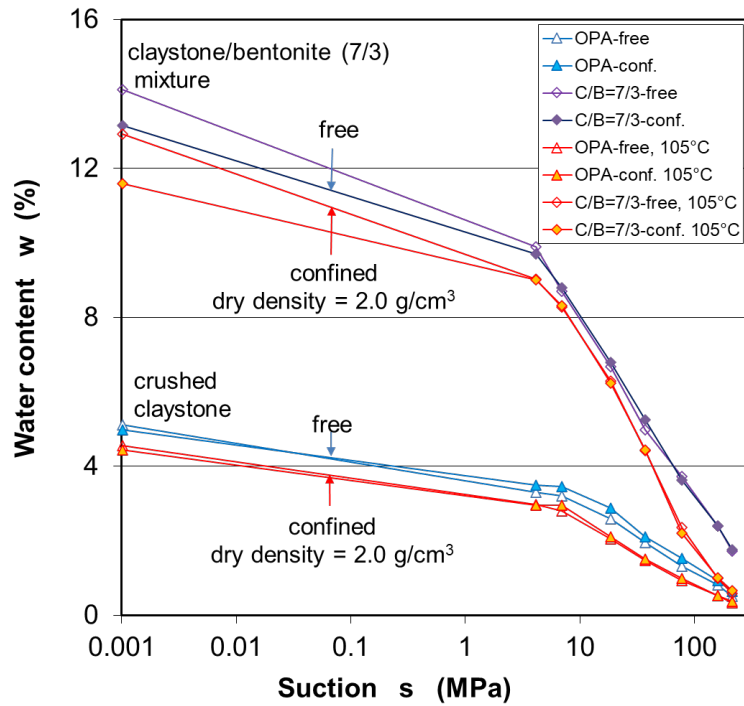


Fig. 2.7 Water retention curves of the crushed OPA claystone and claystone/bentonite (7/3) mixture preheated at 25 - 105 °C under free and confined conditions

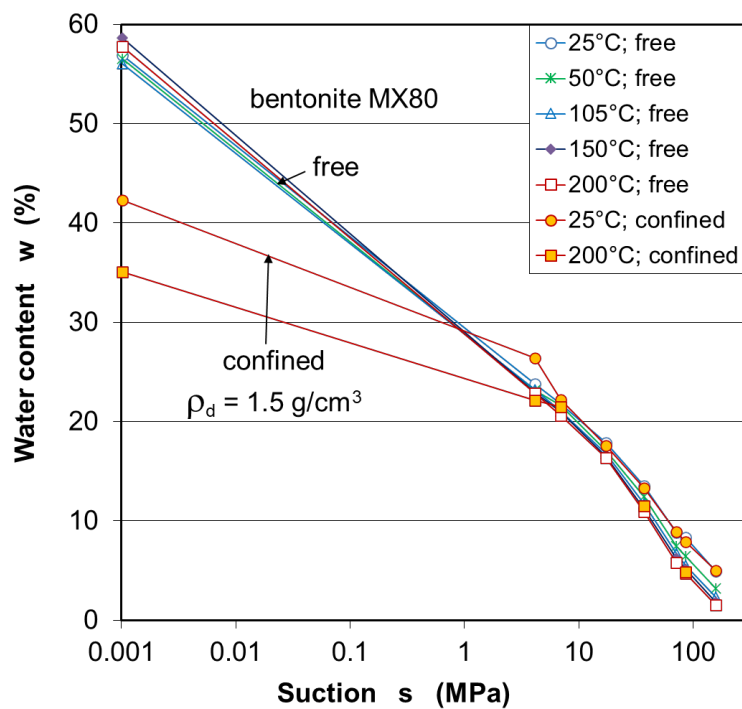


Fig. 2.8 Water retention curves of MX80 bentonite preheated at 25 - 200 °C under free and confined conditions

Taking the density of pure water $\rho_w = 1.0 \text{ g/cm}^3$ for the pore water, the degree of water saturation is calculated for the confined samples at the different suctions. The results are shown in figure 2.9. One can see that the degree of water saturation increases with decreasing suction for each of the compacted materials and with increasing bentonite content at a given suction. Whereas the bentonite at a dry density $\rho_d = 1.5 \text{ g/cm}^3$ (corresponding to a porosity $\phi = 47.7 \%$) can be fully saturated by taking up water from humid air at zero suction, the pore spaces in the highly compacted claystone aggregate ($\rho_d = 2.0 \text{ g/cm}^3$, $\phi = 25.9 \%$) and the claystone/bentonite (7/3) mixture ($\rho_d = 2.0 \text{ g/cm}^3$, $\phi = 25.7 \%$) can only be saturated to low degrees $S_w < 40 \%$ and $S_w < 100 \%$ respectively. The calculated “oversaturation” ($S_w > 100 \%$) for the bentonite is unrealistic. This is because the real density of the pore water in the compacted bentonite is higher than that of the pure water. For instance, a water density of 1.35 g/cm^3 was measured on compacted bentonite FEBEX at a dry density of 1.8 g/cm^3 /VIL 10/, and high values of up to 1.4 g/cm^3 are reported in /MIT 76/ for the density of adsorbed water on sodium montmorillonite.

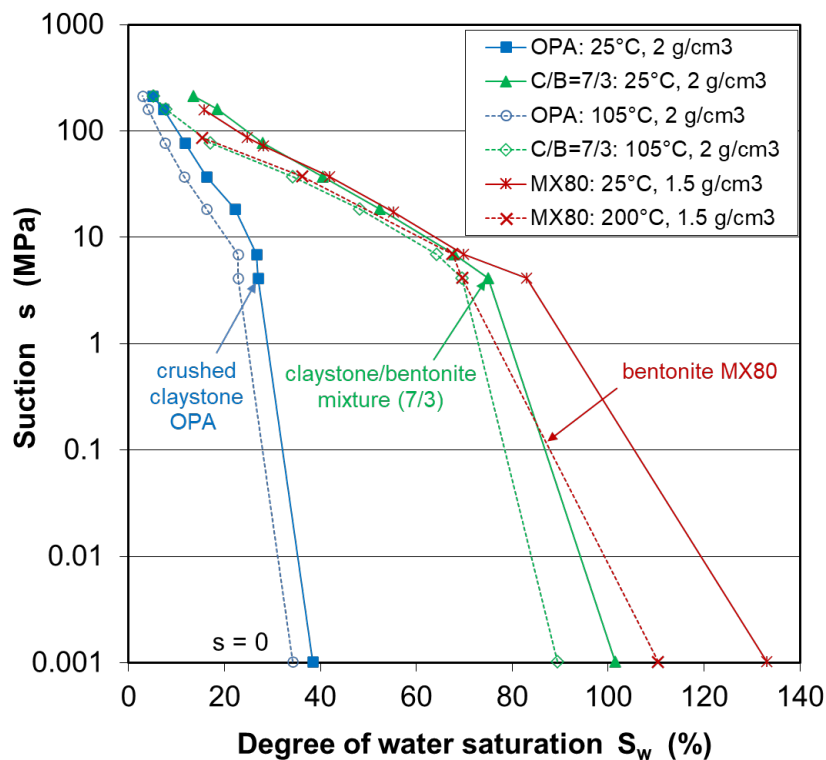


Fig. 2.9 Degree of water saturation as a function of suction for the crushed OPA claystone, claystone/bentonite (7/3) mixture and MX80 bentonite under confined conditions

The unrealistic “oversaturation” problem may be solved by redefining the degree of water saturation

$$S_w = \frac{w}{w_{max}} \quad (2.3)$$

The maximum water content reached at zero suction corresponds to the full saturation and the ratio of water content at any suction to the maximum is referred as the saturation degree.

Usually, the relationship of water saturation degree with suction is approached by the van Genuchten model /VAN 80/. Considering the definitions of the water saturation degree in equations (2.2) and (2.3), the model can be expressed by

$$S_w = \frac{V_w}{V_v} = \left[1 + \left(\frac{s}{P_o} \right)^{\frac{1}{1-\beta}} \right]^{-\beta} \quad (2.4a)$$

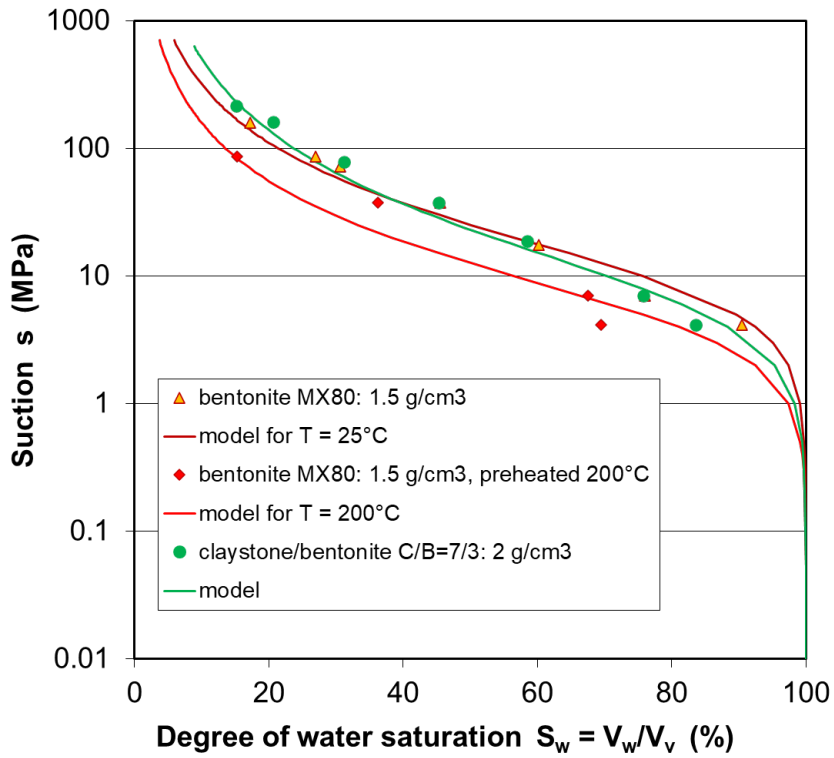
or

$$S_w = \frac{w}{w_{max}} = \left[1 + \left(\frac{s}{P_o} \right)^{\frac{1}{1-\beta}} \right]^{-\beta} \quad (2.4b)$$

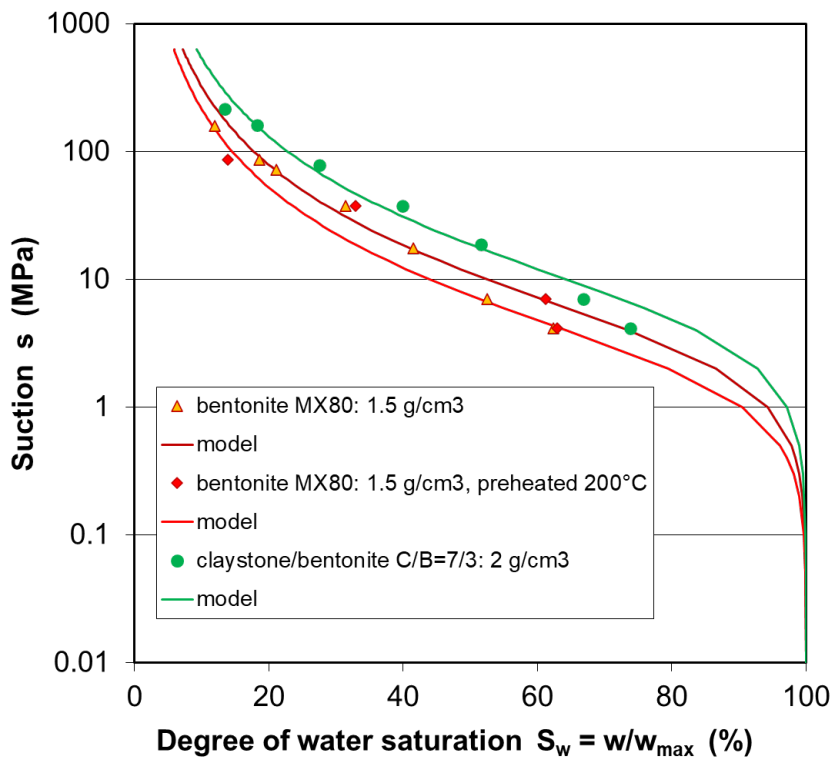
where P_o and β are the material parameters. Fitting the data yields the parameter values for the compacted bentonite samples with and without preheat treatment, and for the claystone/bentonite mixture, as given in table 2.10. Figures 2.10a-b show the curves of models (2.4a) and (2.4b) respectively. A reasonable agreement can be found between the models and data.

Tab. 2.10 The parameters of van Genuchten model for the compacted bentonite (MX80-a unheated; MX-b preheated at 200 °C) and claystone/bentonite (7/3) mixture (unheated)

Parameter	MX80-a	MX80-b	C/B=7/3
Dry density (g/cm ³)	1.5	1.5	2.0
Eq. (2.4a): P_o (MPa)	10	5	7
Eq. (2.4a): β (-)	0.4	0.4	0.35
Eq. (2.4b): P_o (MPa)	2	1.8	3
Eq. (2.4b): β (-)	0.3	0.3	0.3



a. data fitted by model (2.4a)



b. data fitted by model (2.4b)

Fig. 2.10 Modelling of the water retention curves for the compacted bentonite MX80 and claystone/bentonite (7/3) mixture

2.3 Compressibility

Drift seals are mostly designed to consist of precompacted blocks of clay-based material and bentonite pellets filling the remaining gaps between the blocks and the drift wall. The blocks must have sufficiently high densities to ensure the requirements on the sealing functions, which are usually achieved by compacting the loose material in mould. The compressibility of the material is essential for determination of the block density and the required compression energy.

2.3.1 Test methodology

Four mixtures were selected and compacted to blocks:

- crushed OPA claystone with the coarse grains $d < 32$ mm;
- crushed OPA claystone with the sieved grains $d < 10$ mm;
- claystone/bentonite (7/3) mixture with the coarse claystone aggregate ($d < 32$ mm) and the bentonite powder ($d < 2$ mm);
- claystone-bentonite (7/3) mixture with the sieved claystone ($d < 10$ mm) and the bentonite powder ($d < 2$ mm).

The grain size distributions of the samples are illustrated in figure 2.11, while the initial characteristics of the samples are given in table 2.11.

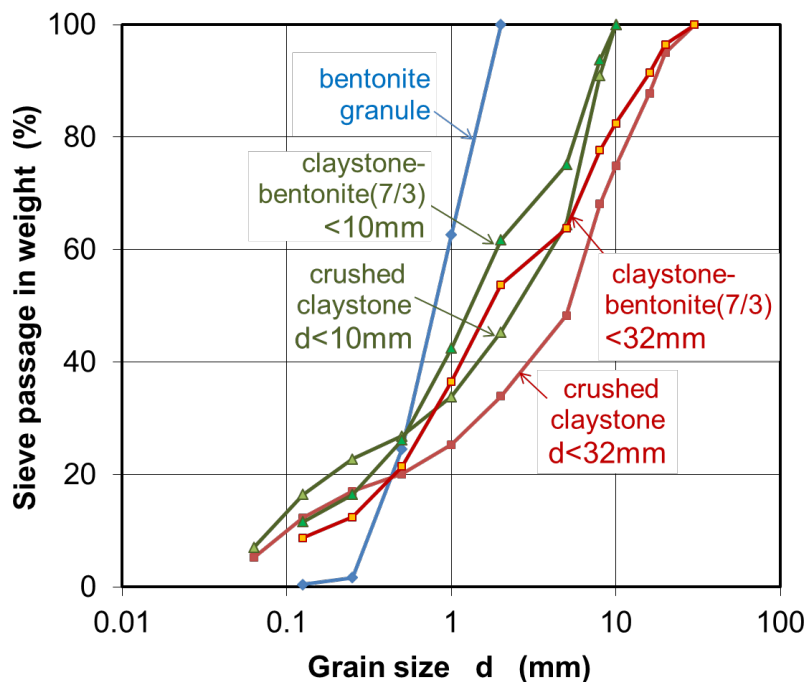


Fig. 2.11 Grain size distributions of the crushed OPA claystone and claystone/bentonite (7/3) mixture for precompacted blocks

Tab. 2.11 Initial characteristics of the crushed OPA claystone and claystone/bentonite mixtures installed in a large oedometer cell

Sample properties	Coarse claystone d < 32 mm	Sieved claystone d < 10 mm	Claystone-bentonite (7/3) d < 32 mm	Claystone-bentonite (7/3) d < 10 mm
Bulk weight M (kg)	13.95	13.84	13.90	13.25
Diameter D (mm)	280.0	280.0	280.0	280.0
Initial height H (mm)	124.0	119.0	131.0	125.0
Grain density ρ_s (g/cm ³)	2.70	2.70	2.69	2.69
Bulk density ρ_b (g/cm ³)	1.83	1.89	1.72	1.72
Dry density ρ_d (g/cm ³)	1.76	1.82	1.63	1.63
Porosity ϕ (%)	34.8	32.6	39.4	39.4
Water content w (%)	3.6	3.6	5.4	5.4
Saturation degree S_w (%)	18.2	20.1	22.3	22.3

Compaction tests were carried out by means of a large oedometer cell of 280 mm diameter and 265 mm height. Figure 2.12 shows the test layout and the cell. First of all, each material was mixed using shovel to an apparently homogenous distribution of the grains, then filled in the cell in 2 layers and stamped by hand. Figure 2.13 shows some pictures of the emplaced samples. The measured data (table 2.11) indicate that the crushed claystone with the relatively small grains $d < 10$ mm reached the maximum initial dry density of $\rho_d = 1.82$ g/cm³, followed by $\rho_d = 1.76$ g/cm³ for the coarse claystone aggregate $d < 32$ mm, and $\rho_d = 1.63$ g/cm³ for both the claystone-bentonite mixtures with the different grain sizes of $d < 32$ mm and 10 mm. The emplaced samples were then compressed by a load piston at a displacement rate of $7 \cdot 10^{-4}$ mm/s up to 21 MPa.

2.3.2 Test results

The compacted dry densities of the samples are depicted in figure 2.14 as function of applied axial load. One can find out that:

- The initial dry densities of the emplaced claystone samples are significantly higher than those of the claystone-bentonite mixtures, which is mainly determined by the grain size distribution. The coarse and sieved claystone grains ($d < 32$ mm, $d < 10$ mm) are favourable for achieving high emplacement densities.
- The density increases with loading. At axial load of 21 MPa, high dry densities were reached to $\rho_d = 2.2$ g/cm³ for both the crushed claystone samples and to $\rho_d = 2.0 - 2.1$ g/cm³ for both mixtures. The final parameters of the compacted samples are summarized in table 2.12.

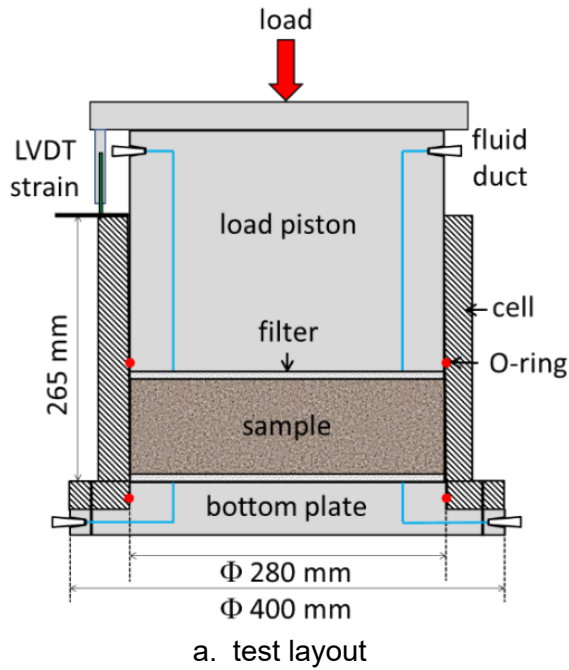


Fig. 2.12 A large oedometer setup for compaction of barrier materials



Fig. 2.13 Pictures of the samples installed in the big cell ($D = 280$ mm, $H = 265$ mm)

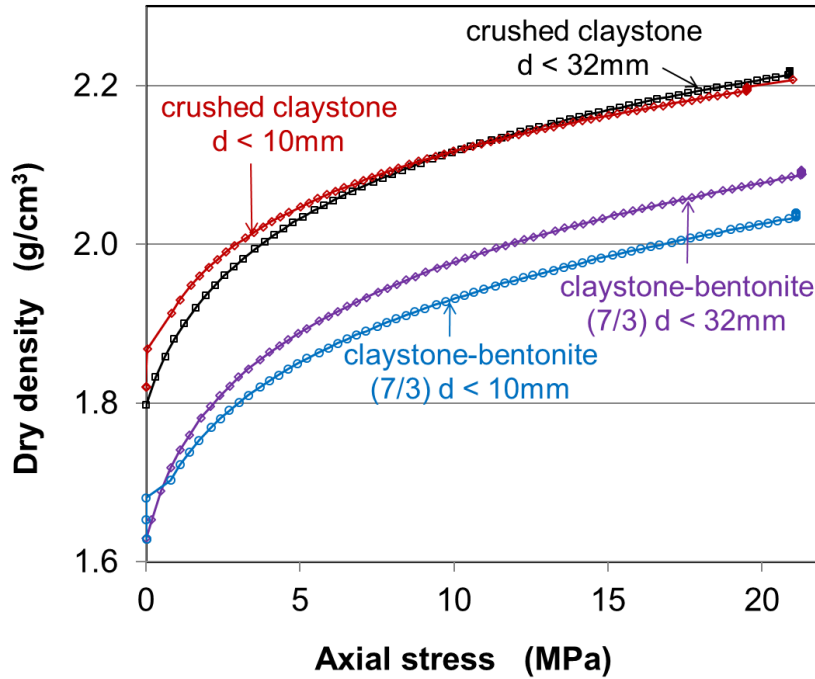


Fig. 2.14 Compacted dry densities of the crushed OPA claystone and claystone-bentonite (7/3) mixture

The repeatability of the results was examined by an additional test on the coarse claystone aggregate, as shown in figure 2.15. Two compaction curves are well consistent with each other.

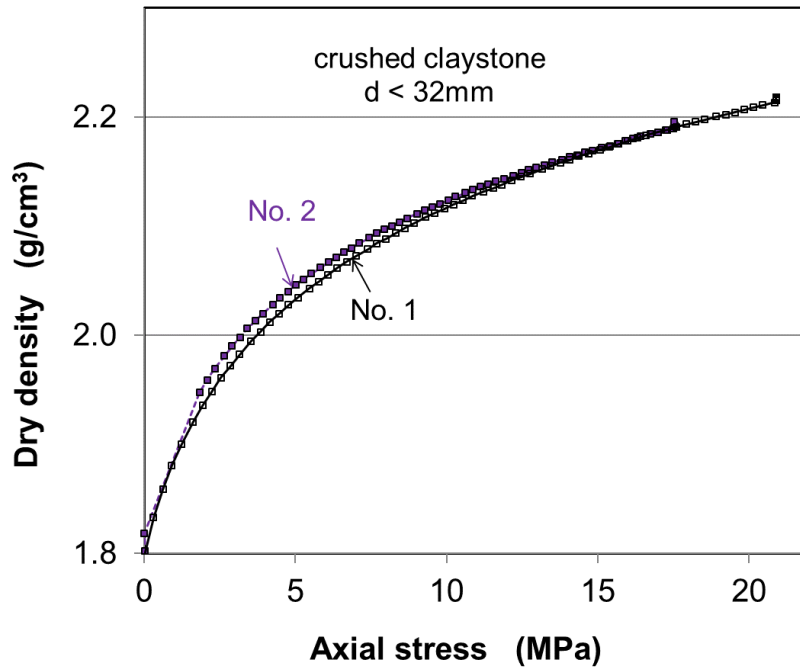


Fig. 2.15 Comparison of the compaction curves of two crushed claystone samples with coarse grains of d < 32 mm

Tab. 2.12 Characteristics of the samples compacted at axial load of 21 MPa

Sample properties	Claystone aggregate d<32mm	Claystone aggregate d<10mm	Claystone/bentonite (7/3) mixture d<32mm	Claystone/bentonite (7/3) mixture d<10mm
Final height H (mm)	98.4	98.1	102.0	99.8
Dry density ρ_d (g/cm ³)	2.21	2.20	2.09	2.02
Porosity ϕ (%)	17.8	18.2	22.4	24.5
Water content w (%)	3.6	3.6	5.4	5.4
Saturation degree S_w (%)	44.8	43.6	50.2	45.0

Figure 2.16 compares the compaction curves with those obtained previously on the crushed COX claystone and mixture with bentonite (C/B = 6/4), pure bentonite and bentonite/sand (7/3) mixture /ZHA 13/14/17a/. The samples in the previous tests were filled in the same oedometer cell but without hand stamping. Therefore, their emplaced densities and hence the compacted densities at a given load are lower than those of the stamped samples.

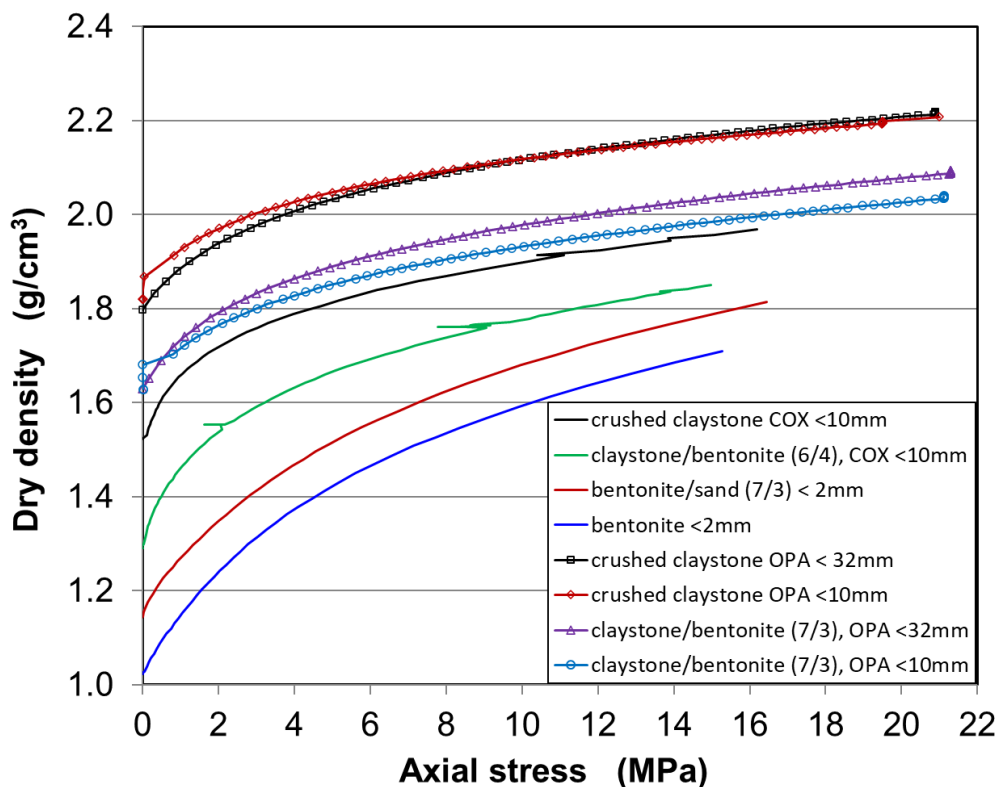


Fig. 2.16 Comparison of the compaction curves of the crushed OPA claystone and mixture with bentonite (pre-stamped by hand) and the crushed COX claystone and mixture with bentonite and pure bentonite as well as bentonite-sand mixture (without hand stamping)

Figure 2.17 show some pictures of the compacted samples. All of them are visually homogeneous in grain distribution, despite of the boundary area where some grains were splitted out by cutting through. The compacted claystone and claystone/bentonite blocks with a dry density of 2.0 g/cm^3 shall be used for bearing of POLLUS casks (figure 1.2) and for sealing of drifts (figure 1.3).

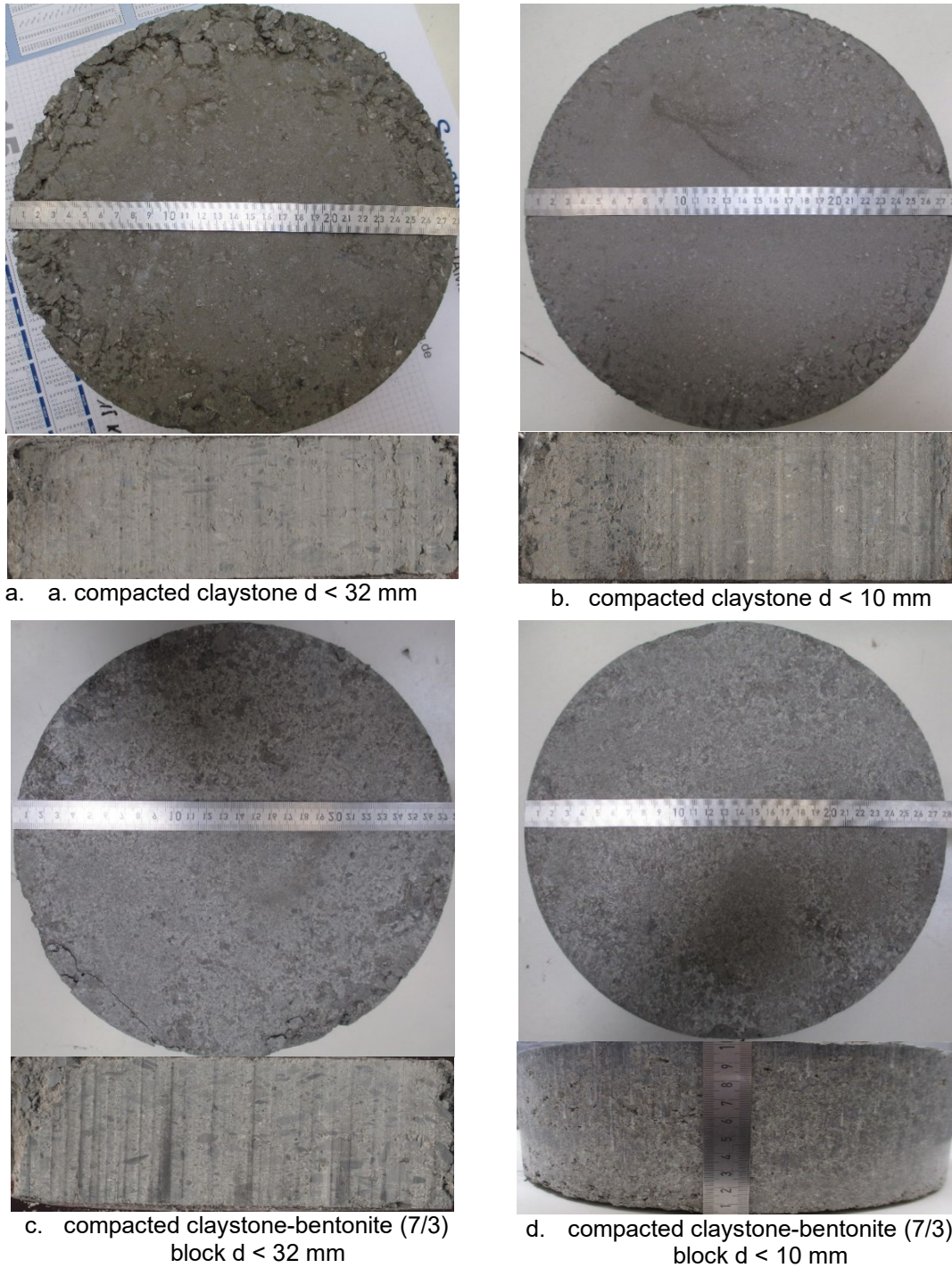


Fig. 2.17 Pictures of the compacted blocks of the crushed claystone and claystone/bentonite (7/3) mixture

2.4 Swelling capacity

Sufficient swelling capacity is required on the barrier materials to seal engineered gaps and voids, to resist propagation of the surrounding EDZ, and to establish a robust integration of the geological and engineered barrier system. The swelling capacity of a clay-based material depends mainly on its mineralogical composition, particularly expansive minerals such as montmorillonite, dry density, water content, and chemistry of contacting water. Swelling capacities of the crushed OPA claystone, MX80 bentonite, and claystone/bentonite mixtures with different ratios were determined by measurement of their swelling pressures at different dry densities.

2.4.1 Test methodology

Following mixtures were selected for testing:

- a. crushed OPA claystone with grains $d < 5$ mm;
- b. MX80 bentonite granules with grains $d < 5$ mm;
- c. claystone/bentonite mixtures C/B=8/2, 7/3, and 6/4 with the crushed claystone ($d < 5$ mm) and the bentonite powder ($d < 2$ mm).

The grain size distributions of the crushed claystone and bentonite are shown in figures 2.2 and 2.3.

The tests were carried out using a specific setup for sequential measurements of swelling pressure, water permeability, and gas penetration of clay-based materials, as shown in figure 2.18. It consists of 16 stainless steel cells arranged in parallel, a syringe pump, hydraulic lines, and measuring instruments. This setup allows parallel testing on different samples under identical conditions, so that one can obtain a great amount of data from each sample and hence save up the total time expenditure. Its another advantage is that one can precisely compare properties of different samples under the same conditions.

Test samples were prepared by compaction of the materials in the cells to a size of 50 mm diameter and 15 mm height and to different dry densities of 1.3 – 2.0 g/cm³ for the bentonite, 1.65 – 2.0 g/cm³ for the crushed claystone and claystone/bentonite mixtures. The selected densities cover the ranges achievable by using the available backfilling/sealing techniques: a) emplacement of loose material with compaction on site and b) construction of precompacted blocks with filling the remaining gaps. The compacted samples were dried at 105 °C for 1 day, which led to a slight contraction and separation

of the samples from the cell wall. This could avoid possible effect of friction between sample and cell wall on the measurement of swelling pressure. The samples were covered by sintered porous discs at the end faces. The setup was placed in an air-conditioned room at a temperature of 22 ± 1 °C. The tests started with hydration by infiltration of the synthetic OPA pore water from the scaled burette into the bottom of each sample, during which swelling pressure built up in the sample. The swelling pressure was measured by a load cell installed between the top cap and the upper piston contacting the sample. Following that, water permeability and gas penetration through the water-saturated samples were measured.

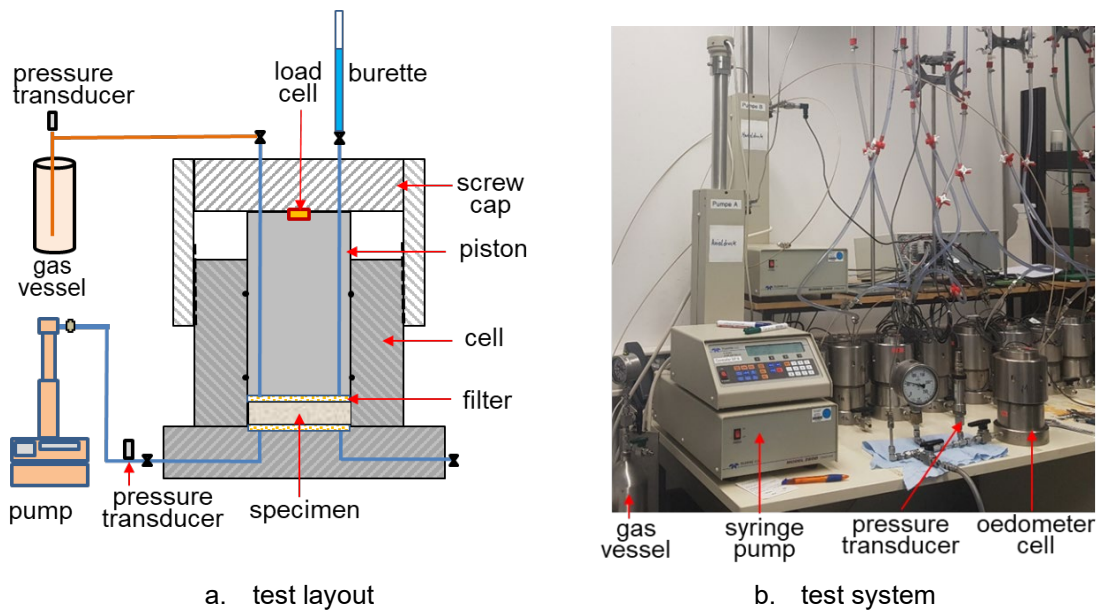


Fig. 2.18 A test setup with parallel arranged oedometer cells for measurements of swelling pressure, water permeability, and gas penetration of clay samples

2.4.2 Test results

Figures 2.19a-e show buildup of swelling pressure observed on each compacted sample of the crushed claystone (a), claystone/bentonite mixtures $C/B = 8/2$, $7/3$ and $1/6/4$ (b-d), and bentonite (e). All samples exhibited a rapid increase in the swelling pressure to a temporary peak at most of the samples, particularly the pure bentonite. Following that, the swelling pressure decreased slowly and then increased gradually again to a maximum until full saturation. The double-peak shape of the swelling pressure evolution is very typical for compacted bentonite and attributed to variations of micro- and macrostructures in compacted bentonite during saturation process /PUS 90/, /IMB 06/, /ZHU 13/, /ZHA 22/. In contrast, the double-peak evolution did not appear on the highly compacted

claystone/bentonite mixtures at the high dry density of 2.0 g/cm³ due to their stable internal structures established by the stiff claystone grains. The final swelling pressures P_s of all samples are summarised in table 2.13 and illustrated figure 2.19f as a function of dry density ρ_d . It is obvious that the swelling pressure increases with increasing dry density and bentonite content. A required swelling pressure at an engineered barrier can be achieved by choosing a suitable claystone/bentonite mixture on the one hand and a suitable emplacement technique for the predefined material density on the other hand.

Tab. 2.13 Summary of welling pressure, water and gas permeabilities measured on the compacted claystone/bentonite mixtures at different dry densities

Samples	Claystone/ bentonite ratio	Dry density (g/cm ³)	Swelling pressure (MPa)	Water permeabil- ity (m ²)	Gas permeability (m ²)
OPA-a	1/0	1.7	0	6.7E-15	1.2E-15
OPA-b	1/0	1.8	0.2	2.1E-15	4.5E-16
OPA-c	1/0	2	1.1	1.6E-16	8.6E-18
CB8/2-a	8/2	1.65	0.2	3.9E-15	1.9E-16
CB8/2-b	8/2	1.8	0.4	4.0E-16	5.3E-17
CB8/2-c	8/2	2	2.2	1.6E-17	5.3E-19
CB7/3-a	7/3	1.65	0.2	1.1E-16	9.1E-17
CB7/3-b	7/3	1.8	0.7	2.5E-17	7.5E-18
CB7/3-c	7/3	2	2.6	3.2E-18	3.4E-19
CB6/4-a	6/4	1.65	0.6	9.2E-17	1.5E-17
CB6/4-b	6/4	1.8	1.5	7.1E-18	6.4E-19
CB6/4-c	6/4	2	3.8	9.3E-19	1.4E-19
MX80-a	0/1	1.3	0.8	8.0E-20	
MX80-b	0/1	1.4	1.1	6.0E-20	
MX80-c	0/1	1.5	1.5	3.0E-20	
MX80-d	0/1	1.5	1.6	3.9E-20	
MX80-e	0/1	1.5	2.2	2.1E-20	
MX80-f	0/1	1.6	3.5	1.5E-20	
MX80-g	0/1	1.6	4.0	2.4E-20	
MX80-h	0/1	1.6	4.3	1.2E-20	
MX80-i	0/1	1.8	13.3	7.3E-21	
MX80-j	0/1	1.8	11.4	1.1E-20	
MX80-k	0/1	1.8	11.5	5.6E-21	
MX80-l	0/1	1.8	12.6	7.6E-21	
MX80-m	0/1	2	22.1	3.6E-21	
MX80-n	0/1	2	22.0	1.7E-21	
MX80-o	0/1	2	22.8	9.8E-22	

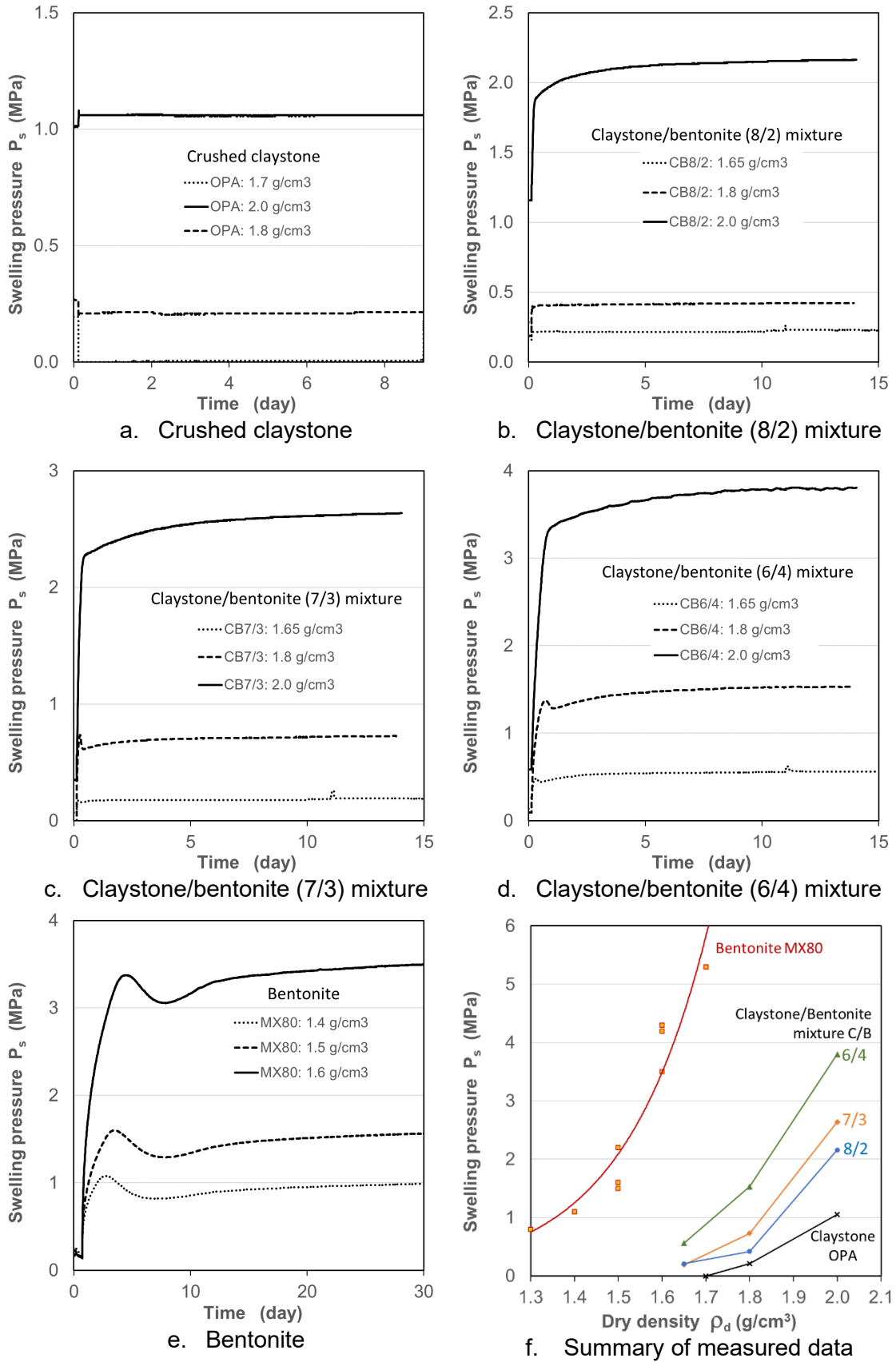


Fig. 2.19 Swelling pressures measured on the compacted claystone/bentonite mixtures

2.5 Water permeability

The main function of the engineering barriers is to prevent fluid access into the repository and the release of radionuclides from it. Therefore, sufficiently low hydraulic conductivities or water permeabilities are required on the barrier materials. This most important parameter was determined for the selected materials as mentioned earlier in section 2.4.

2.5.1 Test methodology

The same test setup illustrated in figure 2.18 was applied for the hydraulic tests. Following the swelling pressure measurement, water permeabilities of the compacted samples were measured by injecting the synthetic OPA pore water at increased pressures of 0.08 to 0.8 MPa. Water outflow was recorded using the scaled burette at atmospheric pressure. During steady-state flow, water permeability was determined by Darcy's law:

$$K_w = \frac{Q_w \mu_w H}{A(P_i - P_o)} \quad (2.5)$$

where K_w is the water permeability (m^2); Q_w is the water flow rate (m^3/s); μ_w is the dynamic viscosity of the synthetic water (9.5×10^{-4} Pa s, figure 2.4b); H is the sample length (m); A is the cross-sectional area of the sample (m^2); and P_i and P_o are the inlet and outlet pressures (Pa), respectively.

2.5.2 Test results

Figure 2.20 depicts water permeabilities measured on the compacted claystone aggregate, claystone/bentonite mixtures C/B = 8/2, 7/3, 1/6/4, and bentonite. The data are summarized in table 2.13. The results indicate that the water permeability of the mixture is dominated by the bentonite content and dry density. The water permeabilities of the bentonite are very low in a range of 10^{-19} to 10^{-21} m^2 for the dry densities of 1.3 to 2.0 g/cm^3 . These values are 3 - 6 orders of magnitude lower than that of the mixture, depending on the bentonite content and density. In the mixture, swelling of bentonite particles can seal macro-pores between claystone particles and thus reduce the effective porosity for water flow through. From the test results, suitable mixtures with a specific density and water permeability can be identified regarding the requirements for the individual elements of the technical barrier system in a repository.

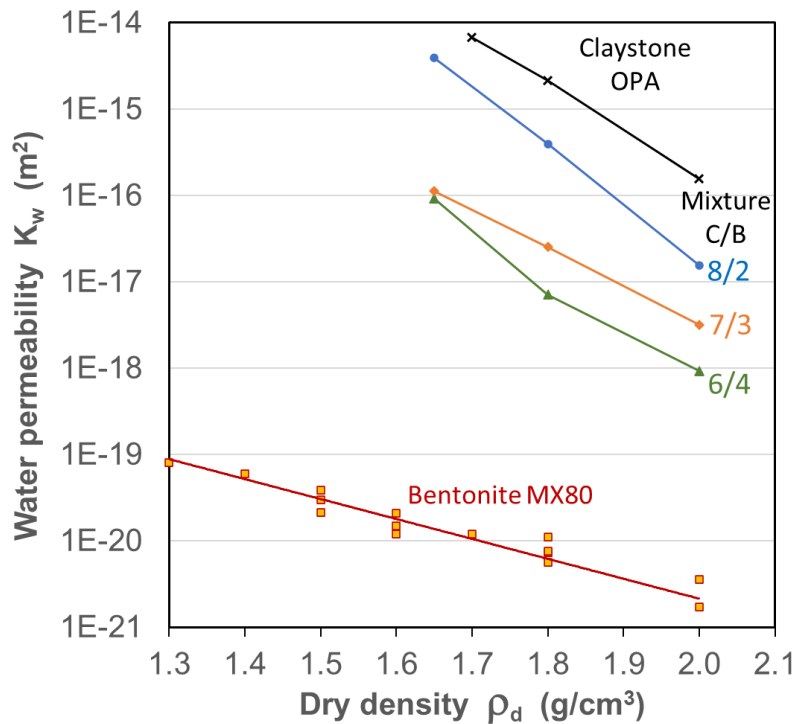


Fig. 2.20 Water permeability of the claystone/bentonite mixtures as a function of dry density

2.6 Gas permeability

When moisture contacts the metallic canisters and components of the construction in a repository, anaerobic corrosion will occur and produce gases. In early stage before full water saturation of the barrier materials the gases can easily escape without build-up of high gas pressure. When the barrier materials are fully saturated, the gas flow may be hindered and accumulated, leading to gas overpressures accessing certain thresholds and impairing the integrity of the geological-engineered barrier system /HOR 96/, /ROD 99/, /SEL 14/, /LEV 20/. Thus, the knowledge of gas migration in the water-saturated barriers is necessary for safety assessment of the repository. In clay-based materials, the gas migration is usually characterized with gas entry/breakthrough pressure and effective permeability. These two gas flow parameters were determined for the selected materials as mentioned earlier in sections 2.4 and 2.5.

2.6.1 Test methodology

The same test setup illustrated in figure 2.18 was applied for the gas flow tests. After the measurement of water permeability as mentioned above, gas flow testing was carried out on the water-saturated and compacted claystone, bentonite, and claystone/bentonite mixtures C/B=8/2, 7/3 and 6/4. Before gas injection, it was tried to remove the water in the inlet and outlet reservoirs. A syringe pump (Model 260D) was applied for gas injection, which allows a maximum volume of 260 mL, a maximum pressure of 500 bar and flow rates in a range of 1 μ L/min to 100 mL/min. Helium gas was then injected into the inlet under increased pressures of 0.1 - 0.2 MPa for the compacted claystone/bentonite samples, while the gas injection to bentonite samples was conducted at low flow rates of 0.02 and 0.08 ml/min. Gas outflow from the claystone/bentonite samples was recorded by the burette at atmospheric pressure, while the outflow from the bentonite samples was accumulated in a steel vessel with a volume of 562 ml. Gas pressures in the inlet and outlet were monitored.

The gas injection lasted for sufficient time periods to examine long-term gas flow process and to determine gas breakthrough pressure and permeability. As soon as gas bubbles in the burette or gas pressure in the outlet vessel were detected, the gas pressure recorded in the inlet is defined as the breakthrough pressure P_b . For the bentonite samples, the gas outflow rate can be estimated from the pressure difference with elapsed time /GUT 21/

$$Q_g = V_g \frac{P_g(t_j) - P_g(t_i)}{P_m} \frac{1}{\Delta t} \quad (2.6)$$

where Q_g is the mean gas flux (m^3/s), V_g is the volume of the outlet reservoir (m^3), $P_g(t_j)$ and $P_g(t_i)$ are the in- or outlet gas pressures (Pa) at time point j and i, P_m is the average gas pressure between the measurement interval $\Delta t = t_j - t_i$ (s). Effective gas permeability K_g (m^2) is then estimated by Darcy's law:

$$K_g = \frac{2 Q_g \mu_g P_o L}{A (P_g^2 - P_o^2)} \quad (2.7)$$

where μ_g is the dynamic viscosity of helium gas (1.96×10^{-5} Pa·s).

2.6.2 Test results

2.6.2.1 Claystone/bentonite mixtures

Figure 2.21 shows gas permeabilities of the water-saturated and compacted claystone and claystone/bentonite mixtures C/B=8/2, 7/3 and 6/4. K_g -values were obtained under gas injection pressures of 0.1 - 0.2 MPa, which are lower than the respective swelling pressures (cf. figure 2.19f). That means that gas can flow through the materials under the low pressures without impairing the integrity of the engineered barrier system. It can also be seen that the gas permeability decreases with increasing bentonite content and dry density.

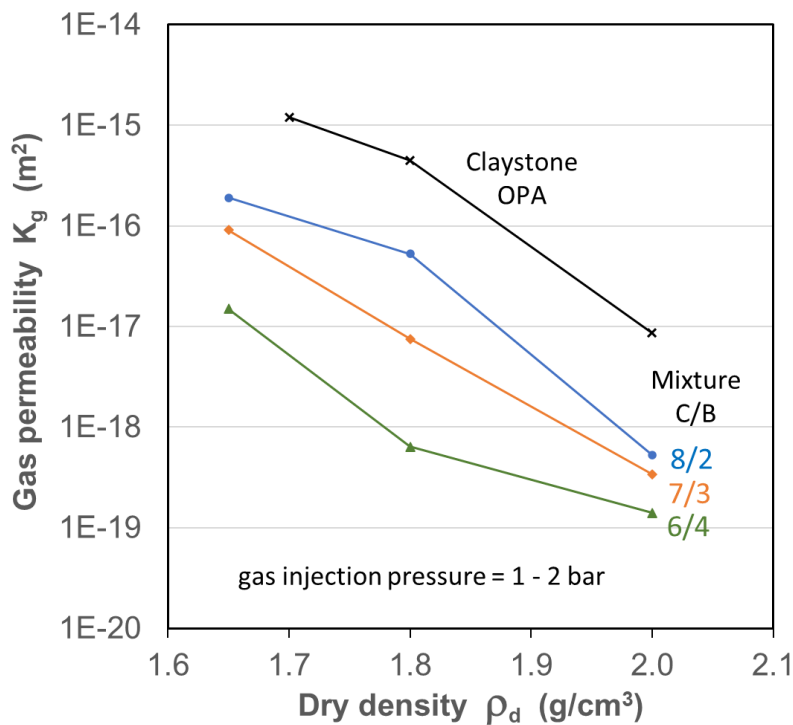


Fig. 2.21 Effective gas permeability of the water-saturated claystone/bentonite mixtures as a function of dry density

2.6.2.2 Bentonite

Four bentonite samples MX80-b/c/d/e were selected for gas penetration testing. Before testing, samples MX80-c/d were saturated by hydration over 0.5 - 1 month with swelling pressure measurement, while samples MX80-b/e were saturated over a longer period of 1 - 2 months with both swelling pressure and water permeability measurements. The dry density, swelling pressure and water permeability obtained on the samples are given in

table 2.13. Figure 2.22 illustrates results of the gas tests in terms of applied gas flow rate (Q_g), induced up- and downstream pressures (P_g, P_o), axial total stress (σ_a), and outflow rate (Q_o) versus elapsed time. At samples MX80-b/c/d, the gas was injected at a low flow rate of 0.02 ml/min, while the injection to MX80-e was carried out at flow rates of 0.02 and 0.08 ml/min. All samples showed a similar evolution of gas pressure, gas outflow, and stress response.

The gas injection led to a gradual build-up of the upstream pressure (P_g). As a peak pressure P_b was reached, gas breakthrough occurred, which caused a release of gas and thus a drop in the upstream pressure and an increase in the backpressure (except MX80-c at $P_o = 0$ applied). When the upstream pressure dropped to a certain value P_c , the swelling of the bentonite locally clogged the path network, which impeded the flow of gas and increased the injection pressure again. Following the first gas breakthrough/sealing event, further gas injection caused more cyclic rising/dropping episodes of the upstream pressure, reflecting local opening/closing cycles of the network. Correspondingly, the resulting gas flow was unstable. The fluctuations in gas injection pressure and flow rate reduced over time. If the gas injection were to continue for a sufficiently long period of time, the pathway tends to stable and thus a steady flow of gas can be expected.

In the closed downstream, the backpressure (P_o) increased with the accumulation of the flowing gas and at the same time the average pore pressure ($P_m = (P_g + P_o)/2$) increased. The elevated pore pressures kept the gas pathway open. However, due to the corresponding reduction in pressure gradient or difference ($\Delta P_g = P_g - P_o$), the gas flow through the pathway slowed down. In order to examine the influence of the backpressure on the gas flow, it was lowered down to zero at samples MX80-b/d/e. Almost no injection pressure response was observed. This means that the pathway was not noticeably affected by the backpressure.

The gas injection initially caused a gradual increase in stress (σ_a) over the initial swelling pressure, indicating that the samples were gas-tight and subjected to compression against the rigid confinement by the gas pressure. Before the first gas breakthrough, a peak stress was already reached and then dropped slightly. However, what caused this is unclear. Continued gas injection increased the stress further up to the next peak σ_b at the gas breakthrough event. All samples showed that the gas breakthrough pressure is slightly higher than the stress, $P_b > \sigma_b$. Their values are summarized in table 2.14. This

observation confirms that gas penetration into water-saturated bentonite under constrained volume conditions requires high overpressures that exceed the total stress and tensile strength of the material to create local microcracks for gas passage /PUS 87/, /HOR 96/, /ROD 99/, /SEL 14/, /GRA 16/, /HAR 17/, /LEV 20/, /ZHA 22/. After gas breakthrough, the gas injection pressure decreased below the stress. and had no further influence on the stress. The further variation of the stress was exclusively determined by the gas backpressure acting on the load piston and the load cell (figure 2.18a). According to /ZHA 22/, the gas breakthrough pressure can be expressed as

$$P_b = \sigma_{min} + \sigma_T \quad (2.8a)$$

where σ_{min} is the minor principal stress and σ_T is the tensile strength of the material. In case of the oedometer test condition (figure 2.18), the stress in the sample is quasi-hydrostatic, $\sigma_{min} = \sigma_r \approx \sigma_a \approx \sigma$, and thus equation (2.8a) can be rewritten by

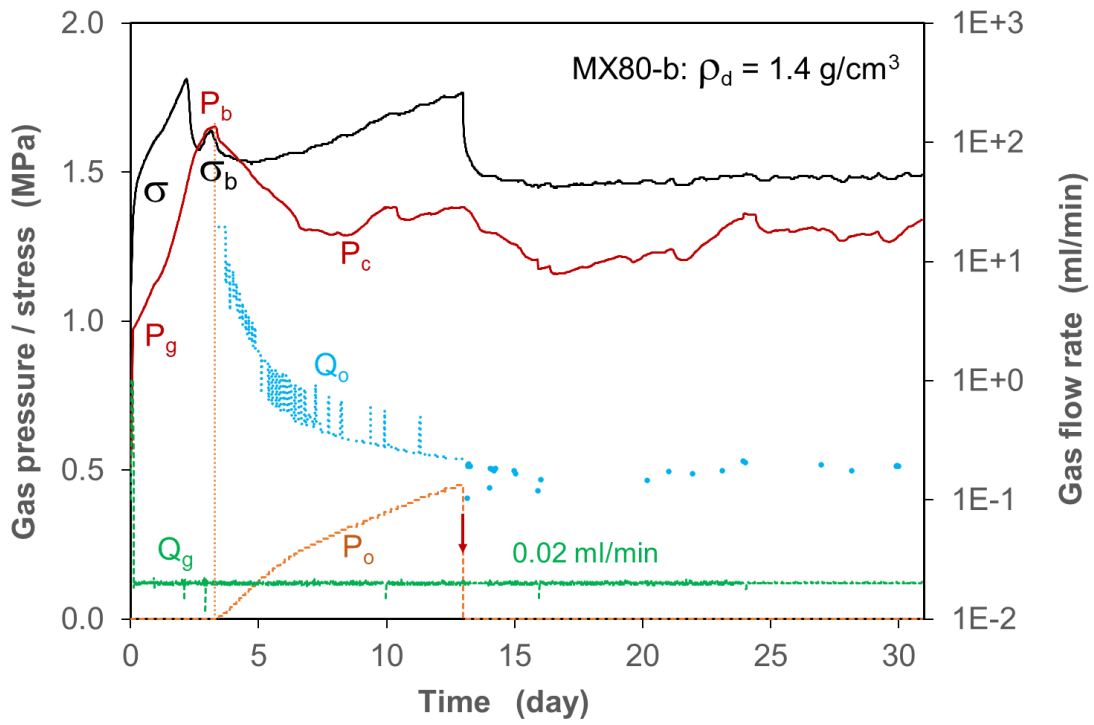
$$P_b = \sigma_b + \sigma_T \quad (2.8b)$$

$$P_b = (1 + b) \times \sigma_b \quad (2.8c)$$

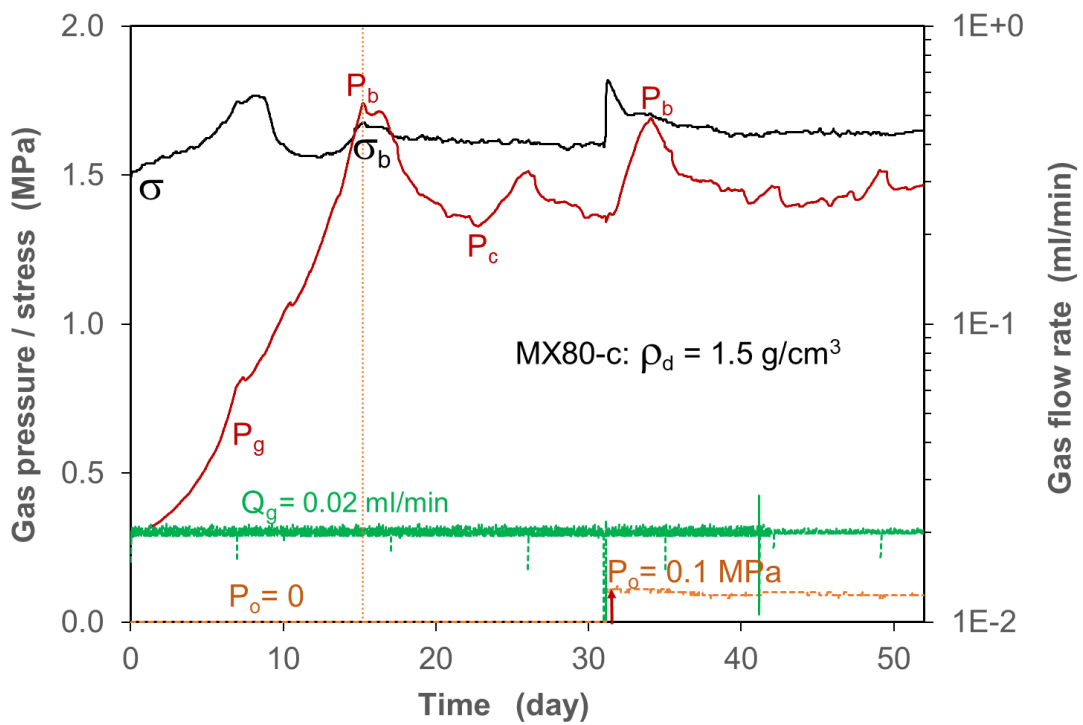
where the tensile strength is assumed to be linearly related with the stress, $\sigma_T = b \times \sigma_b$. The parameter $b = 0.09$ was determined from the previous tests on different bentonites /ZHA 22/. Figure 2.23 shows that the present data from the samples MX80-b/c/d/e are consistent with the model.

Tab. 2.14 Results of the gas penetration tests on the water-saturated bentonite MX80 samples under volume-constrained conditions

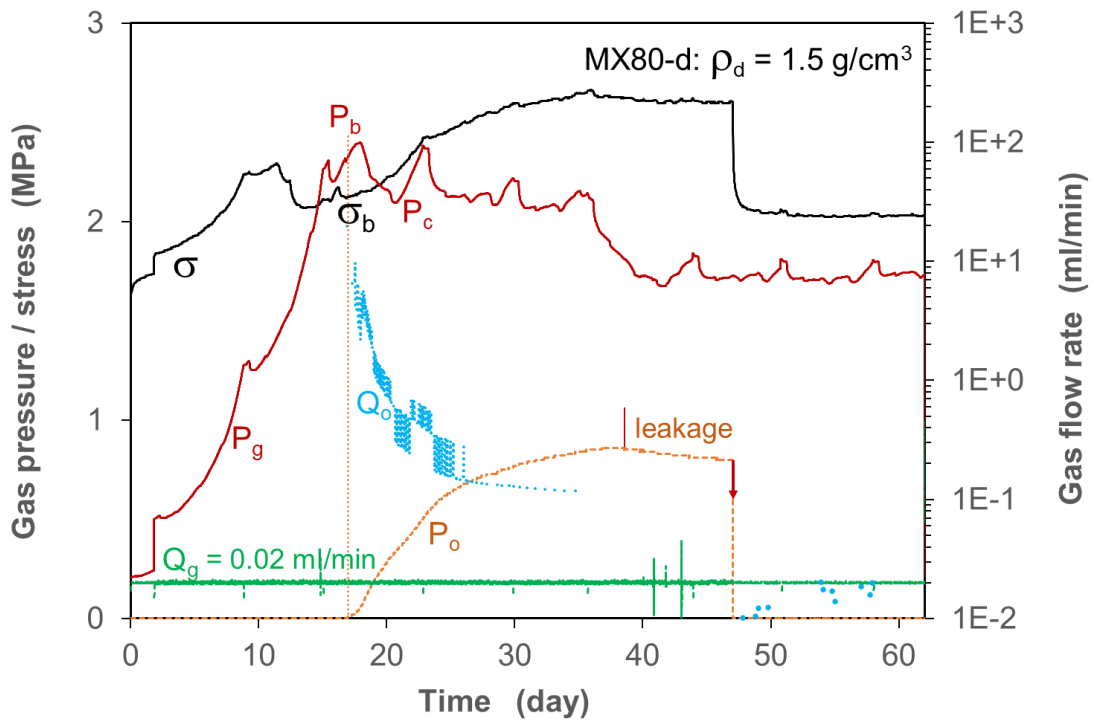
Samples	Dry density ρ_d (g/cm ³)	Swelling pressure P_s (MPa)	Gas breakthrough pressure P_b (MPa)	Stress at gas breakthrough σ_b (MPa)	Gas permeability K_g (m ²)
MX80-b	1.4	1.1	1.6	1.6	5.2E-19
MX80-c	1.5	1.5	1.7	1.7	-
MX80-d	1.5	1.6	2.3	2.1	2.5E-20
MX80-e	1.5	2.2	3.4	3.2	-



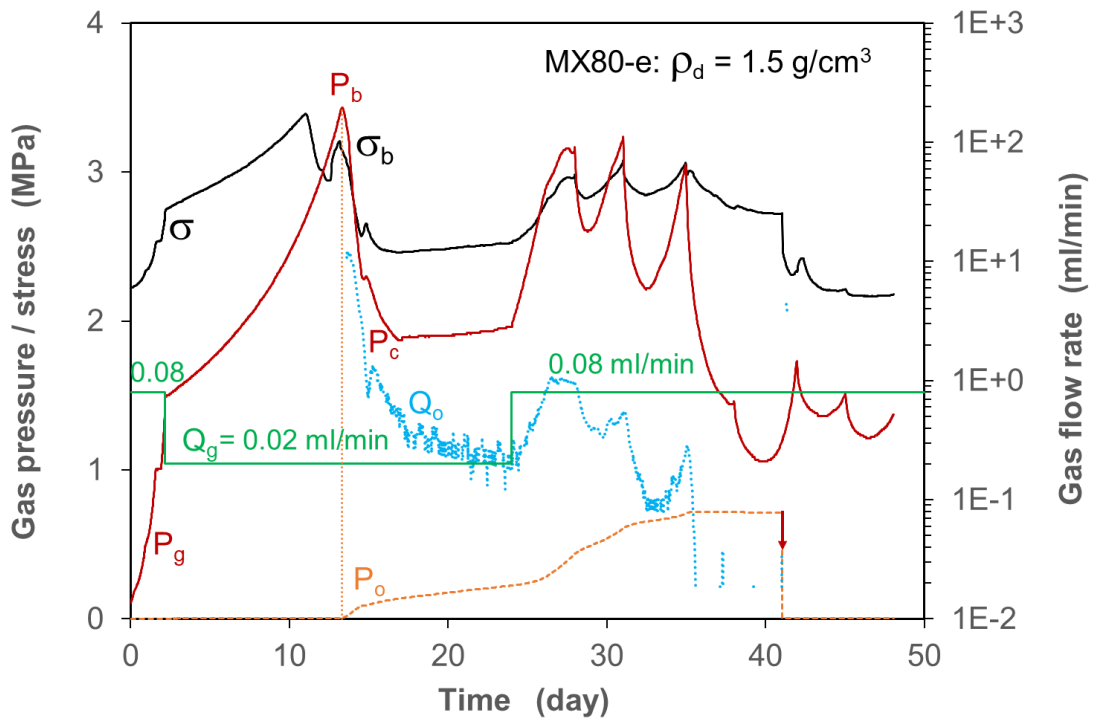
a. MX80-b with a dry density of 1.4 g/cm^3



b. MX80-c with a dry density of 1.5 g/cm^3



c. MX80-d with a dry density of 1.5 g/cm^3



d. MX80-e with a dry density of 1.5 g/cm^3

Fig. 2.22 Developments of gas pressure and confining stress with the gas injection to the water-saturated bentonite under volume-constrained conditions

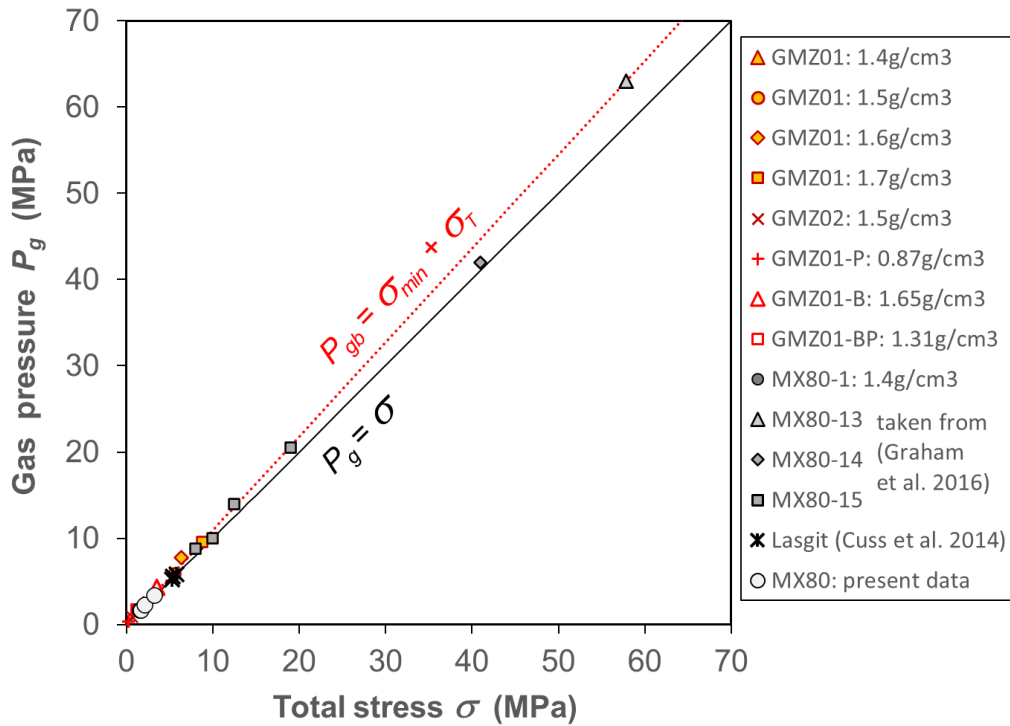


Fig. 2.23 Gas breakthrough pressure in relation to the total stress

The gas breakthrough pressure of water-saturated bentonite is determined by many factors, particularly by its mineralogical composition, dry density, homogeneity, and swelling pressure. Figure 2.24 summarises the present data of MX80 together with those from other kinds of bentonites MX80 /PUS 87/, FEBEX /GUT 21/, GMZ01 and GMZ02 /XU 17/, /ZHA 22/. It shows that the gas breakthrough pressure of each bentonite increases exponentially with increasing dry density. The differences of the breakthrough pressures between the different bentonites are attributed to the different fractions of montmorillonite, which dominate the proportions of bound and free pore water, effective pore space and connectivity for gas flow. The present data of MX80 also show an increase of the gas breakthrough pressure with the swelling pressure, as shown in figure 2.25. The relationship is quite similar like that obtained on FEBEX bentonite /GUT 21/. The gas breakthrough pressure is about twice the swelling pressure.

The gas permeability (K_g) was measured on two samples MX80-b/d at the lowered back-pressure to atmospheric pressure. Figure 2.26 shows evolution of the gas permeability measured on MX80-d with a dry density of 1.5 g/cm³. K_g -values increased slightly with time and then maintained relatively constant at 2.5×10^{-20} m². Sample MX80-b with a dry density of 1.4 g/cm³ showed a higher K_g -value of 5.2×10^{-19} m².

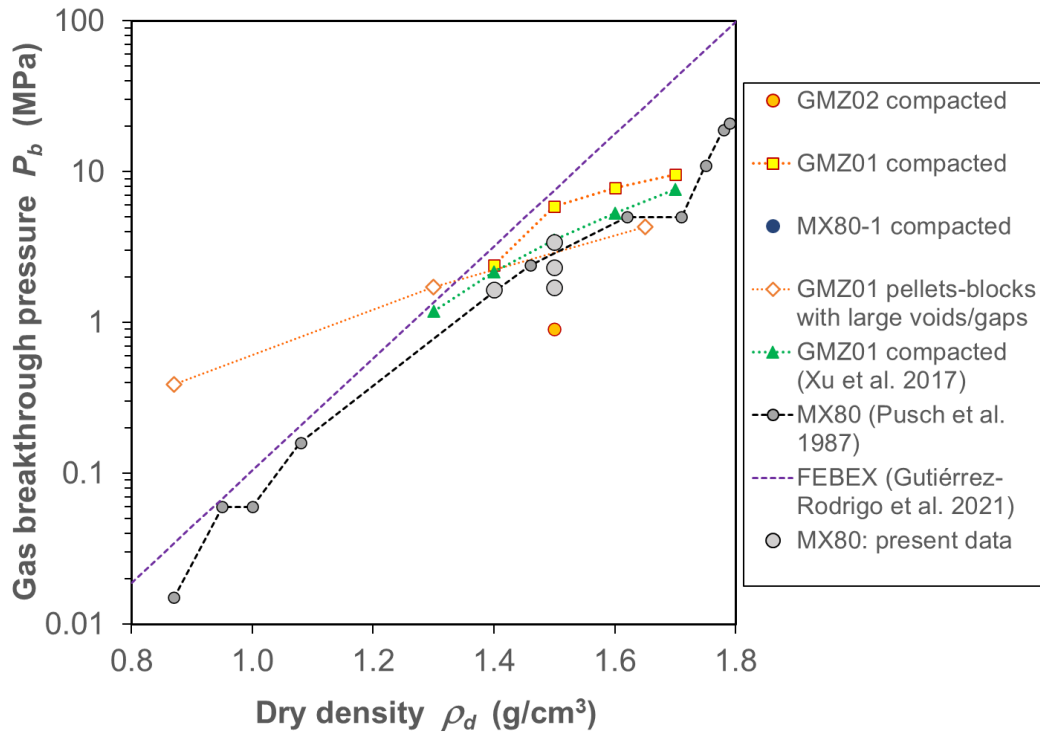


Fig. 2.24 Gas breakthrough pressures of the different bentonites as a function of dry density

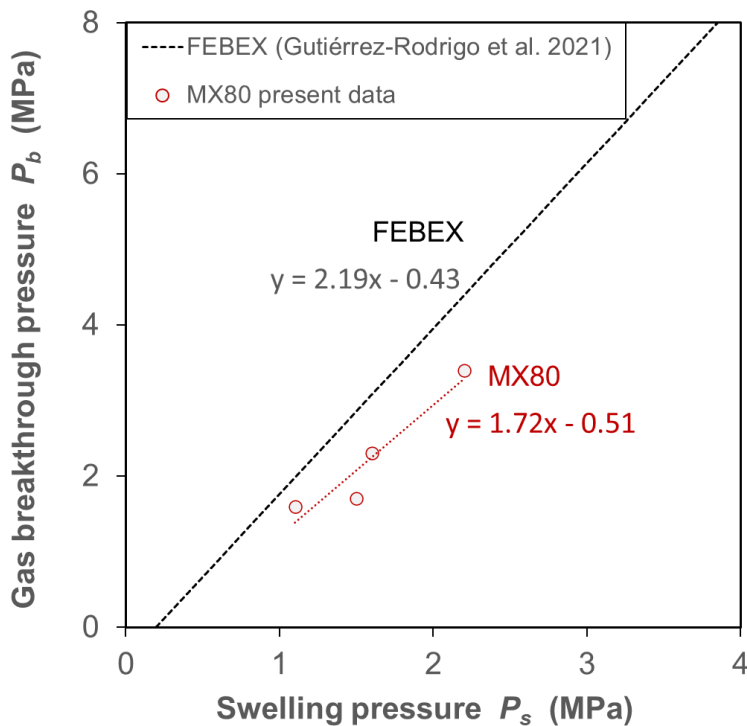


Fig. 2.25 Gas breakthrough pressure in relation to swelling pressure

In order to examine self-sealing of gas pathways in bentonite, water permeability was measured by injecting the synthetic OPA water into sample MX80-d after the gas penetration testing. The measured data are depicted in figure 2.26. An average value can be estimated to $K_w = 1.7 \times 10^{-20} \text{ m}^2$, which is consistent with the data obtained on the fully saturated samples in table 2.13 and figure 2.20. This implies that the gas pathway in the bentonite can reseal completely due to the swelling effect.

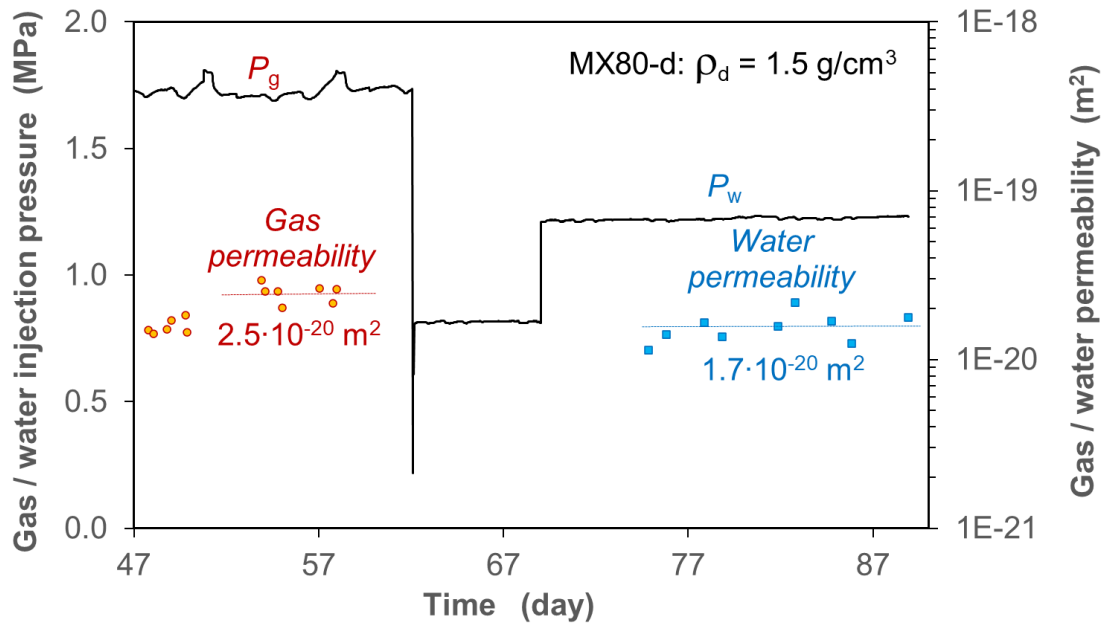


Fig. 2.26 Gas and water permeability obtained on a bentonite sample MX80-d with a dry density of 1.5 g/cm^3

3 Barrier performance of selected claystone/bentonite mixtures

3.1 Repository relevant conditions considered

Barrier performance of the crushed claystone, pure bentonite and claystone/bentonite mixtures was examined considering repository-relevant conditions, which will vary over hundreds and thousands of years. In most of the repository concepts, clay-based materials will be used for backfilling and sealing the remaining openings after deposition of radioactive waste.

When the openings are backfilled and sealed, the clay-based barrier materials will firstly be saturated by uptaking water from the humid surrounding environment. Hydration will cause the clay to swell towards the gaps left in the system and then development of swelling pressure against the concrete lining installed to support the rock. The lining will be altered with time under chemical and mechanical effects. When the lining fails, the engineering barriers will be subject to compression from the rheological deformation of the surrounding rock. This increases the density, stiffness, and backpressure of the barrier materials. Additionally, the pore water pressure will build up in the engineered barrier system due to water intrusion on the hand and rock compression on the other hand. Under the rock compression, the porosity and hydraulic conductivity of the barrier materials will decrease, which enhances the functions of the engineered barrier system. The hydro-mechanical interactions between the engineering barriers and the surrounding lining-rock will progress until an equilibrium is reached. When moisture contacts the metallic canisters and other metallic components, anaerobic corrosion will occur and produce gases. In early stage before full water saturation of the barrier materials, the gases can easily release without buildup of high gas pressure. When the materials are highly saturated, the gas flow will be hindered and accumulated, which could lead to high pressures accessing certain thresholds and impairing the integrity of the geological-engineered barrier system. The buffer around HLW will be additionally subjected to thermal loading from decayed heat emission of the waste. The most concern is whether and how the barrier properties of the buffer will be altered during the thermal period over several thousands of years. Within the project, the crushed OPA claystone, MX80 bentonite, and a claystone/bentonite (7/3) mixture were selected and tested for examination of their barrier performance under the repository relevant conditions.

3.2 Test methodology

3.2.1 Equipment and samples

Two test equipments were used for long-term testing of the crushed claystone, bentonite and claystone/bentonite mixtures as barrier material under dynamic THM conditions expected in the repository.

As backfill material, the excavated claystone with coarse grains $d < 32$ mm was taken and tested in a large stainless steel oedometer cell of a diameter of $D = 280$ mm and a height of $H = 265$ mm. Figure 3.1 shows the oedometer setup. The OPA aggregate of 23 kg was filled in 2 layers of 100 mm each in the cell and stamped by hand to a height of 200 mm. An initial bulk density of 1.88 g/cm^3 was achieved, corresponding to a dry density of 1.81 g/cm^3 for the water content of 3.6 %. Two metallic filter platen of 5 mm thickness were placed respectively at the top and bottom of the sample for fluid flow. Filter paper was also inserted between the sample and the filter platen to avoid possible elution of fine particles with water flow. The upper load piston and the lower basic plate were manufactured with two thin holes for fluid flow. A syringe pump (Model 260D) was used for water or gas injection to the bottom of the sample, while outflow was collected by a bottle for water or a burrito for gas. Axial deformation was measured using two linear variable differential transducers (LVDTs) deformation transducers installed between the upper load plate and the top of the cell. Axial load was applied by means of a servo-controlled load apparatus allowing a maximum stress of 75 MPa. The test was carried out at ambient temperature of ~ 22 °C.

For testing seal materials, two coupled rigs were used, each of which allows two samples in stainless steel cells of 120 mm diameter and 160 mm height one upon another, as illustrated in figure 3.2. They are installed in separated thermal chambers allowing high temperatures up to 200 °C. Each sample is covered with sintered porous plates and connected to thin holes through the upper load piston and the lower basic plate for fluid flow. A syringe pump (Model 260D) is used for fluid injection at the bottom, while fluid outflow is measured at the top by means of scaled burette at atmospheric pressure. Axial load is applied by means of another syringe pump. Axial deformation is monitored using two LVDTs mounted between the upper load piston and the cell top. Identical THM conditions can be simultaneously applied to four samples in the individual cells. The parallel testing under the same conditions provides an opportunity of direct comparison of different samples.

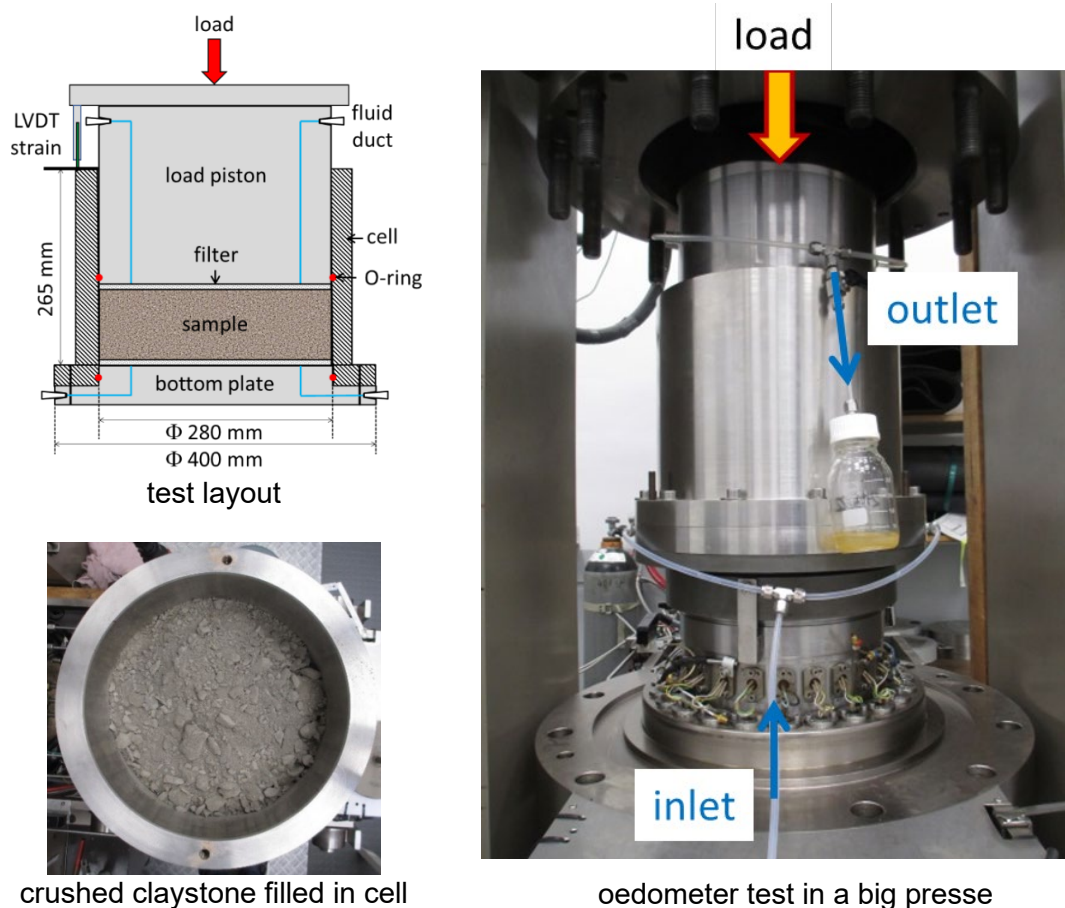


Fig. 3.1 A large oedometer setup for hydro-mechanical testing of backfill material

Four seal samples were prepared in the oedometer cells of 120 mm diameter to different thicknesses:

1. Seal sample 1 (S1) is a bentonite pellets/powder mixture, which was installed by emplacing the pellets ($d = 7$ mm) in seven layers and by filling the powder ($d < 2$ mm) into the voids between pellets. This yielded a pellet/powder ratio of 4/1 and a sample height of 46 mm. The achieved dry density of 1.44 g/cm^3 is consistent with that achieved in the full-scale drift emplacement experiments /FOI 15/ and /MÜL 17/.
2. Seal sample 2 (S2) is a claystone/bentonite (7/3) mixture, which was mixed with the crushed claystone ($d < 10$ mm) and the bentonite powder ($d < 2$ mm) to a mass ratio of 7/3. The mixture was filled and stamped by hand to a height of 73 mm, yielding a dry density of 1.58 g/cm^3 .
3. Seal sample 3 (S3) is an assembly of claystone/bentonite (7/3) blocks, which was firstly precompacted to a cylinder of 110 mm in diameter and 67 mm in height with a dry density of 2 g/cm^3 and then vertically cut through the central cross-sections into four sector subblocks. They were installed in the middle of a cell. The annular

gap of 5 mm in width and the joints within the subblocks were filled with the bentonite powder to a dry density of 1.27 g/cm^3 , which led to an average dry density of 1.74 g/cm^3 of the block-powder assembly.

4. Seal sample 4 (S4) is an assembly of precompacted blocks of the crushed claystone, for which the same preparing method for seal material 3 was adopted. The crushed claystone ($d < 10 \text{ mm}$) was compacted to a dry density of 2.1 g/cm^3 . The four sector subblocks were installed in a cell by filling the bentonite powder into the gaps and joints. An average dry density of 1.85 g/cm^3 was achieved.

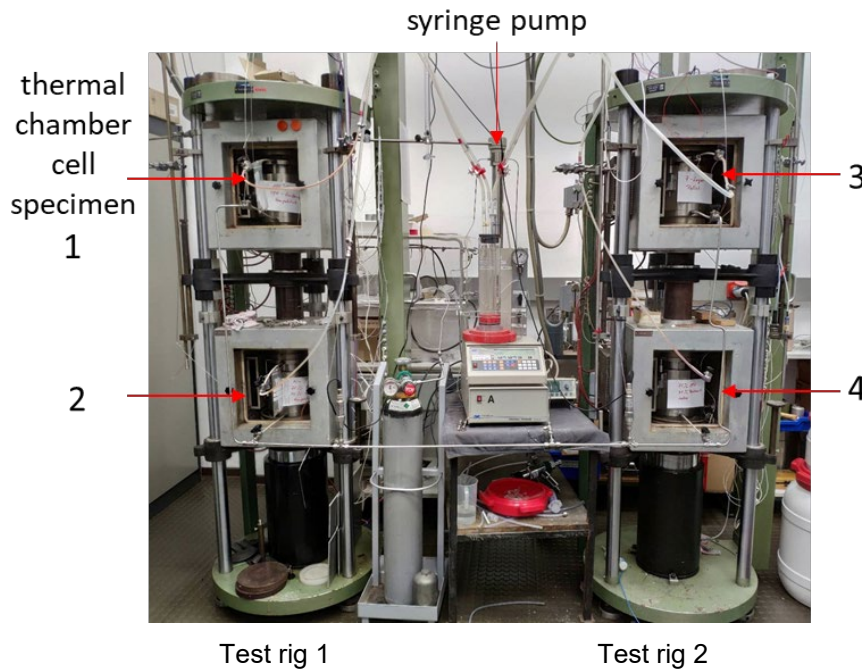
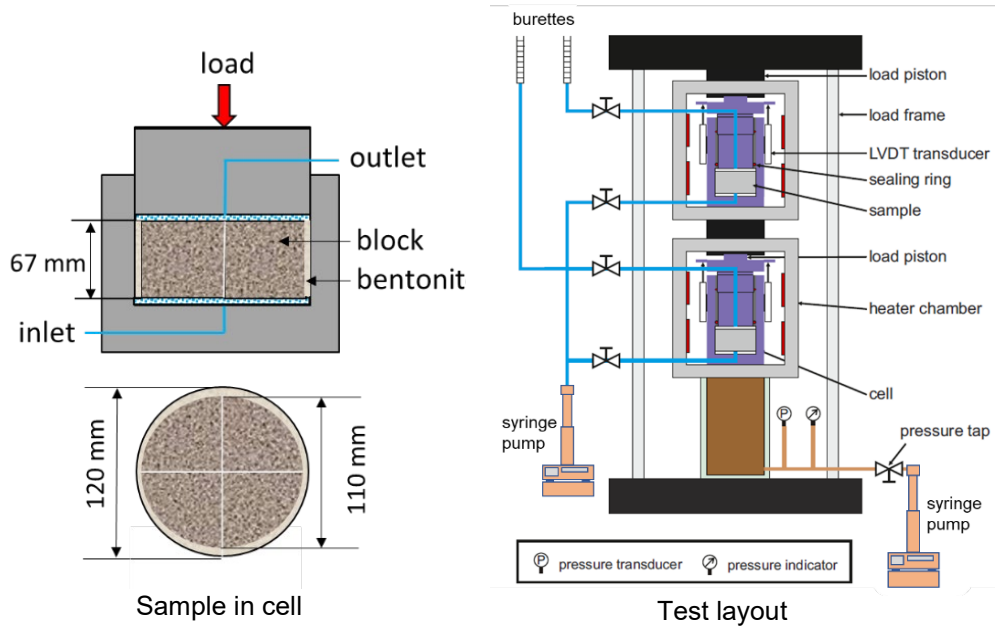
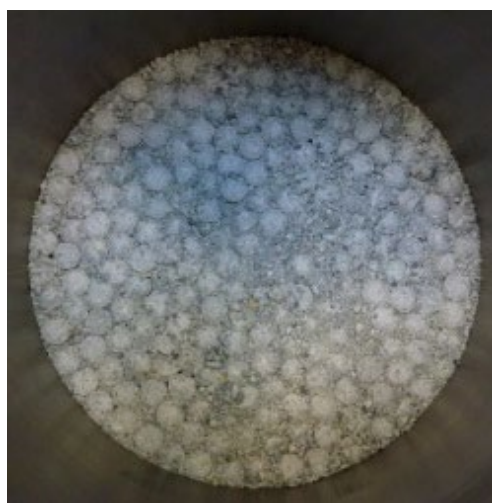
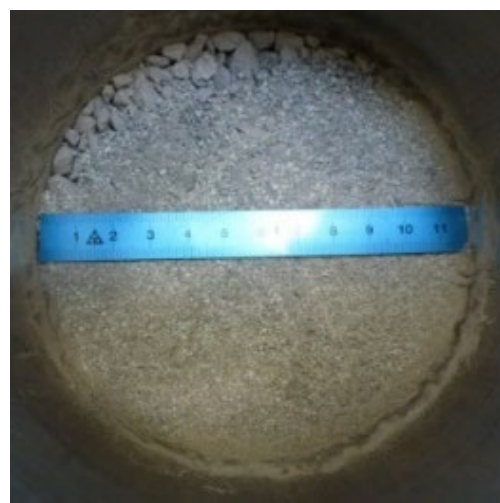


Fig. 3.2 Setup of the oedometer tests on four seal samples in two coupled load rigs

Figure 3.3 pictures the seal samples, while the average characteristics are summarised in table 3.1. It is noted that the sample height was selected to gather representative pathways for fluid flow in the coarse-grained materials by assuming an adequate ratio of sample height to maximum grain size $H/d > 6$. As consequence, the ratio of sample height to diameter ($H/D=0.6 - 0.7$) becomes larger compared with the normal values of 0.3 - 0.4 in conventional oedometer tests. This might yield a remarkable friction along cell wall and hence non-uniform stresses along the sample, which was not yet examined in the tests. However, an adequate sample thickness needs to be determined for coupled hydro-mechanical oedometer testing on coarse-grained materials in the future.



Seal 1
bentonite pellets/powder mixture



Seal 2
claystone/bentonite (7/3) mixture



Seal 3
assembly of claystone/bentonite (7/3)
blocks with bentonite powder filling gaps



Seal 4
assembly of claystone blocks with
bentonite powder filling gaps

Fig. 3.3 Pictures of the seal samples emplaced in oedometer cells

Tab. 3.1 Initial characteristics of the backfill/seal samples for hydro-mechanical testing

Sample Parameter	Backfill Crushed claystone d < 32 mm	Seal 1 Bentonite pellets/powder	Seal 2 Claystone/bentonite mixture (7/3)	Seal 3 Claystone/bentonite blocks (7/3)	Seal 4 Crushed claystone blocks
Diameter (mm)	280	120	120	120	120
Height (mm)	200	46	73	67	67
Grain density (g/cm ³)	2.70	2.67	2.69	2.68	2.70
Bulk density (g/cm ³)	1.88	1.56	1.70	1.85	1.97
Dry density (g/cm ³)	1.81	1.44	1.58	1.74	1.85
Porosity (%)	33.0	46.0	41.0	35.5	31.0
Water content (%)	3.6	5.54	6.68	4.80	4.80
Water saturation (%)	20.0	12.5	25.5	23.5	28.5
Mass ratio (-)	-	79/21 ^a	70/30 ^b	88/12 ^c	89/11 ^c

59 a: mass ratio of pellets to powder; b: mass ratio of claystone to bentonite; c: mass ratio of block to bentonite filled in gaps and joins.

Tab. 3.3 Main results determined on the studied barrier materials at different stages

Test stage	Properties of sample	Backfill	Seal 1	Seal 2	Seal 3	Seal 4
Initial state	Dry density (g/cm ³)	1.81	1.44	1.58	1.74	1.85
	Porosity (%)	33.0	46.0	41.0	35.0	31.5
Free swelled state after hydration over a month	Dry density (g/cm ³)	-	1.19	1.49	1.80	1.46
	Porosity (%)	-	55.5	44.5	45.8	33.3
Consolidated state under 5 MPa for seals and 17.3 MPa for backfill	Dry density (g/cm ³)	2.22	1.67	1.87	1.88	2.04
	Porosity (%)	17.9	37.9	30.2	30.0	24.3
	Water permeability (m ²)	1·10 ⁻¹⁸	8·10 ⁻²¹	3·10 ⁻¹⁹	2·10 ⁻¹⁹	6·10 ⁻¹⁸
	Gas breakthrough pressure P _b (MPa)	0.25	4.81	0.92	0.98	0.21
	Parameter B in (Eq. 3.3) (m ² /MPa)	4·10 ⁻¹⁹	-	3·10 ⁻¹⁸	6·10 ⁻¹⁹	2·10 ⁻¹⁷
Unloaded state	Dry density (g/cm ³)	2.21	1.61	1.73	1.64	1.92
	Porosity (%)	18.2	40.5	35.8	39.0	29.0

Thermal effects were investigated on two same bentonite and two same mixture (C/B=7/3) samples, which were prepared using the bentonite pellets with grains $d < 5$ mm (figure 2.3) and the crushed claystone with $d < 10$ mm (figure 2.2). The materials were filled in four individual cells of 120 mm diameter to a height of 43 mm for the bentonite samples (S1, S2) and 65 mm for the mixture ones (S3, S4). Figure 3.4 pictures the prepared samples. The bentonite samples reached an initial dry density of 1.39 g/cm^3 and/or a bulk density of 1.47 g/cm^3 , which is consistent with that achieved in the full-scale drift emplacement experiments /FOI 15/, /MÜL 17/. A higher dry density of 1.57 g/cm^3 was achieved at both mixture samples. This is probably attributed to the favourable grain size distribution (figure 2.11). The initial characteristics of the samples are given in table 3.2.

Tab. 3.2 Initial characteristics of the prepared bentonite samples (S1, S2) and claystone/bentonite (C/B=7/3) samples (S3, S4) for thermal testing

Property	S1: MX80	S2: MX80	S3: C/B=7/3	S4: C/B=7/3
Sample size D/H (mm/mm)	120/43	120/43	120/65	120/65
Grain size (mm)	< 5	< 5	< 10	< 10
Bulk density (g/cm^3)	1.47	1.47	1.67	1.67
Dry density (g/cm^3)	1.39	1.39	1.57	1.57
Porosity (%)	47.8	47.8	41.8	41.8
Water content (%)	5.6	5.6	7.0	7.0
Saturation degree (%)	16.4	16.4	26.0	26.0

3.2.2 Test procedure

3.2.2.1 Hydro-mechanical testing

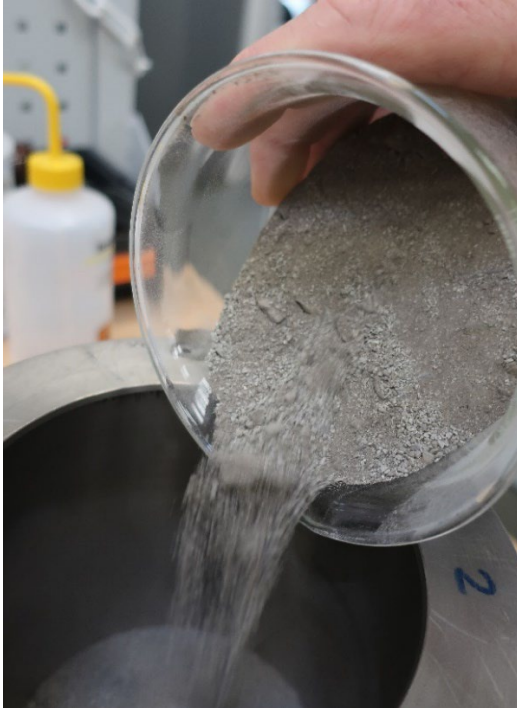
A common procedure was conducted on the backfill and seal samples (table 3.1) in the big and normal oedometer cells (figures 3.1-2) under relevant hydro-mechanical conditions expected in the backfilled/sealed drifts without thermal loading: (i) hydration by taking up water from the surrounding humid environment; (ii) consolidation under rheological rock compression and water flow from the surroundings; and (iii) gas generation and migration from corrosion of metallic components within a repository. These conditions were sequentially applied to the samples to investigate the responses of the materials:



bentonite pellets $d < 5$ mm



Crushed claystone $d < 10$ mm



filling the mixture in cell



claystone-bentonite (7/3) mixture



compaction by hand stamping



bentonite sample



claystone-bentonite (7/3) sample

Fig. 3.4 Pictures of the samples prepared with the bentonite pellets ($d < 5$ mm) and crushed claystone ($d < 10$ mm) by mixing, filling and stamping the mixtures in oedometer cells of 120 mm diameter

- (1) Hydration was conducted on the samples without mechanical loads. The synthetic clay water was introduced from the scaled burette into the bottom of each sample at small height differences of 0.5 – 0.8 m. Water uptake and axial strain of the samples were monitored for evaluation of their hydration processes and swelling capacities.
- (2) Consolidation and water injection started upon the full water-saturated samples. Axial load was stepwise increased to different levels up to 5 MPa on the seal material samples and 17 MPa on the backfill material one. Each load step was kept for time periods of weeks to months until the consolidation rates reached the measurable limit of 10^{-10} s^{-1} . Under the load, the synthetic water was injected at pressures of 0.1 – 0.7 MPa to the seal material samples and 0.1 – 0.3 MPa to the backfill material one. The pressure gradients over 1000 were selected for precise measurement of water flow through the low permeable materials within acceptable durations of days to weeks, as done in the previous experiments /ZHA 14/18a/. At high external stresses, the internal structures of the samples could not be remarkably altered by the slow water flow under the relatively low injection pressures. During steady-state water flow, apparent water permeability can be determined by Darcy's law (equation 2.5).
- (3) Following the water flow at the final step load, gas penetration testing was carried out on the water-saturated and compacted materials. Firstly, it was tried to remove the water in the external reservoirs, but it could not be completely removed from the filters with small pores. Nitrogen gas was injected into the inlet by stepwise increasing pressure with small increments of 0.1 – 0.2 MPa at time intervals of 1 – 3 days, while the outlet was kept at atmospheric pressure. As soon as gas bubbles were detected at the outlet, the gas pressure in the inlet was considered as the gas breakthrough pressure P_b . Beyond the breakthrough, the gas injection continued for determination of apparent gas permeability by Darcy's law (equation 2.6).
- (4) Finally, the compacted samples were unloaded and dismantled for visual inspection.

3.2.2.2 Thermal testing

Thermal tests were conducted on two same samples of the bentonite and the clay-stone/bentonite (7/3) mixture (table 3.2) to investigate thermal effects on their hydro-mechanical properties and behaviour such as swelling, consolidation, water permeability, and gas migration. A common procedure followed in several stages:

- (1) Initial conditions were adjusted to an axial load of 0.2 MPa for the samples (S1-S4), and temperatures of 23 °C for S1 & S3 and 90 °C for S2 & S4 respectively;

- (2) Hydration was performed by infiltration of the synthetic pore water from the burette to the bottom of each sample, whereby axial deformation was monitored;
- (3) Consolidation was conducted under axial loads of 3 and 4 MPa for 1 – 2 months;
- (4) Water was injected at a pressure of 0.4 MPa to measure water permeabilities; and
- (5) Gas injection followed at a flow rate of 0.03 ml/min to examine gas penetration behaviour of the water-saturated samples.

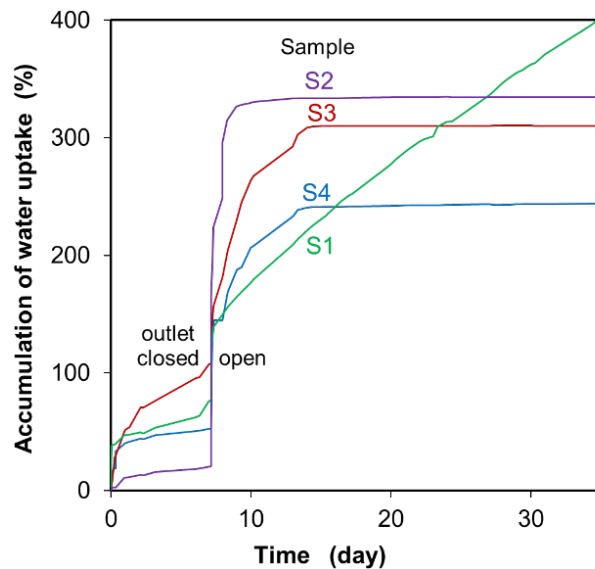
3.3 Results of hydro-mechanical testing

3.3.1 Hydration and swelling

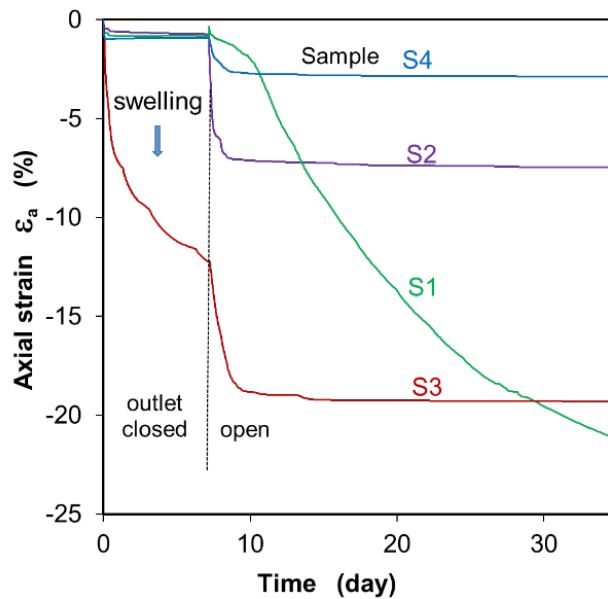
Figure 3.5 shows the amounts of absorbed water and axial strains of the seal samples during hydration at atmospheric pressure. First, the outlet was closed. Under suction effect, the initially unsaturated materials took up water quickly in the beginning and then slowed down. As the outlet was opened, the water uptake was accelerated. This phenomenon suggests that the air in the pore space at closed outlet is compressed by increasing water content and thus the pore air pressure rises and impedes more water moving into the pores. As the outlet is opening, the compressed air releases and the reduced pore air pressure allows more water moving into the pores. The materials showed different hydration processes (figure 3.5a). Whereas the claystone block S4 as well as the claystone/bentonite mixture S2 and block S3 reached full saturation within 10 - 15 days, the bentonite S1 was still not fully saturated even over a longer period to a month. Obviously, the hydration is dominated by bentonite content and dry density of the mixtures. At a given dry density, more water can be absorbed for higher contents of bentonite due to its high adsorption capacity, but more time is also needed for full saturation. Moreover, the associated swelling of bentonite particles decreases the effective porosity, which slows down the hydration too. At a given bentonite content, the pore volume decreases with increasing dry density, which slows down and limits the water uptake.

The hydration results in swelling of the clay materials (figure 3.4b). At full saturation, a maximum swelling strain is achieved, which strongly depends on bentonite content and dry density. The bentonite S1, even at a low dry density of 1.44 g/cm^3 , exhibited a large swelling strain of 21% and more when the hydration continued till full saturation. A similar swelling strain of 20% was achieved by the claystone/bentonite block S3 at a high dry density of 1.74 g/cm^3 . The other two samples (claystone/bentonite mixture S2 and

claystone block S4) showed smaller swelling strains of 7.5 % and 3 %, respectively, because of either a low dry density (1.58 g/cm³) for S2 or a low bentonite content filling the voids between blocks in S4. However, a rapid contraction occurred as water was introduced to the crushed claystone subjected to a small load of 0.2 MPa from the piston weight (figure 3.6). This can be attributed to collapse of the inner soil structure due to water-induced weakening of claystone particles and friction reduction between neighbouring particles. In practice, such contraction shall be avoided or minimised by adding bentonite to the aggregate with a small content like the claystone/bentonite (7/3) mixture S2, and/or by increasing emplacement density by mechanical compressing on site. The densities reached after hydration are summarised in table 3.3 for the samples.



a. water uptake



b. axial strain

Fig. 3.5 Water uptake and induced swelling of the seal samples S1-S4

3.3.2 Consolidation and water permeability

The saturated samples were consolidated in drained conditions under repeatedly increased axial stresses and water injection pressures. The results are shown in figure 3.6 for the backfill and in figure 3.7 for the seal materials in evolution of applied axial stress and water injection pressure, and resulting axial strain, porosity as well as water permeability.

3.3.2.1 Consolidation

The multistep loading compacted the materials and decreased their porosities (figures 3.6c, 3.7b). All samples exhibited a similar multiple consolidation behaviour with a rapid decrease, followed by a gradual decrease of porosity under increasing load. The strain rates decreased steadily to a low level of $\sim 10^{-10} \text{ s}^{-1}$ over days to months during each stage (figure 3.6b). The low strain rates are close to the rock strain rates observed around drifts in URL Bure /GUA 16/. Quantitatively, the different materials showed different reductions in porosity (figure 3.7b). The bentonite S1 was mostly consolidated with a high porosity of 55% to 33% at 5 MPa. The claystone/bentonite (7/3) mixture S2 and block S3 exhibited a similar reduction of the porosity from 45% to 30% at 5 MPa. The crushed claystone (figure 3.6c) and block S4 (figure 3.7b) were less compacted due to relatively lower initial porosities and thus higher stiffnesses.

The consolidation of crushed claystone and mixtures with bentonite is mostly governed by variations of the interparticle macropores, as the micropores in the claystone particles are hardly compressible under the lithostatic stresses. The stress and time-dependent variation in porosity can be approached by /ZHA 13/

$$\sigma'_a = \left(\frac{\dot{\epsilon}_a}{C}\right)^{\frac{1}{n}} \left\{ \ln \left[\frac{\phi_o(1-\phi_e)}{\phi_e(1-\phi_o)} \right] \right\}^{\frac{m}{n}} \quad (3.1)$$

where σ'_a is the effective axial stress, $\sigma'_a = \sigma_a - (P_i - P_o)$, in which σ_a is the total stress; $\dot{\epsilon}_a$ is the axial strain rate; ϕ_o and ϕ_e are the initial and current macro-porosities, respectively; and C , n and m are the empirical parameters. The macro-porosity ϕ_e is defined as the total porosity ϕ minus the micro-porosity ϕ_m , i. e. $\phi_e = \phi - \phi_m$. Figure 3.8 shows two fitting curves for the claystone aggregate with $\phi_m \approx 10\%$ for the average strain rates of $\dot{\epsilon}_a = 1 \times 10^{-7} \text{ s}^{-1}$ for the onset of the loading stage and $\dot{\epsilon}_a = 5 \times 10^{-10} \text{ s}^{-1}$ for the end of the loading stage. The data are reasonably described by the model with the parameter values of $C = 3 \times 10^{-16} \text{ MPa s}^{-1}$, $n = 12$ and $m = 37$.

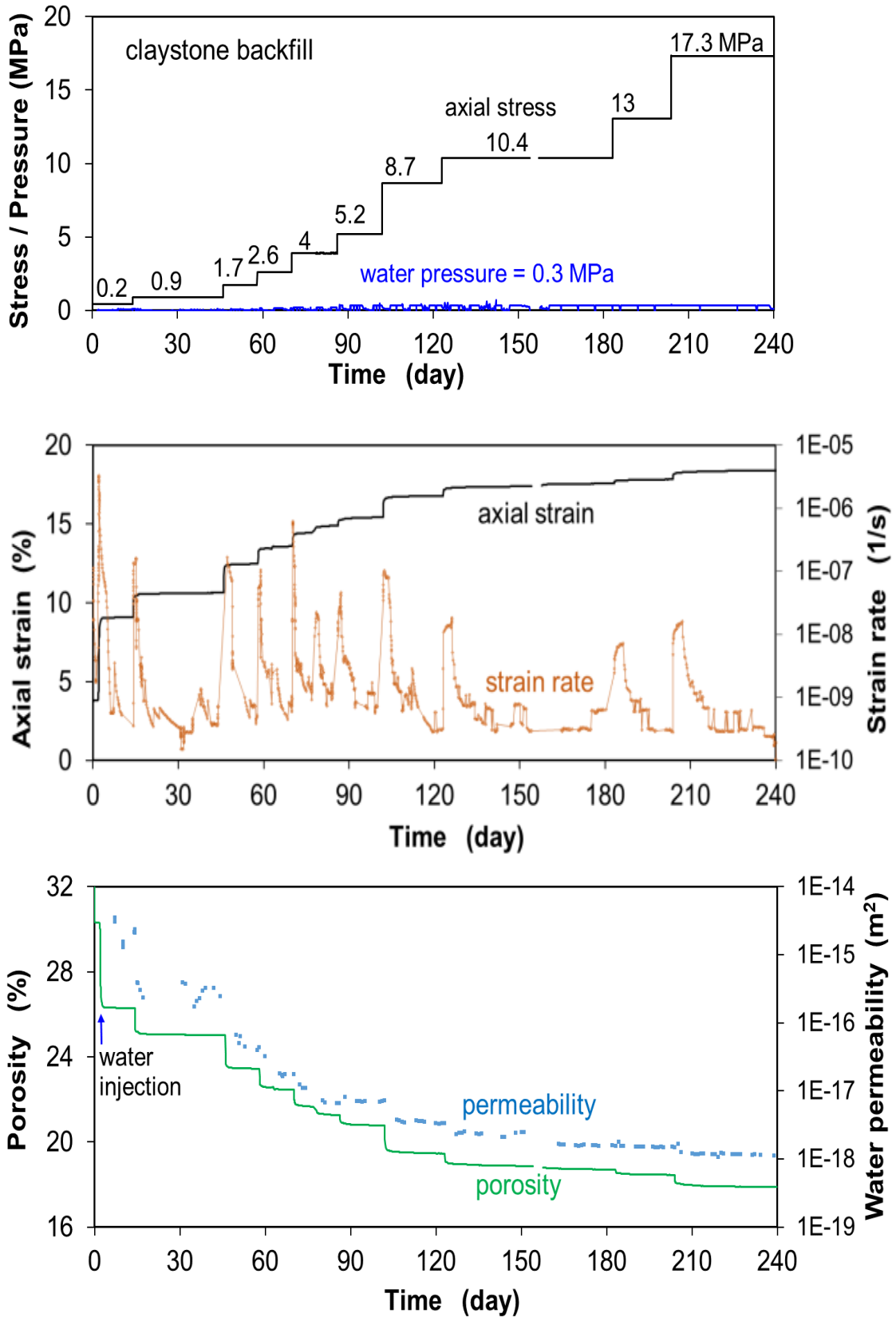


Fig. 3.6 Multistep consolidation behaviour and variation in water permeability of the claystone aggregate: (a) axial stress and water injection pressure; (b) axial strain and strain rate; and (c) porosity and water permeability

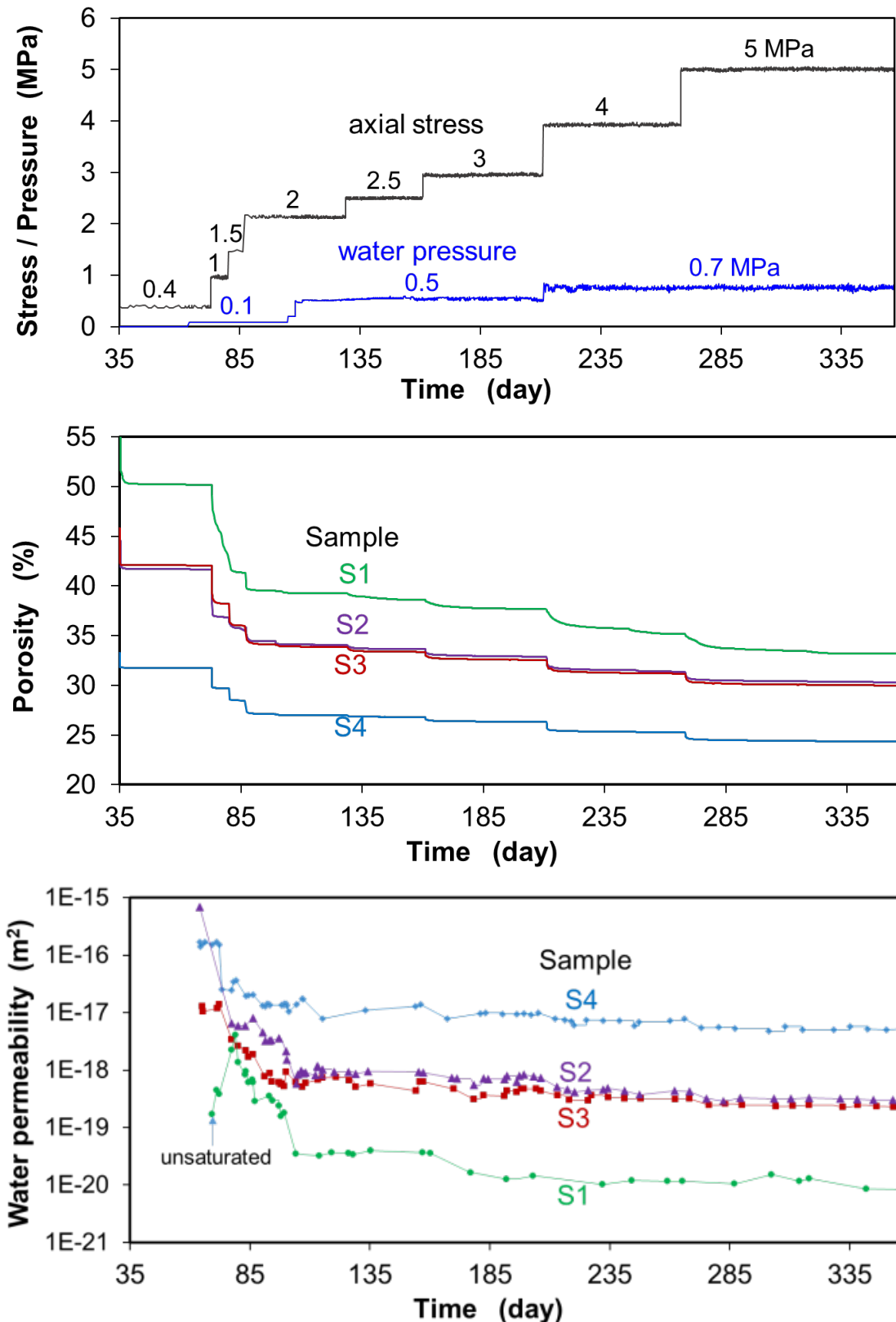


Fig. 3.7 Multistep consolidation behaviours and variations in water permeability of the seal materials: (a) axial stress and water injection pressure; (b) porosity; and (c) water permeability

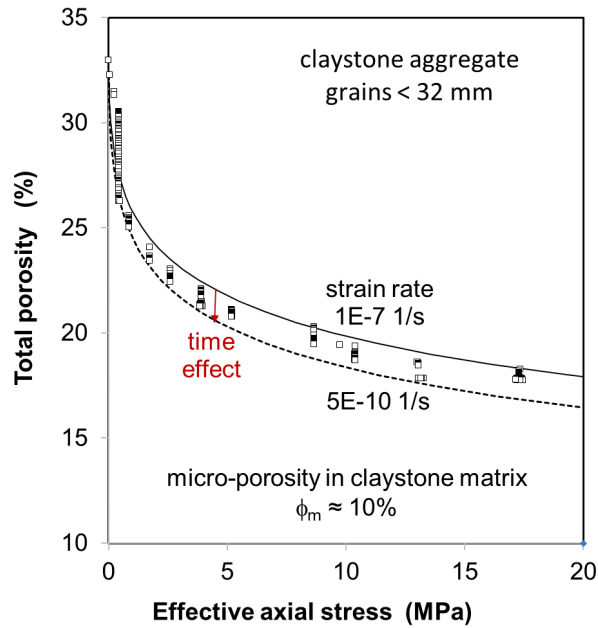


Fig. 3.8 Stress-porosity relationship for the crushed claystone

Furthermore, the consolidation increases the density and the mechanical stiffness, which can be quantified by bulk modulus:

$$K = \frac{\Delta\sigma'_a}{\Delta\varepsilon_a} \tag{3.2}$$

where $\Delta\sigma'_a$ and $\Delta\varepsilon_a$ are the increments of effective axial stress and axial strain under rapid loading. Figure 3.9 shows that the bulk modulus increases exponentially with increasing dry density.

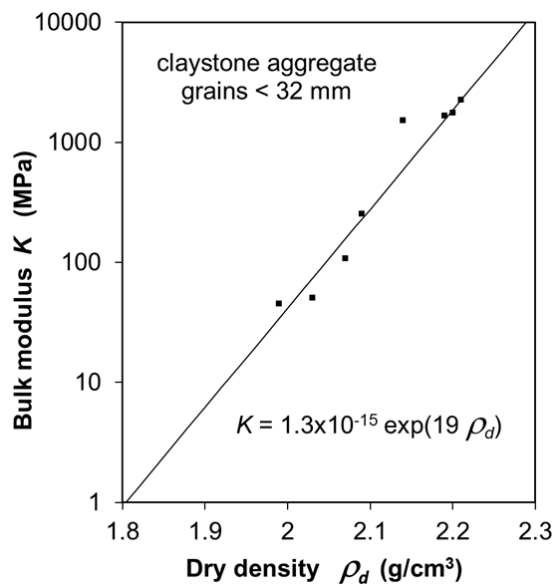


Fig. 3.9 Bulk modulus of the crushed claystone as a function of dry density

3.3.2.2 Water permeability

Along with porosity reduction, water permeability decreased either. Particularly, the permeability is decreased by 2-3 orders of magnitude at low stresses (below 2 MPa) (see figures 3.6c; 3.7c): from $3 \times 10^{-15} \text{ m}^2$ to $2 \times 10^{-17} \text{ m}^2$ at the crushed claystone; $4 \times 10^{-18} \text{ m}^2$ to $4 \times 10^{-20} \text{ m}^2$ at the bentonite S1; $7 \times 10^{-16} \text{ m}^2$ to $9 \times 10^{-19} \text{ m}^2$ at the claystone/bentonite (7/3) mixture S2; $1 \times 10^{-17} \text{ m}^2$ to $7 \times 10^{-19} \text{ m}^2$ at the claystone/bentonite block S4; and $2 \times 10^{-16} \text{ m}^2$ to $2 \times 10^{-17} \text{ m}^2$ at the claystone block S3. Note that because the bentonite was not fully saturated in the beginning, the water permeability was relatively low ($2 \times 10^{-19} \text{ m}^2$) and then increased to the maximum with the increase in water saturation due to porosity reduction. Beyond 2 MPa, the porosity and permeability varied insignificantly.

The dependence of water permeability on porosity is illustrated in figure 3.10. It is obvious that the permeability decreases exponentially with decreasing porosity for each material studied. Moreover, the water permeability decreases significantly with increasing bentonite content. Because major part of the bentonite porewater is strongly bounded and becomes immobile under the applied pressure gradients, only a small fraction of the porewater is mobile within the limited pathways of smaller effective pores.

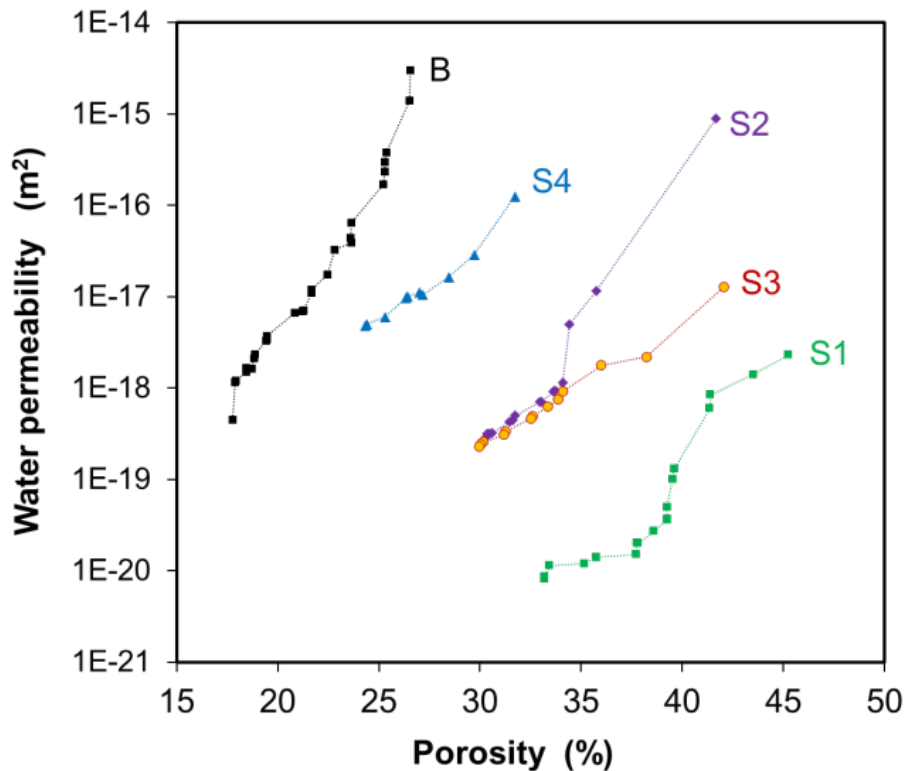


Fig. 3.10 Water permeability-porosity relationships of the crushed claystone B and the seal materials S1-S4

3.3.3 Gas penetration and impact

3.3.3.1 Gas penetration

Gas penetration testing followed the last consolidation stage at axial stresses of 5 MPa on the seal material samples and 17.3 MPa on the backfill material one, respectively. Figure 3.11 depicts the results obtained from the parallel tests on the seal material samples with consolidated porosities (table 3.3), in terms of applied gas injection pressure and permeability versus elapsed time.

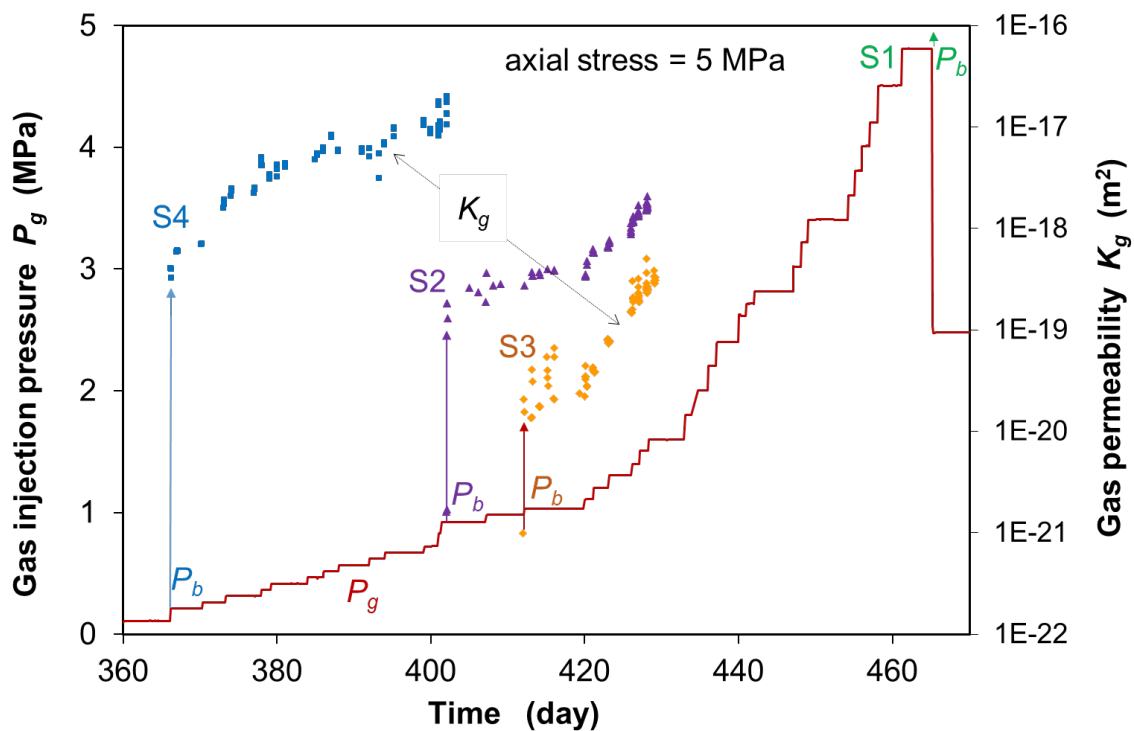


Fig. 3.11 Gas breakthrough pressures and permeabilities of the water-saturated seal materials compressed under axial stress of 5 MPa

The measured data indicate that:

- (1) No advective gas flow occurred before the breakthrough threshold P_b for each material;
- (2) The breakthrough event occurred in the claystone block S4 at the lowest pressure $P_b = 0.2$ MPa followed by the claystone/bentonite (7/3) mixture S2 and block S3 at pressures $P_b = 0.9$ MPa and 1 MPa, respectively. The breakthrough of bentonite S1 was observed at the highest pressure $P_b = 4.8$ MPa; and
- (3) The gas permeability increased with increasing injection pressure beyond the breakthrough. Obviously, the gas breakthrough pressures of the compacted claystone

aggregate and claystone/bentonite mixture were much lower than that of the bentonite. The large discrepancies are mostly due to different states of porewater in the materials.

Many studies /HOR 96/, /ROD 99/, /BIR 13/, /HAR 17/, /ZHA 22/ suggested that porewater in compacted bentonite is preferentially bound to interlayers and external surfaces of the particles and cannot be easily displaced by gas pressures, when the external confining stress is not exceeded. In contrast, porewater in claystone aggregate and mixtures with limited bentonite contents is either less strong bound or free. As gas pressure exceeds the local capillary thresholds of pores, interparticle porewater in such claystone-based mixtures can be displaced by pressuring gas. When gas pressure increases, higher capillary thresholds in narrower pore channels can be exceeded and additional pathways are created for increased gas flow. Increase in gas permeability is linearly related to the increase in injection pressure according to the equation:

$$K_g = B(P_g - P_b) \quad (P_g \geq P_b) \quad (3.3)$$

In the equation, the linear factor B is obtained by fitting the data for each sample and is given in table 3.3. The linear relationship does not appear as a line in the $\log_{10}K_g$ - P_g plot as shown in figure 3.12 for the claystone aggregate B and block S4 as well as for the claystone/bentonite mixture S2 and block S3.

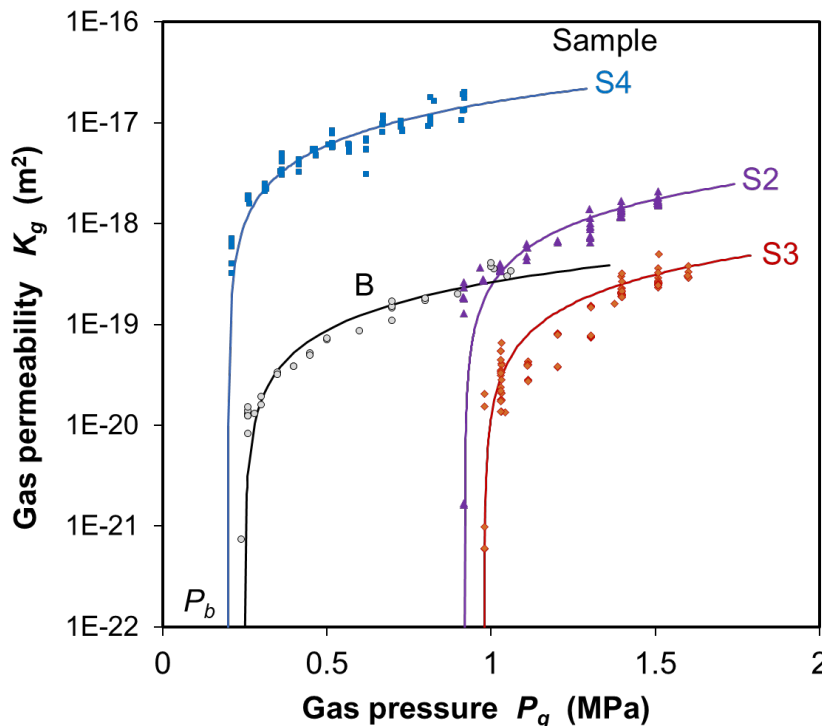


Fig. 3.12 Gas permeabilities of the water-saturated and compacted claystone aggregate B and seal materials S2-S4 as a function of gas injection pressure

As mentioned above, a much higher gas pressure is needed to create a pathway in bentonite. During the increase of gas injection pressure from 2.8 MPa to 4.8 MPa, a water outflow instead of a gas outflow occurred unexpectedly. This might be caused by the movement of the residual water remained in the inlet into the sample. That means that the real pressurised fluid in the sample was water rather than gas. The gas pressure was transferred to the porewater at the sample end ($P_g = P_w$). The increased pressure gradients drove the residual water into the pores displacing mobile water out of sample. The apparent water permeability values K_w estimated are presented in figure 3.13. Moreover, the increased porewater pressure in the sample (mean value of $P_w/2$) decreased the effective stress and thus led to a gradual expansion of the sample (figure 3.14). This could be the reason for the increase in water permeability from $5 \times 10^{-21} \text{ m}^2$ to $3 \times 10^{-19} \text{ m}^2$ (figure 3.13). Only at the maximum pressure P_b , a sharp gas release was observed, indicating creation of a pathway through the sample. Following that, the gas pressure dropped sharply down to $P_c = 2.5 \text{ MPa}$, accompanied by a rapid reduction of gas permeability K_g to zero. This implies that the gas pathway became closed at the gas residual or shut-off pressure P_c .

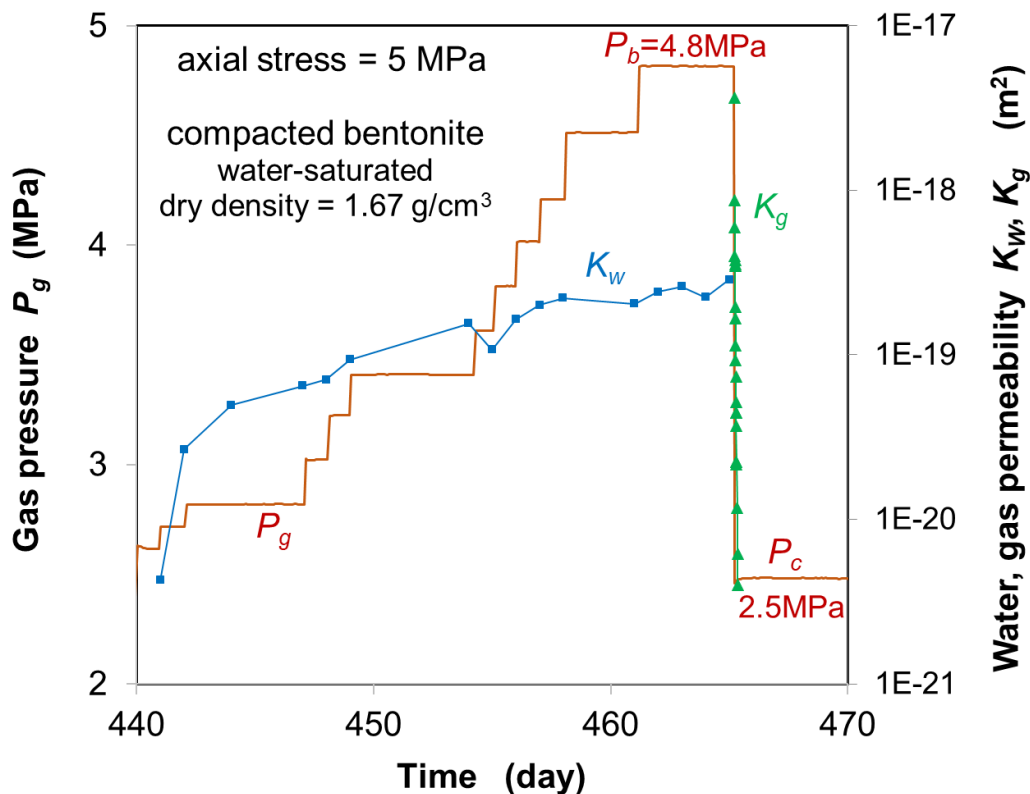


Fig. 3.13 Evolution of gas injection pressure, water permeability before gas breakthrough and gas permeability at breakthrough observed on the bentonite sample

Theoretically, the gas penetration in water-saturated bentonite is not dominated by displacement of porewater, but by creation and dilation of micro-fissures as the gas pressure exceeds the local confining stress and tensile strength /HOR 96/, /ROD 99/, /BIR 13/17/, /GUT 15/, /HAR 17/, /ZHA 22/. In practice, the gas penetration often occurs in relatively weak regions, e.g., through joints between bentonite blocks, seal-rock interfaces, or sample-cell interfaces in laboratory tests. Therefore, the gas breakthrough pressures observed in field and laboratory tests under flexible and constraint boundary conditions (including the present one) are usually slightly lower than the boundary confining stresses /CUS 14/, /BIR 17/, /HAR 17/, /ZHA 22/.

3.3.3.2 Impact of gas pressure

In order to examine self-sealing behaviour of the gas pathway in bentonite, gas injection continued at controlled flow rates. Responses of gas pressure in the inlet and axial strain are plotted in figure 3.14. The gas pressure started rising from the shut-off point P_c at a flow rate of 0.12 mL/h and then accelerated at a higher rate of 0.6 mL/h until a new breakthrough at a pressure of $P_b = 4$ MPa occurred, which was close to the first break-through pressure of the intact sample. This implies that the previously induced pathway was resealed nearly to the previous intact state. The closure of the pathway is mainly caused by the mechanical compression ε_a under the constant external stress. The gas pressure has no mechanical impact on water-saturated bentonite at pressures below the external stress /BIR 17/.

Following the second breakthrough, the gas pressure dropped sharply to a new shut-off point of 1.6 MPa. The continuation of the gas supply led to two further pressure rising/dropping cycles with a duration of one month for each. The repeated breakthrough pressures are within a narrow range of 4 - 4.4 MPa, while the shut-off pressures are within a narrow range of 1.6–1.8 MPa. The repeated breakthrough and shut-off pressures are slightly lower than those of the intact bentonite. Similar multiple cyclic pressure rising/dropping processes were also observed on water-saturated bentonites in some other experiments /VOK 14/, /GUT 15/, /HAR 17/. In fact, the cyclic gas pressure rising/dropping process reveals closing/opening cycles of migration pathways.

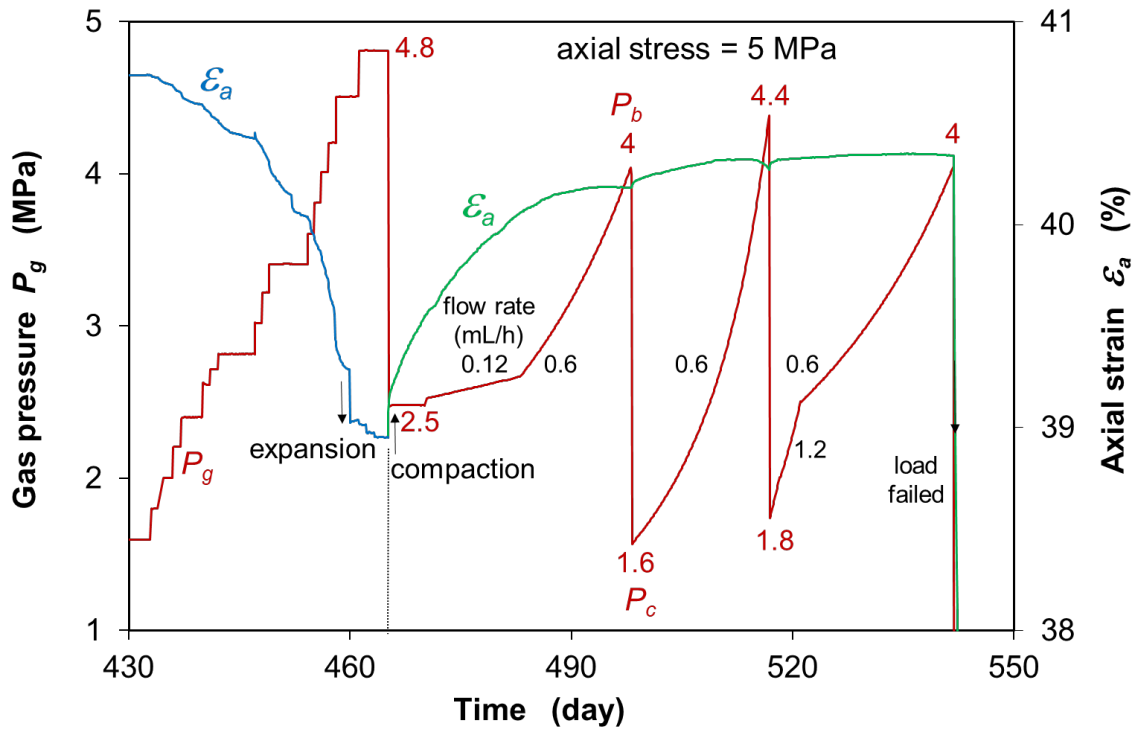


Fig. 3.14 Evolution of the gas injection pressure and resulting deformation of water-saturated and compacted bentonite

3.3.4 Dismantled samples

The tests on the seal material samples were terminated due to a failure in axial loading. The unloading led to expansion of the samples (figure 3.15) with a gradual increase in porosity by 6 % over 6 d at the bentonite S1, 6 % and 9% at the claystone/bentonite mixture S2 and block S3, respectively, and 5 % at the claystone block S4. After dismantling, the porosity of the bentonite increased further by 5.5 %.

The dismantled samples can be seen in figure 3.16 and described as follows:

- (1) The coarse claystone particles are homogeneously distributed in the compacted aggregate and claystone/bentonite mixture;
- (2) The annular gaps and joints within the assembled blocks are completely sealed with bentonite; and
- (3) The initially heterogenous bentonite pellets/powder mixture became very homogeneous. The homogenisation of the bentonite pellets/powder mixture is mainly dominated by swelling of the pellets during the first hydration phase, as demonstrated by a simple experiment (figure 3.17). Bentonite pellets ($d = 7$ mm) were employed in a glass and flooded with the synthetic porewater. Within 1 hour, the pellets swelled into the interparticle pores to be a homogeneous bentonite-water mass at a ratio of 3/1.

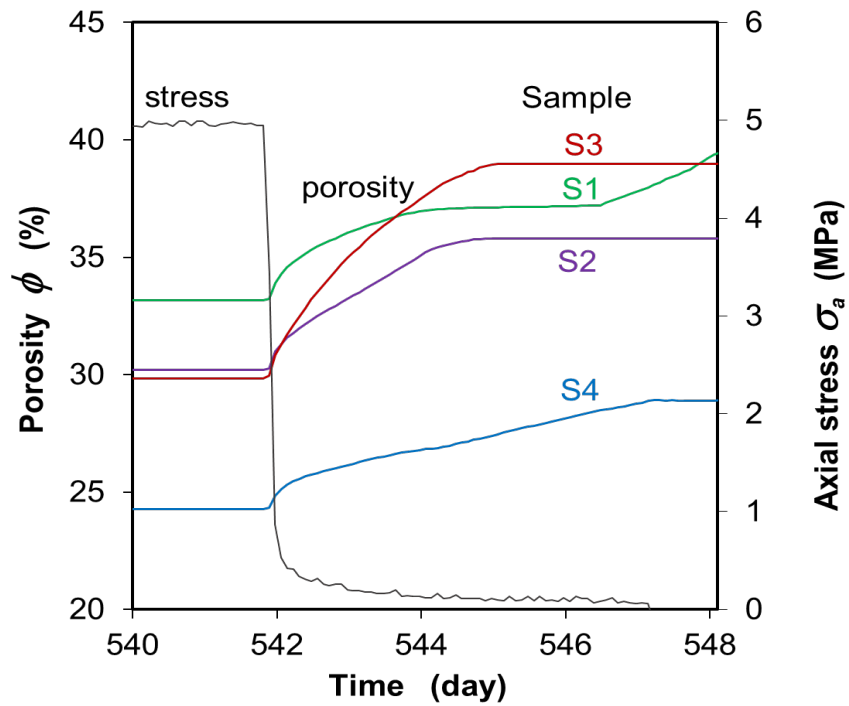


Fig. 3.15 Swelling of the compacted seal material samples S1-S4 after unloading



Backfill: compacted claystone
dry density = 2.2 g/cm³



Seal 1: compacted bentonite pellets/powder mixture
dry density = 1.61 g/cm^3



Seal 2: compacted claystone/bentonite (7/3) mixture
dry density = 1.73 g/cm^3



Seal 3: claystone/bentonite (7/3)-blocks with bentonite-filled gap and joints
dry density = 1.64 g/cm^3

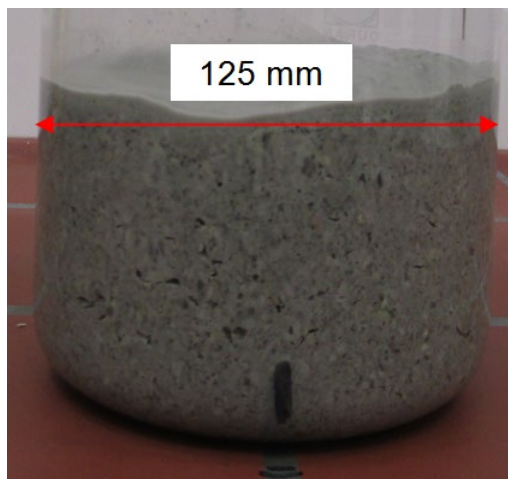


Seal 4: claystone-blocks with bentonite-filled gap and joints
dry density = 1.92 g/cm^3

Fig. 3.16 Pictures of the dismantled backfill and seal samples



(a)



(b)

Fig. 3.17 Demonstration of the homogenisation of bentonite pellets ($d = 7 \text{ mm}$) immersed in the synthetic clay water: (a) before and (b) after wetting for 1 hour

3.4 Results of thermal testing

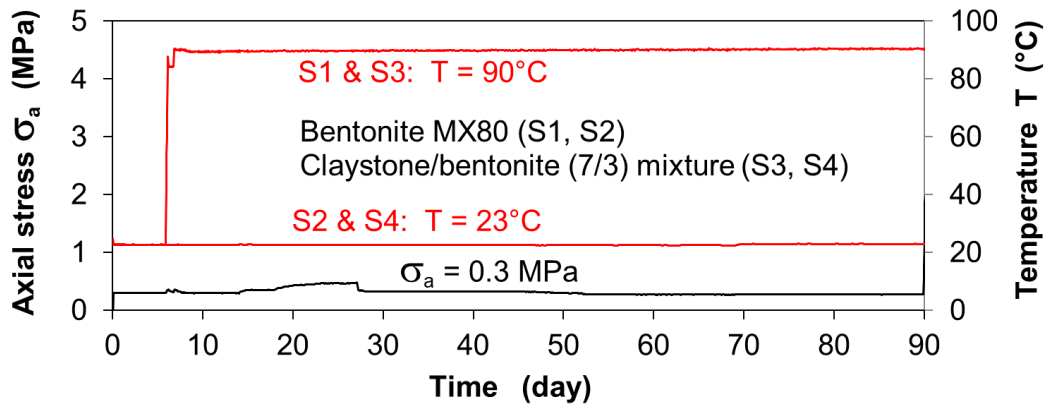
3.4.1 Thermal effects on hydration and swelling

Figure 3.18 shows the amounts of absorbed water and axial strains of the bentonite samples (S1, S2) and claystone/bentonite (7/3) mixture (S3, S4) during hydration at hydraulic gradients of 25 - 40 m/m. First, the samples were loaded at a low axial stress of 0.3 MPa and heated to 23 °C at S2 & S4 and 90 °C at S1 & S3, respectively. The initial loading did not cause remarkable deformation. As the synthetic water was introduced into the samples, a rapid hydration process took place. The water uptake of both mixture samples (S3, S4) reached the respective maximum values within 2 - 3 days, while the bentonite samples (S1, S2) took much longer time over 1 – 2 months to full saturation. The saturation process in the bentonite at 90 °C was faster but the amount of water uptake at the final saturation was less than at 23 °C. This indicates that the water absorption capacity of the bentonite decreases with increasing temperature /MIT 76/, /HOR 96/. Obviously, the bentonite can take up more water than the mixture due to the high absorption capacity of the dominating mineral montmorillonite in the bentonite.

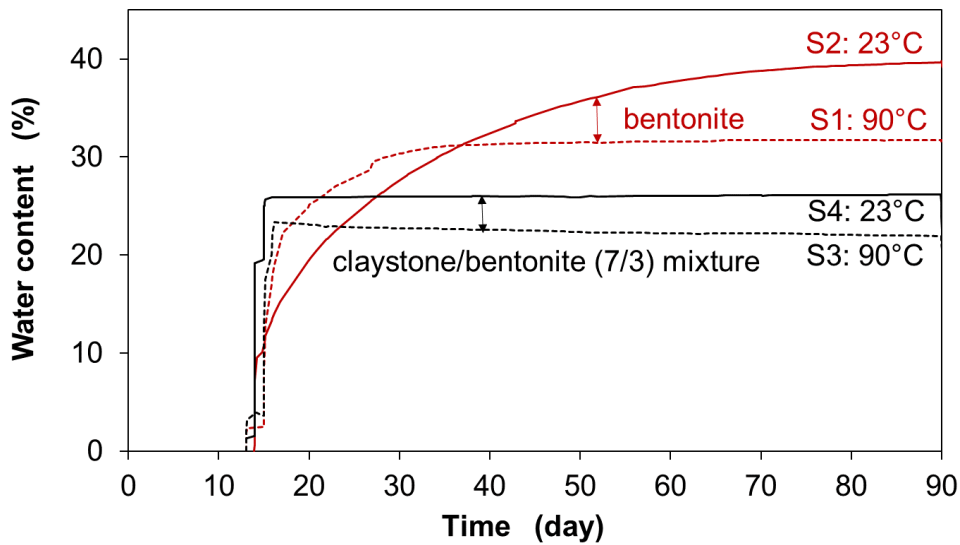
The hydration led to different responses of the bentonite and the claystone/bentonite mixture. Whereas the bentonite samples expanded gradually with time to a maximum volumetric strain of $\varepsilon_v = 5.5\%$ at 90 °C (S1) and 13% at 23 °C (S2), the claystone/bentonite mixture contracted to $\varepsilon_v = -0.7\%$ at 90 °C (S3) and -0.1% at 23 °C (S4). The swelling of the bentonite is a direct consequence of the water uptake and associated expansion of montmorillonite interlayers, while the contraction of the mixture is resulted from collapse of the internal structure through water-induced reduction of friction resistance between clay particles, where the swelling effect of the small bentonite content was relatively smaller. Moreover, the relatively smaller swelling of the bentonite at the high temperature is resulted from the thermal reduction of its water absorption capacity mentioned above.

3.4.2 Thermal effects on consolidation and water permeability

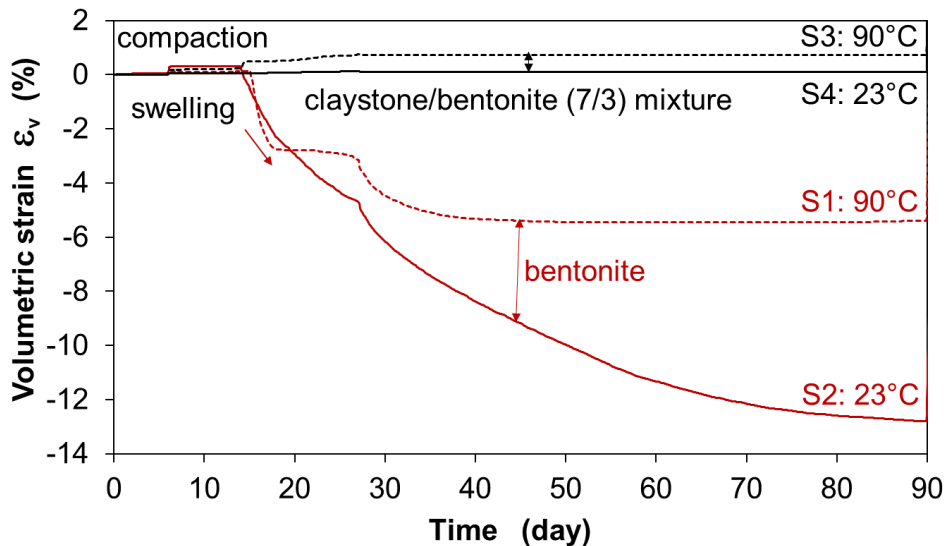
The saturated samples were consolidated in drained conditions under increased axial stresses of 3 and 4 MPa. The water injection pressure was stepwise increased to 0.4 MPa, while the outlet pressure maintained atmospheric. The temperature was elevated step-by-step from 23 to 49, 69 and 90 °C at samples S2 & S4, and lowered from 90 to 70, 50, and 26 °C at S1 & S3. Results are summarized in figure 3.19.



a. Applied axial load and temperature



b. Water uptake



c. Volumetric deformation

Fig. 3.18 Evolution of water uptake and induced swelling of the bentonite and claystone/bentonite (7/3) mixture during hydration with synthetic OPA clay water at a low axial load of 0.3 MPa and temperatures 23 °C and 90 °C

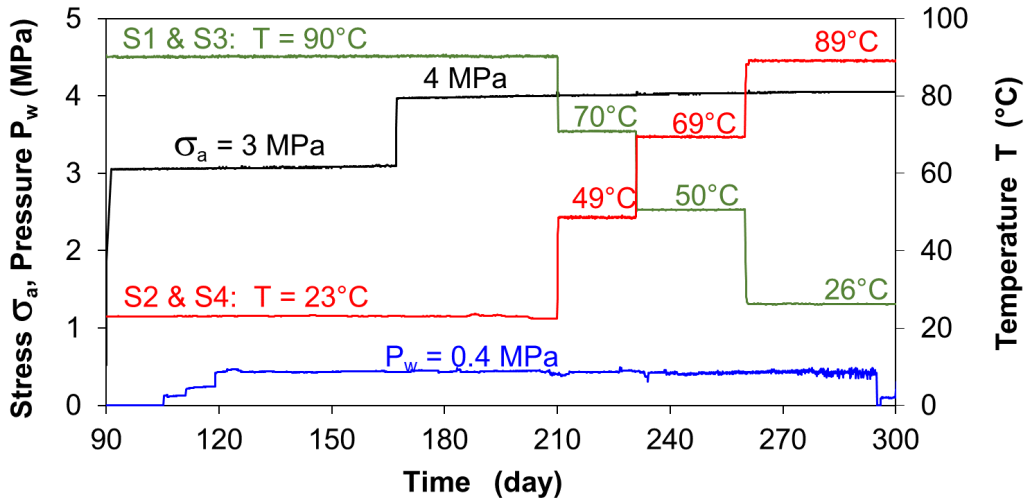
3.4.2.1 Consolidation

The mechanical loading compacted the materials (figures 3.19b-c). Under each increased load, the different samples exhibited a similar consolidation behaviour with rapid decreased rates, followed then by a gradual decrease of porosity to a quasi-stable state after 1-2 months. The consolidation at the high temperature of 90 °C (S1, S3) was more significant than at 23 °C (S2, S4). This should be attributed to the fact that the porewater at high temperatures is less absorbed, less viscous, more mobile, and more easily expelled out of the pore under external loading.

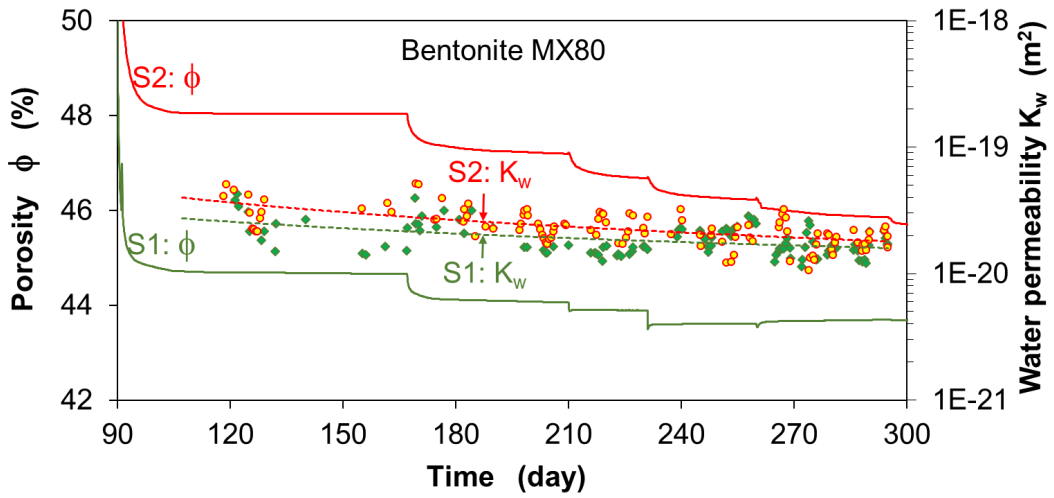
At the constant load of 4 MPa, the temperature was stepwise increased at samples S2 & S4 and decreased at S1 & S3, respectively. The strain measurements indicated that the samples were compacted by both heating or cooling. Theoretically, sample expansion should appear by heating or contraction inversely by cooling. The same response of the material to heating and cooling was caused by the testing system. The thermal deformation measured practically consists of two parts: one from the sample itself and another one from the load piston. They cannot be distinguished and thus the true thermal deformation of the samples cannot be determined from the testing system.

3.4.2.2 Water permeability

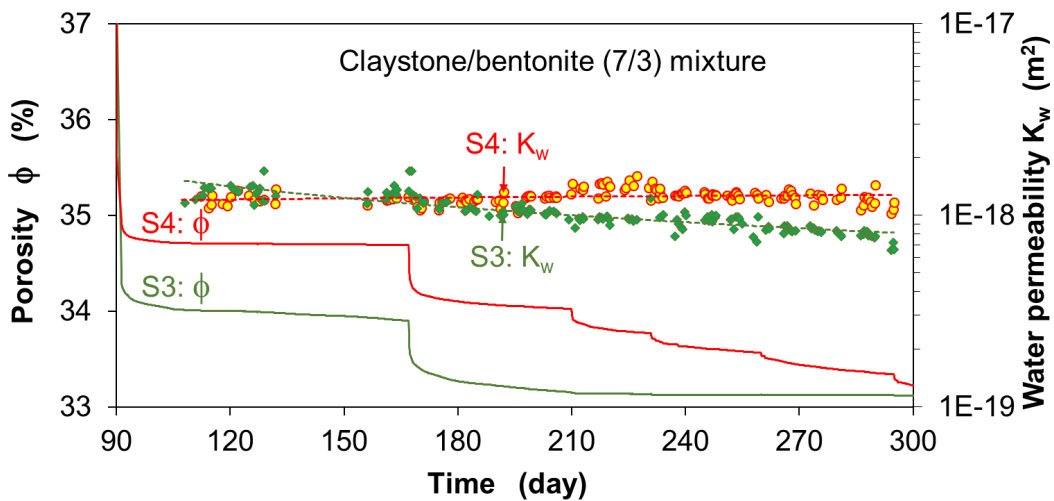
Along with the thermally induced reduction in porosity ϕ , water permeability K_w decreased either. However, the permeability variations are limited within small ranges, as shown in figure 3.20 illustrating K_w -values determined at the end of each temperature step in correlation with ϕ -values. The permeability varied with change in porosity. As observed on the bentonite S2, K_w decreased from 2.5×10^{-20} m² to 1.8×10^{-20} m² with ϕ -reduction from 47.2% to 45.8% during heating from 24 °C to 90 °C; and on the mixture S3, K_w from 1.2×10^{-18} m² to 7.8×10^{-19} m² with ϕ -reduction from 33.2 % to 33.1 % during cooling from 90 °C to 26 °C. These results indicate a negligible temperature influence on the intrinsic water permeability of both the bentonite and claystone/bentonite mixture. Correspondingly, the hydraulic conductivity is influenced mainly by thermally induced variations in viscosity and density of liquid water at a given porosity of the material. Moreover, it was also observed that the water permeabilities of the bentonite are about two orders of magnitude lower than those of the claystone/bentonite (7/3) mixture, even though the total porosities of the bentonite are much larger. This is because major part of the porewater in the bentonite is strongly bonded and immobile, and the remaining effective porosity is limited for flow of free water.



a. applied axial load, temperature and water injection pressure

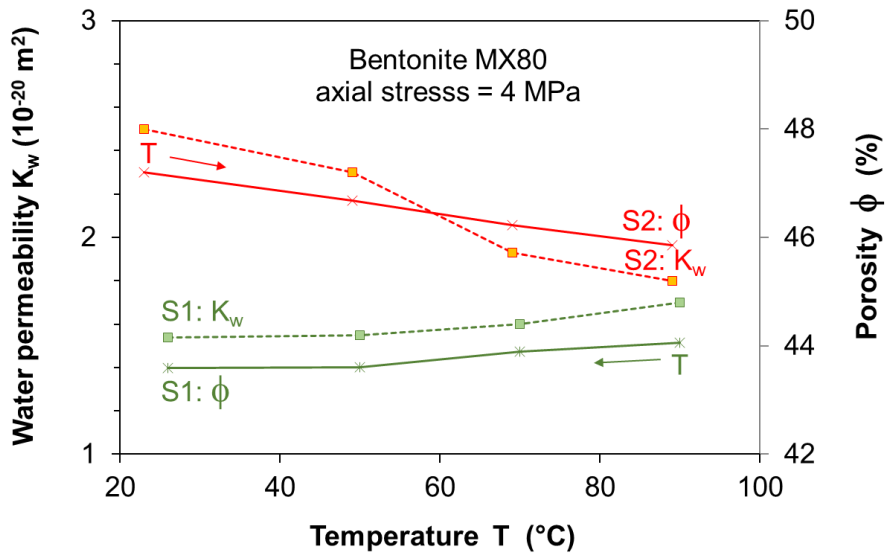


b. porosity and water permeability of the bentonite

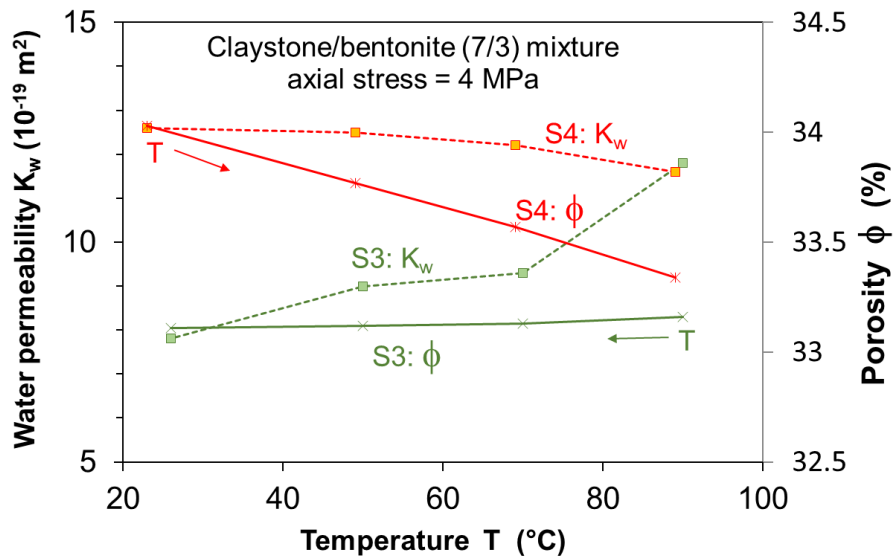


c. porosity and water permeability of the claystone/bentonite (7/3) mixture

Fig. 3.19 Consolidation and water permeability changes of the bentonite and claystone/bentonite (7/3) mixture under different loads and temperatures



a. Bentonite



b. Claystone/bentonite (7/3) mixture

Fig. 3.20 Thermally induced variations of porosity and water permeability of the bentonite and claystone/bentonite (7/3) mixture under axial stress of 4 MPa

3.4.3 Thermal effect on gas penetration

Gas penetration testing followed the last consolidation stage at axial stress of 4 MPa and at temperatures of 26 °C for samples S1 & S3 and 90 °C for S2 & S4. Figure 3.21 depicts results obtained from the claystone/bentonite (7/3) mixture S3 and S4. Both samples had the same dry density of 1.8 g/cm³ reached before. The data indicate relatively low gas breakthrough pressures $P_b = 0.8 - 0.9$ MPa, almost independent of the applied temperatures. The gas permeability increased with increasing injection pressure. Obviously,

gas can easily penetrate and migrate in the water-saturated and compacted claystone/bentonite (7/3) mixture at pressures much below the applied confining stress.

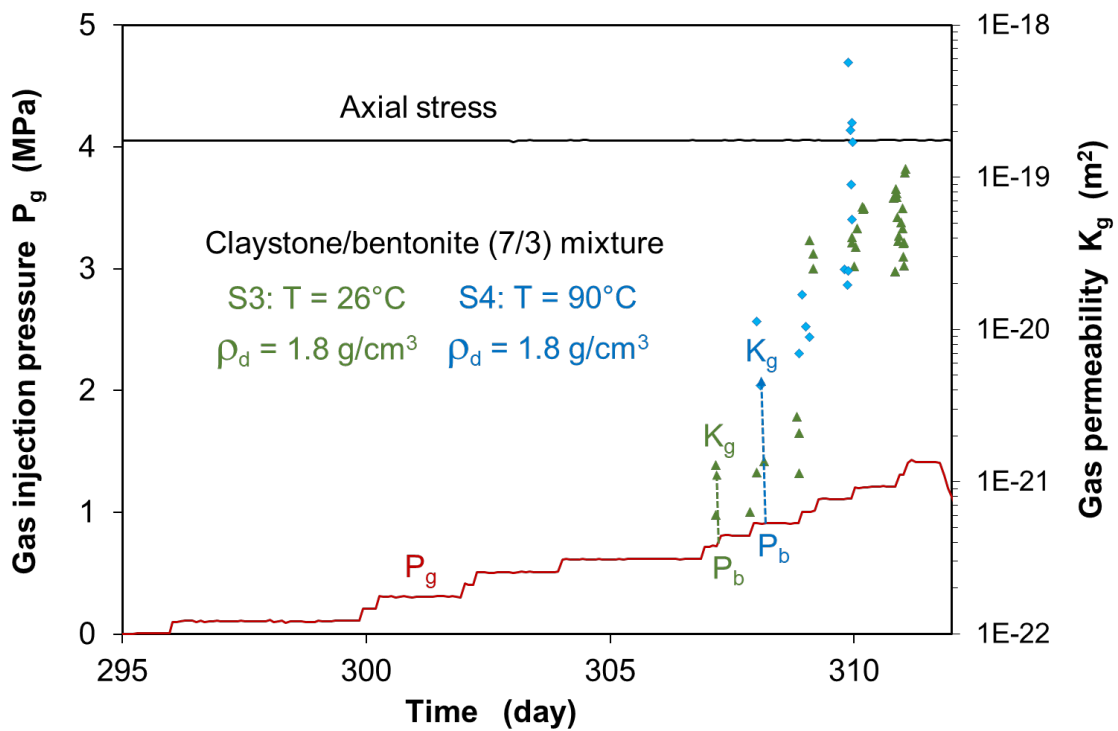
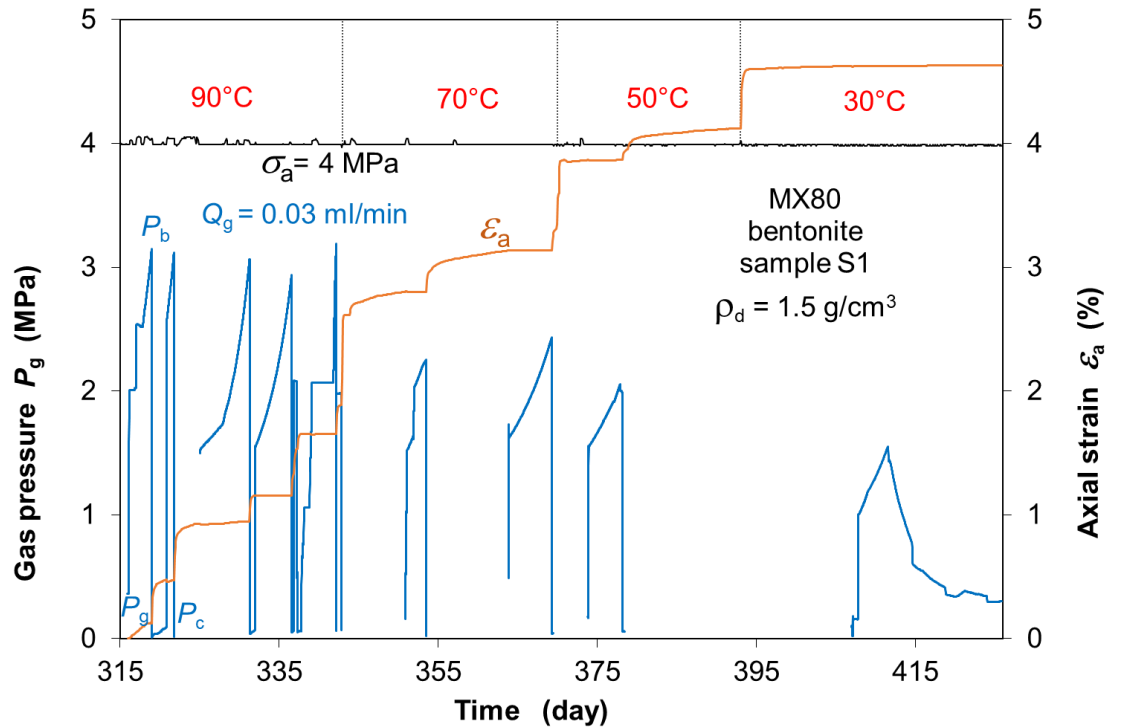
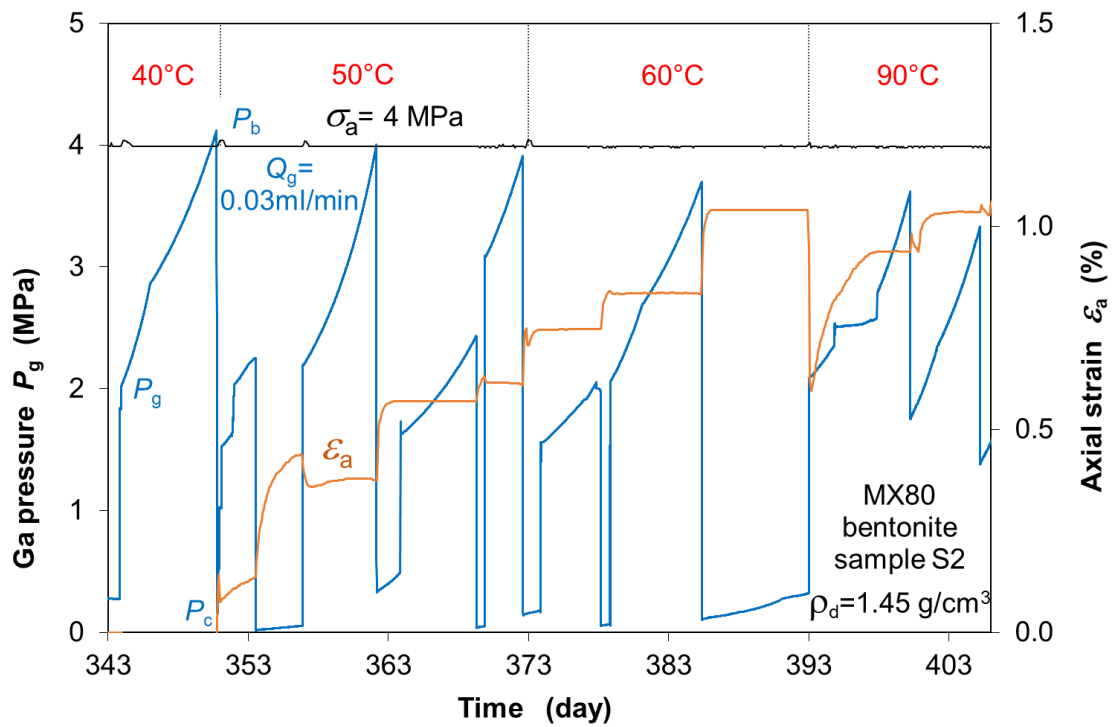


Fig. 3.21 Gas breakthrough pressures and permeabilities of the water-saturated claystone/bentonite mixture at temperatures of 26 °C and 90 °C

In contrast, much higher gas pressures are needed to create pathways in the water-saturated bentonite, as shown in figure 3.22. The gas was injected to both samples S1 and S2 in parallel at a controlled flow rate of 0.03 ml/min. While the gas supply to S1 was switched off on several times during the injection over three months, the gas injection to S2 was continuing over 2 months. Figure 2.22a shows that the gas breakthrough occurred at S1 at 90 °C five times at similar repeated pressures $P_b = 3.1 \pm 0.1$ MPa. The repeated pressure rising/dropping reflects opening/closing cycles of the pathway network due to the ductile deformation of the bentonite under interactions between gas pressure and confining stress. Subsequently, the stepwise cooling led the gas breakthrough pressure dropping down. At sample S2 at 40 °C, the first gas breakthrough occurred as the pressure reached to $P_b = 4.1$ MPa over the confining stress (figure 3.22b). At an increased temperature of 50 °C, the gas breakthrough pressures were still high close to the confining stress. Further increasing temperature to 60°C and 90 °C lowered the gas breakthrough pressure down to 3.6 – 3.5 MPa.



a. Sample 1



b. Sample 2

Fig. 3.22 Evolution of gas pressure of the water-saturated bentonite in correlation with temperature variation

The gas breakthrough pressures measured at the axial stress of 4 MPa are illustrated in figure 3.23 as a function of temperature. Both samples showed reverse tendencies: P_b decreased not only by heating at S2 but also by cooling at S1. The confused phenomena were in fact resulted from different degrees of water saturation in the samples caused by different thermal loading path. The water content and saturation were measured after testing. Sample S1 showed a significant desaturation to a degree of 79%, while a full saturation still maintained at S2. Under ambient temperature, porewater in bentonite is strongly bonded in interlayers and on external surfaces of clay particles. Gas penetration needs high pressures exceeding the total stress and tensile strength of the material to create micro-pathways. As temperature increases, a part of the absorbed water tends to desorption from solid surfaces and can be moved by gas pressures when local capillary thresholds are exceeded. Thus, the gas breakthrough pressure decreases with increasing temperature.

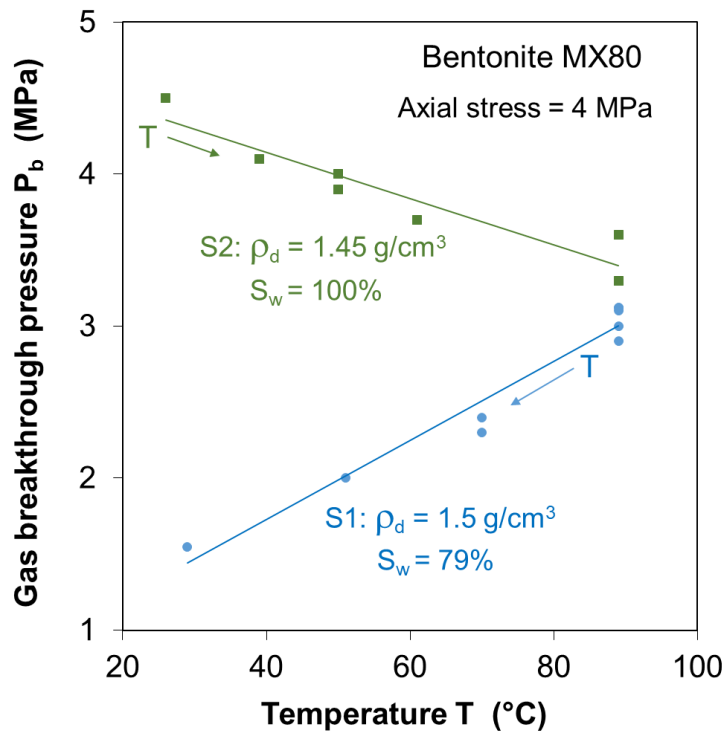


Fig. 3.23 Gas breakthrough pressure of the compacted bentonite as a function of on temperature and water saturation

Moreover, figure 3.22 also shows response of axial strain to gas pressure at each bentonite sample. Before gas breakthrough, the pressure increase did not cause significant deformation. As gas broke through, the rapid gas release led to a drop of the pore gas pressure ($P_p = (P_b + P_o)/2$) and thus an increase in the effective stress ($\sigma_{\text{eff}} = \sigma - P_p$).

Consequently, the material was somewhat compacted. As mentioned earlier, the sudden compaction caused by rising and dropping temperature was partly attributed to the thermal deformation of the test system, so that the thermal deformation of the samples could not be identified and evaluated here.

4 Summary and conclusions

As the engineered barrier material for the disposal of radioactive waste in clay host rock, crushed claystone, bentonite, and claystone/bentonite mixtures have been investigated regarding safety-related properties and performance. For laboratory testing, the crushed Opalinus claystone and sodium MX80 bentonite were taken. Both materials and the mixtures with claystone/bentonite mass ratios of 8/2, 7/3 and 6/4 were characterized by determination of key geotechnical properties:

- petrophysical properties (mineralogical composition, grain size distribution, grain density, water content)
- water absorption/retention capacity
- compressibility for fabrication of compacted blocks
- swelling pressure in relation to dry density
- water permeability in relation to dry density
- gas migration behaviour under water-saturated conditions.

Regarding the German generic repository models and the available emplacement techniques (emplacing and compacting granular material on site; setting up precompacted blocks and filling the remaining gaps with bentonite powder), the crushed claystone, granular bentonite, and a mixture of claystone/bentonite (7/3) were selected for investigating the barrier performance as

- *Buffer material*: precompacted blocks of the crushed claystone and the claystone/bentonite (7/3) mixture with a dry density of 2.0 g/cm^3 for supporting HLW-POLLUS casks as well as the bentonite granules for backfilling the rest space in the deposition drifts/holes;
- *Seal material*: precompacted blocks of the crushed claystone and the claystone/bentonite (7/3) mixture with a dry density of 2.0 g/cm^3 as well as the bentonite granules for sealing the boreholes, drifts and shafts at selected locations;
- *Backfill material*: the crushed claystone and the claystone/bentonite (7/3) mixture for backfilling the rest space in the repository.

The barrier performance of the selected materials was examined under dynamic repository conditions with three main phases: (i) hydration by taking up water from the surrounding humid environment; (ii) consolidation under the combined effect of the rock

stress and porewater pressure; and (iii) gas generation and migration in water-saturated barrier materials. Specific methods were developed and successfully applied for the tests. Synthetic pore water of the Opalinus clay and helium gas were used for respective water and gas flow testing. Key barrier parameters were determined by the measurements of swelling pressure and strain upon hydration, porosity and water permeability under increased loads, gas threshold pressure and permeability, and thermal responses. The following conclusions can be drawn from the experiments:

- The compressibility of the clay materials is mainly determined by grain size distribution and the claystone/bentonite mixing ratio. The crushed claystone with the coarse and sieved grains ($d < 32$ mm, $d < 10$ mm) can be easily compacted to a desired dry density compared to the pure bentonite and the mixtures. The targeted dry density of 2.0 g/cm³ for blocks can be achieved by the crushed claystone and claystone/bentonite (7/3) mixture under axial compression loads of 5 - 15 MPa in a mould.
- The water absorption and retention capacity of the claystone/bentonite mixtures is largely determined by the bentonite content. The amount of water absorption in the vapor reaches the maximum of about 57% for the bentonite in the free state, which corresponds to about 4 and 10 times that of the claystone/bentonite mixture and the claystone. The maximum water content is limited in the compacted blocks with reduced porosities.
- The swelling capacity of the claystone/bentonite mixtures is measured by the swelling pressure at full water saturation, which increases exponentially with increasing bentonite content and dry density. The swelling pressures were determined to be around 2 MPa for the bentonite with the targeted dry density of 1.5 g/cm³, 1 MPa for the compacted claystone blocks with a dry density of 2.0 g/cm³, and 2.5 MPa for the compacted claystone/bentonite (7/3) blocks with a dry density of 2.0 g/cm³. The swelling capacities are sufficiently high for the materials to be able to seal engineered voids/gaps in the barrier systems.
- The water permeability of the claystone/bentonite mixtures decrease exponentially with increasing bentonite content and dry density. At a given porosity, the water permeability of the bentonite is about four to six orders of magnitude lower than that of the claystone/bentonite (7/3) mixture and the crushed claystone.
- The gas migration in the water-saturated clay materials is significantly dependent on bentonite content. Gas flow in a water-saturated clay usually requires high gas pressure to overcome the capillary threshold or to create a local micro-pathway. The gas entry/breakthrough pressure observed for the bentonite is close to and even higher

than the confining stress, depending on the boundary confinement. The pathway can be locally clogged by the bentonite swelling. Under interactions between gas pressure and confining stress, the gas breakthrough/sealing event repeats itself periodically until the network is opened continuously. In contrast to the bentonite, the compacted claystone/bentonite mixtures allow for gas release at significantly lower gas pressures. The gas permeability of the induced pathway decreases exponentially with increasing bentonite content and dry density.

- The time-dependent consolidation of the claystone/bentonite mixtures increases nonlinearly with increasing effective stress, which causes a reduction of the porosity and the permeability. With the precompacted blocks of the crushed claystone and claystone/bentonite (7/3) mixture as well as the loosely emplaced bentonite, low water permeabilities of $10^{-18} - 10^{-20} \text{ m}^2$ can be achieved by increasing the stress up to 5 MPa.
- Thermal effects on the bentonite and claystone/bentonite (7/3) mixture were observed in the tested temperature range of 25 – 100 °C: a) increasing temperature reduces the water absorption capacity and thus the swelling capacity; b) the water permeability decreases with thermally induced decrease in effective porosity due to variations between bound and free porewater; c) increasing temperature increases the mobility and evaporation of bound porewater and thus lowers the pressure threshold for gas entry and penetration; and d) these thermal effects on the barrier performance of the studied materials are generally insignificant.

In general, the crushed claystone, bentonite, and mixtures studied exhibit favourable properties and barrier performance. The test results can be used for the design of the engineered barrier system in a repository.

Acknowledgements

The research work was funded by the Federal Ministry for the Environment, Nature Conservation, Nuclear Safety and Consumer Protection (BMUV) under contract number 02E11627.

References

- /AND 05/ ANDRA DOSSIER (2005): Synthesis – Evaluation of the feasibility of a geological repository in an argillaceous formation.
- /AND 15/ ANDRA (2015): Status of the Cigéo Project in France - French Industrial Geological Disposal Project, in the Proceedings of the LUCOEX Conference and Workshop, June 2-4, 2015, Oskarshamn, Sweden.
- /ARM 14/ Armand, G., Leveau, F., Nussbaum, C., de La Vaissiere, R., Noiret, A., Jaeggi, D., Landrein, P., Righini, C. (2014): Geometry and Properties of the Excavation-Induced Fractures at the Meuse/Haute-Marne URL Drifts, *Rock Mech Rock Eng* (2014) 47, 21-41.
- /BIR 13/ Birgersson, M., Karnland O. (2013): Gas intrusion in bentonite – Results of small scale experiments, FORGE International Symposium and Workshop on Gas Generation and Migration, February 5-7, 2013, Luxembourg.
- /BIR 17/ Birgersson M, Hedström M, Karnland O, Sjöland A (2017): Bentonite buffer: macroscopic performance from nanoscale properties. *Geological Repository Systems for Safe Disposal of Spent Nuclear Fuels and Radioactive Waste*. <http://dx.doi.org/10.1016/B978-0-08-100642-9.00012-8>
- /BOS 16/ Bosgiraud J.M. and Foin R. (2016): DOPAS WP3 Deliverable D3.7 - Test report on FSS metric clayish material emplacement tests with clayish material definition and laboratory work on its performance.
- /CON 18/ Conil N, Talandier J, Djizanne H, de La Vaissière R, Righini-Waz C, Auvray C, Morlot C, Armand C (2018): How rock samples can be representative of in-situ condition: a case study of Callovo-Oxfordian claystones, *Journal of Rock Mechanics and Geotechnical Engineering* 10 (2018) 613-623.
- /CUS 14/ Cuss, R.J., Harrington, J.F., Noy, D.J., Graham, C.C., Sellin, P., 2014. Evidence of localized gas propagation pathways in a field-scale bentonite engineered barrier system; results from three gas injection tests in the large scale gas injection test (Lasgit). *Appl. Clay Sci.* 102, 81–92. <http://dx.doi.org/10.1016/j.clay.2014.10.014>.

- /FOI 15/ Foin, R., Bosgiraud, J.-M., Armand, G., Noiret, A. (2015): Technical feasibility of the Cigéo Project seals, the Proceedings of the LUCOEX Conference and Workshop “Full-scale demonstration tests in technology development of repositories for disposal of radioactive waste”, June 2-4, 2015, Oskarshamn, Sweden.
- /FRE 93/ Fredlund, D.G., Rahardjo, H. (1993): Soil Mechanics for Unsaturated Soils. John Wiley & Sons, INC.
- /GRA 16/ Graham C.C., Harrington J.F., Sellin P., 2016. Gas migration in precompacted bentonite under elevated pore-water pressure conditions. Applied Clay Science 132, 353–365.
- /GUT 21/ Gutiérrez-Rodrigo, V., Martín, P. L., Villar, M. V, 2021. Effect of interfaces on gas breakthrough pressure in compacted bentonite used as engineered barrier for radioactive waste disposal, Process Safety and Environmental Protection 149 (2021) 244–257. <https://doi.org/10.1016/j.psep.2020.10.053>.
- /GUA 16/ Guayancan-Carrillo LM, Sulem J, Seyedi DM, Ghabezloo S, Noiret A, Armand G. Analysis of Long-Term Anisotropic Convergence in Drifts Excavated in Callovo-Oxfordian claystone. Rock Mechanics and Rock Engineering 2016; 49: 97-114.
- /HAR 17/ Harrington J. F., Graham C. C., Cuss R. J. and Norris S., 2017. Gas network development in a precompacted bentonite experiment. evidence of generation and evolution. Applied Clay Science 147, 80–89.
- /HOR 96/ Horseman, S.T., Higgs, J.J.W., Alexander, J., Harrington, J.F. (1996): Water, Gas and Solute Movement through Argillaceous Media. Report CC-96/1
- /IAE 92/ IAEA (1992): Performance of Engineering barriers in Deep Geological Repositories. Technical Report Series No. 342.
- /IMB 06/ Imbert, C. and Villar, M.V., 2006. Hydro-mechanical response of a bentonite pellets/powder mixture upon infiltration. Applied Clay Science 32(3-4), 197–209.

- /JOB 17/ Jobmann, M., Bebiolka A., Burlaka V., Herold P., Jahn S., Lommerzheim A., Maßmann J., Meleshyn A., Mrugalla S., Reinhold K., Rübél A., Stark L., Ziefle G. (2017): Safety assessment methodology for a German high-level waste repository in clay formations, *Journal of Rock Mechanics and Geotechnical Engineering* 9 (2017) 856-876. <https://doi.org/10.1016/j.irmge.2017.05.007>
- /KAU 11/ Kaufhold A, Dohrmann R, Siegesmund S, Gräsle W, Plischke I. Mineralogical and microfabric investigations of the sandy facies of Opalinus Clay (Mont Terri), *Clay Characterisation from Nanoscopic to Microscopic Resolution*. In: *Proceedings of the NEA Clay Club Workshop*. NEA; 2011. 53–7.
- /KÖH 15/ Köhler S, Sakaki T, Weber H, Garitte B, Müller HR (2015): Backfilling a Horizontal Tunnel with Granular Bentonite –Machine Development, Pre- & Mock-up Tests and Application at the Mont Terri URL, the *Proceedings of the LUCOEX Conference and Workshop “Full-scale demonstration tests in technology development of repositories for disposal of radioactive waste”*, June 2-4, 2015, Oskarshamn, Sweden.
- /LEV 20/ Levasseur, S., Collin, F., Daniels, K., Dymitrowska, M., Harrington, J., Jacobs, E., Kolditz, O., Marschall, P., Norris, S., Sillen, X., Talandier, J., Truche, L., Wendling, J., 2020. Initial State-of-the-Art on Gas Transport in Clayey Materials. Final version as of 30.11.2020 of deliverable D6.1 of the HORIZON 2020 project EURAD. EC Grant agreement no: 847593.
- /LOM 15/ Lommerzheim, A. & Jobmann, M. (2015): *Endlagerkonzept sowie Verfüll- und Verschlusskonzept für das Endlagerstandortmodell NORD*, Technischer Bericht (Entwurf), DBE TECHNOLOGY GmbH, Peine (in German).
- /MID 20/ Middelhoff M, Cuisinier O, Masrouri F, Talandier J, Conil N. (2020): Combined impact of selected material properties and environmental conditions on the swelling pressure of compacted claystone/bentonite mixtures. *Applied Clay Science* 2020; 184: 105389.
- /MIT 76/ Mitchell, J.K. (1976): *Fundamentals of Soil Behavior*. University of California, Berkeley, USA

- /MÜL 17/ Müller H.R., Garitte B., Vogt T., Köhler S., Sakaki T., Weber H., Spillmann T., Hertrich M., Becker J.K., Giroud N., Cloet V., Diomidis N. (2017): Implementation of the full-scale emplacement (FE) experiment at the Mont Terri rock laboratory, *Swiss J Geosci* (2017) 110:287-306.
- /NAG 02/ NAGRA (2002): Project Opalinus Clay, Models, Codes and Data for Safety Assessment – Demonstration of disposal feasibility for spent fuel, vitrified high-level waste and long-lived intermediate-level waste
- /OEC 03/ OECD (2003): Engineered Barrier Systems and the Safety of Deep Geological Repositories – State-of-the-art Report. EUR 19964 EN.
- /PEA 99/ Pearson F.J. (1999): WS-A Experiment: Artificial waters for use in laboratory and field experiments with Opalinus clay, Status June 1998. – Mont Terri Project, Technical Note 99-31, January 1999.
- /PEA 03/ Pearson FJ, Arcos D, Bath A, Boisson JY, Fernandez AM, Gäbler FE, Gaucher E, Gautschi A, Griffault L, Hernan P, Waber HN. (2003): Mont Terri Project–Geochemistry of Water in the Opalinus Clay formation at the Mont Terri Rock Laboratory. Reports of the Federal Office for Water and Geology (FOWG) Geology Series No. 5. FOWG; 2003.
- /PUS 87/ Pusch, R., Hökmark, H., Börgesson, L., 1987. Outline of Models of Water and Gas Flow through Smectite Clay Buffers. SKB Technical Report 87-10, Stockholm, Sweden.
- /PUS 90/ Pusch, R., Karnland, O., Hokmark, H., 1990. GMM - A general microstructural model for qualitative and quantitative studies of smectite clays. SKB Technical Report 90-43, Swedish Nuclear Fuel and Waste Management, Stockholm, Sweden.
- /ROB 21/ Robinet J.-C., Tyri D., Djeran-Maigre I. (2021): Hydro-mechanical response of crushed argillite and bentonite mixtures as sealing material, *Engineering Geology* 288 (2021) 106140. <https://doi.org/10.1016/j.enggeo.2021.106140>

- /ROD 99/ Rodwell, W.R., Harris, A.W., Horseman, S.T., Lalieux, P., Müller, W., Ortiz, A.L., Pruess, K., 1999. Gas Migration and Two-Phase Flow through Engineered and Geological Barriers for a Deep Repository for Radioactive Waste. A Joint EC/NEA Status Report, European Commission, EUR 19122 EN.
- /SEL 14/ Sellin, P. (editor), 2014. Experiments and modelling on the behaviour of EBS. FORGE Report D3.38. 426pp.
- /TOU 07/ Tournassat C, Gaucher EC, Fattahi M, Grambow B. On the mobility and potential retention of iodine in the Callovian-Oxfordian formation. *Physics and Chemistry of the Earth* 2007; 32(8-14): 539-51.
- /VAN 80/ Van Genuchten, M.T. (1980): A Closed-Form Equation for predicting the hydraulic Conductivity of Unsaturated Soils. -*Soil Sci. Soc. Am. J.*, 44:892-898
- /VIL 10/ Villar M.V., Gómez-Espina R., Lloret A. (2010): Experimental investigation into temperature effect on hydro-mechanical behaviours of bentonite. *Journal of Rock Mechanics and Geotechnical Engineering*. 2010, 2 (1): 71–78.
- /VIL 20/ Villar, M.V., Armand, G., Conil, N., de Lesquen, C., Herold, P., Simo, E., Mayor, J.C., Dizier, A., Li, X., Chen, G., Leupin, O., Niskanen, M., Bailey, M., Thompson, S., Svensson, D., Sellin, P., Hausmannova, L., 2020. Initial State-of-the-Art on THM behaviour of i) Buffer clay materials and of ii) Host clay materials. Deliverable D7.1 HITEC. EURAD Project, Horizon 2020, No. 847593. 214 pp.
- /VOK 14/ Vokál A., Polívka P., Dobrev D., 2014. Experimental investigation of migration of hydrogen through compacted bentonite, in FORGE Report D3.38 (edited by Sellin P) - Experiments and modelling on the behaviour of EBS.
- /XU 17/ Xu L, Ye WM, Ye B., 2017. Gas breakthrough in saturated compacted GaoMiaoZi (GMZ) bentonite under rigid boundary conditions. *Canadian Geotechnical Journal* 2017; 54: 1139-49.

- /ZEN 19/ Zheng Z.X., Cui Y.J., Zhang F., Conil N., Talandier J. (2019): Investigation of swelling pressure of bentonite/claystone mixture in the full range of bentonite fraction. *Applied Clay Science* 178 (2019) 105137.
- /ZHA 10/ Zhang, C.L., Czaikowski, O., Rothfuchs, T. (2010): Thermo-Hydro-Mechanical Behaviour of the Callovo-Oxfordian Clay Rock – Final report of the BURE-HAUPT/EC-TIMODAZ project, Bericht GRS-266, Gesellschaft für Anlagen- und Reaktorsicherheit (GRS), Braunschweig.
- /ZHA 13/ Zhang, C.L., Czaikowski, O., Rothfuchs, T., Wieczorek, K. (2013): Thermo-Hydro-Mechanical Processes in the Nearfield around a HLW Repository in Argillaceous Formations - Volume I: Laboratory Investigations, Gesellschaft für Anlagen- und Reaktorsicherheit (GRS) mbH, Braunschweig, GRS-312.
- /ZHA 14/ Zhang, C.L. (2014): Characterization of Excavated Claystone and Claystone-Bentonite Mixtures as Barrier material, Geological Society Special Publication 400 – Clays in Natural and Engineering barriers for Radioactive Waste Confinement (edited by Norris et al.), The Geological Society of London, 2014, 323-337.
- /ZHA 17a/ Zhang, C.L. (2017): Sealing Performance of Fractured Claystone and Clay-Based Materials, Final report of the German Project THM-TON and the EC Project DOPAS, Gesellschaft für Anlagen- und Reaktorsicherheit (GRS), Braunschweig, GRS-451.
- /ZHA 17b/ Zhang C.L. (2017): Response of clay rock to moisture change. In: Ferrari A, Laloui L, editors. *Advances in Laboratory Testing and Modelling of Soils and Shales (ATMSS)*. Springer; 2017.
- /ZHA 18a/ Zhang, C.L. and Kröhn, K.P. (2019): Sealing Behaviour of Crushed Claystone-Bentonite Mixtures, *Geomechanics for Energy and the Environment* 17 (2019) 90–105.
- /ZHA 18b/ Zhang C.L. (2018): Thermo-hydro-mechanical behaviour of clay rock for deep geological disposal of high-level radioactive waste. *Journal of Rock Mechanics and Geotechnical Engineering* 2018; 10(5): 992-1008.

- /ZHA 20/ Zhang C.L., Laurich B. Mechanical behaviour of sandy facies of Opalinus Clay under different load conditions. *Journal of Rock Mechanics and Geotechnical Engineering* 2020; 12(2): 223-41.
- /ZHA 22/ Zhang C.L., Wang J., Kaufhold S., Liu Y.M., Czaikowski, O. (2022): Buffering Performance of GMZ and MX80 Bentonites for Geological Disposal of High-Level Radioactive Waste, Final report of the joint German and Chinese Research Project (ELF-China, Pilot Phase), Gesellschaft für Anlagen- und Reaktorsicherheit (GRS), Braunschweig, GRS-702.
- /ZHU 13/ Zhu, C.M., Ye, W.M., Chen, Y.G., Chen, B., Cui, Y.J., 2013. Influence of salt solutions on the swelling pressure and hydraulic conductivity of compacted GMZ01 bentonite. *Engineering Geology*, 166: 74–80.
doi: 10.1016/j.enggeo.2013. 09.001.

List of figures

Fig. 1.1	Sketch of the proposed backfilling/sealing concept /JOB 17/	3
Fig. 1.2	HLW disposal concept in horizontal drifts in Opalinus Clay /JOB 17/	3
Fig. 1.3	Concept for backfilling and sealing horizontal drifts /LOM 15/	4
Fig. 2.1	Sampling of the crushed claystone from excavation of Gallery 18 in the sandy facies of Opalinus Clay at Mont-Terri rock Laboratory	7
Fig. 2.2	Pictures of crushed OPA claystone with different grain sizes and the corresponding distribution curves compared with crushed COX claystone	8
Fig. 2.3	Grain size distributions of the granules, crushed and fabricated pellets of MX80 bentonite	11
Fig. 2.4	Density and viscosity of synthetic OPA and COX porewaters as a function of temperature in comparison with pure water	13
Fig. 2.5	Pictures of the samples placed in desiccators for the measurement of water uptake and retention capacities at different humid conditions.....	15
Fig. 2.6	Evolution of water uptake measured on the crushed OPA claystone, claystone/bentonite (7/3) mixture and MX80 bentonite under free and confined conditions	18
Fig. 2.7	Water retention curves of the crushed OPA claystone and claystone/bentonite (7/3) mixture preheated at 25 - 105 °C under free and confined conditions	20
Fig. 2.8	Water retention curves of MX80 bentonite preheated at 25 - 200 °C under free and confined conditions	20
Fig. 2.9	Degree of water saturation as a function of suction for the crushed OPA claystone, claystone/bentonite (7/3) mixture and MX80 bentonite under confined conditions.....	21
Fig. 2.10	Modelling of the water retention curves for the compacted bentonite MX80 and claystone/bentonite (7/3) mixture	23
Fig. 2.11	Grain size distributions of the crushed OPA claystone and claystone/bentonite (7/3) mixture for precompact blocks.....	24
Fig. 2.12	A large oedometer setup for compaction of barrier materials	26
Fig. 2.13	Pictures of the samples installed in the big cell (D = 280 mm, H = 265 mm)	26

Fig. 2.14	Compacted dry densities of the crushed OPA claystone and claystone-bentonite (7/3) mixture	27
Fig. 2.15	Comparison of the compaction curves of two crushed claystone samples with coarse grains of $d < 32$ mm	27
Fig. 2.16	Comparison of the compaction curves of the crushed OPA claystone and mixture with bentonite (pre-stamped by hand) and the crushed COX claystone and mixture with bentonite and pure bentonite as well as bentonite-sand mixture (without hand stamping)	28
Fig. 2.17	Pictures of the compacted blocks of the crushed claystone and claystone/bentonite (7/3) mixture	29
Fig. 2.18	A test setup with parallel arranged oedometer cells for measurements of swelling pressure, water permeability, and gas penetration of clay samples	31
Fig. 2.19	Swelling pressures measured on the compacted claystone/bentonite mixtures	33
Fig. 2.20	Water permeability of the claystone/bentonite mixtures as a function of dry density	35
Fig. 2.21	Effective gas permeability of the water-saturated claystone/bentonite mixtures as a function of dry density	37
Fig. 2.22	Developments of gas pressure and confining stress with the gas injection to the water-saturated bentonite under volume-constrained conditions	41
Fig. 2.23	Gas breakthrough pressure in relation to the total stress	42
Fig. 2.24	Gas breakthrough pressures of the different bentonites as a function of dry density	43
Fig. 2.25	Gas breakthrough pressure in relation to swelling pressure	43
Fig. 2.26	Gas and water permeability obtained on a bentonite sample MX80-d with a dry density of 1.5 g/cm^3	44
Fig. 3.1	A large oedometer setup for hydro-mechanical testing of backfill material	47
Fig. 3.2	Setup of the oedometer tests on four seal samples in two coupled load rigs	48
Fig. 3.3	Pictures of the seal samples emplaced in oedometer cells	49

Fig. 3.4	Pictures of the samples prepared with the bentonite pellets ($d < 5$ mm) and crushed claystone ($d < 10$ mm) by mixing, filling and stamping the mixtures in oedometer cells of 120 mm diameter	52
Fig. 3.5	Water uptake and induced swelling of the seal samples S1-S4	55
Fig. 3.6	Multistep consolidation behaviour and variation in water permeability of the claystone aggregate: (a) axial stress and water injection pressure; (b) axial strain and strain rate; and (c) porosity and water permeability	57
Fig. 3.7	Multistep consolidation behaviours and variations in water permeability of the seal materials: (a) axial stress and water injection pressure; (b) porosity; and (c) water permeability	58
Fig. 3.8	Stress-porosity relationship for the crushed claystone	59
Fig. 3.9	Bulk modulus of the crushed claystone as a function of dry density	59
Fig. 3.10	Water permeability-porosity relationships of the crushed claystone B and the seal materials S1-S4	60
Fig. 3.11	Gas breakthrough pressures and permeabilities of the water-saturated seal materials compressed under axial stress of 5 MPa	61
Fig. 3.12	Gas permeabilities of the water-saturated and compacted claystone aggregate B and seal materials S2-S4 as a function of gas injection pressure.	62
Fig. 3.13	Evolution of gas injection pressure, water permeability before gas breakthrough and gas permeability at breakthrough observed on the bentonite sample	63
Fig. 3.14	Evolution of the gas injection pressure and resulting deformation of water-saturated and compacted bentonite	65
Fig. 3.15	Swelling of the compacted seal material samples S1-S4 after unloading	66
Fig. 3.16	Pictures of the dismantled backfill and seal samples	67
Fig. 3.17	Demonstration of the homogenisation of bentonite pellets ($d = 7$ mm) immersed in the synthetic clay water: (a) before and (b) after wetting for 1 hour	67
Fig. 3.18	Evolution of water uptake and induced swelling of the bentonite and claystone/bentonite (7/3) mixture during hydration with synthetic OPA clay water at a low axial load of 0.3 MPa and temperatures 23 °C and 90 °C	69

Fig. 3.19	Consolidation and water permeability changes of the bentonite and claystone/bentonite (7/3) mixture under different loads and temperatures	71
Fig. 3.20	Thermally induced variations of porosity and water permeability of the bentonite and claystone/bentonite (7/3) mixture under axial stress of 4 MPa	72
Fig. 3.21	Gas breakthrough pressures and permeabilities of the water-saturated claystone/bentonite mixture at temperatures of 26 °C and 90 °C	73
Fig. 3.22	Evolution of gas pressure of the water-saturated bentonite in correlation with temperature variation	74
Fig. 3.23	Gas breakthrough pressure of the compacted bentonite as a function of on temperature and water saturation	75

List of tables

Tab. 2.1	Grain densities measured on different grain fractions of crushed OPA claystone	9
Tab. 2.2	Main mineralogical components of the OPA sandy claystone determined on drilled cores BPE-1-2/3	10
Tab. 2.3	Grain densities of the different fractions of tested MX80 bentonite.....	12
Tab. 2.4	Mineralogical components of tested MX80 bentonite	12
Tab. 2.5	Main chemical components of synthetic OPA clay water	13
Tab. 2.6	Main chemical components of synthetic COX clay water	13
Tab. 2.7	Salt solutions used for the measurement of water retention capacities of the selected barrier materials at different relative humidities	16
Tab. 2.8	Initial characteristics of the crushed OPA claystone and claystone/bentonite mixture (7/3) for the measurement of water uptake and retention	17
Tab. 2.9	Initial characteristics of MX80 bentonite samples for the measurement of water uptake and retention	17
Tab. 2.10	The parameters of van Genuchten model for the compacted bentonite (MX80-a unheated; MX-b preheated at 200 °C) and claystone/bentonite (7/3) mixture (unheated)	22
Tab. 2.11	Initial characteristics of the crushed OPA claystone and claystone/bentonite mixtures installed in a large oedometer cell	25
Tab. 2.12	Characteristics of the samples compacted at axial load of 21 MPa.....	28
Tab. 2.13	Summary of welling pressure, water and gas permeabilities measured on the compacted claystone/bentonite mixtures at different dry densities	32
Tab. 2.14	Results of the gas penetration tests on the water-saturated bentonite MX80 samples under volume-constrained conditions	39
Tab. 3.1	Initial characteristics of the backfill/seal samples for hydro-mechanical testing	50
Tab. 3.2	Initial characteristics of the prepared bentonite samples (S1, S2) and claystone/bentonite (C/B=7/3) samples (S3, S4) for thermal testing	51

**Gesellschaft für Anlagen-
und Reaktorsicherheit
(GRS) gGmbH**

Schwertnergasse 1
50667 Köln

Telefon +49 221 2068-0

Telefax +49 221 2068-888

Boltzmannstraße 14

85748 Garching b. München

Telefon +49 89 32004-0

Telefax +49 89 32004-300

Kurfürstendamm 200

10719 Berlin

Telefon +49 30 88589-0

Telefax +49 30 88589-111

Theodor-Heuss-Straße 4

38122 Braunschweig

Telefon +49 531 8012-0

Telefax +49 531 8012-200

www.grs.de